1 of 2

DOE/ER/40459--6

PROGRESS REPORT

NUCLEAR PHYSICS RESEARCH

at

THE UNIVERSITY OF RICHMOND

Submitted to

THE UNITED STATES DEPARTMENT OF ENERGY

From

M. F. VINEYARD, G. P. GILFOYLE, AND R. W. MAJOR

DEPARTMENT OF PHYSICS

UNIVERSITY OF RICHMOND, VA 23173

Period: November 1, 1992 to October 31, 1993

Contract Number: DE-FG05-88ER40459

Contents

Preface

Summarized in this report is the progress achieved during the period from November 1, 1992 to October 31, 1993 under Contract Number DE-FG05-88ER40459. The experimental work described in this report is in electromagnetic and heavy-ion nuclear physics. The effort in electromagnetic nuclear physics is in preparation for the research program at the Continuous Electron Beam Accelerator Facility (CEBAF) and is focussed on the construction and use of the CEBAF Large Acceptance Spectrometer (CLAS). The heavy-ion experiments were performed at the Argonne National Laboratory ATLAS facility and the University of Pennsylvania. Seventeen undergraduate students, S. E. Atencio, A. Anderson, C. Cardounel, J. F. Crum, G. Kline, M. M. Mawicke, M. McGhee, B. M. McKeever, M. Nimcheck, R. G. Ohl, J. H. Rollinson, B. Sabloff, S. Sigworth, C. Smith, A. S. Snyder, R. S. Trotter, and P. Woods participated in these projects. In addition, numerous collaborators are associated with this work and are listed at the end of the report. The Principal Investigators would like to express their sincere appreciation for the hospitality and support they have received from all of their collaborators.

M. F. Vineyard, G. P. Gilfoyle, and R. W. Major

CEBAF Program Advisory Committee Six (PAC6) Proposal Cover Sheet

This proposal must be received by close of business on April 5, 1993 at:

CEBAF
User Liaison Office
12000 Jefferson Avenue
Newport News, VA 23606

Proposal Title

Inclusive η Photoproduction in Nuclei

Contact Person

Name: Michael F. Vineyard
Institution: University of Richmond
Address: Department of Physics
Address: University of Richmond
City, State ZIP/Country: Richmond, VA 23173
Phone: (804) 289-8257 **FAX:** (804) 289-8482
E-Mail → BITnet: VINEYARD@URVAX **Internet:** VINEYARD@URVAX.URICH.EDU

If this proposal is based on a previously submitted proposal or letter-of-intent, give the number, title and date:

CEBAF Use Only

Receipt Date: _____ Log Number Assigned: _____

By: _____

Inclusive η Photoproduction in Nuclei

M. F. Vineyard (Spokesperson),[1] S. Ahmad,[2] B. E. Bonner,[2] S. Dytman,[3]
H. Funsten,[4] G. P. Gilfoyle,[1] C. E. Hyde-Wright,[5] B. J. Lieb,[6] R. W. Major,[1]
B. A. Mecking,[7] R. A. Miskimen,[8] G. S. Mutchler,[2] B. G. Ritchie,[9]
P. D. Rubin,[4] J. B. Seaborn,[1] H. Stroeher,[10] and A. Yegneswaran[7]

[1]*University of Richmond*
[2]*Rice University*
[3]*University of Pittsburgh*
[4]*College of William and Mary*
[5]*University of Washington*
[6]*George Mason University*
[7]*CEBAF*
[8]*University of Massachusetts*
[9]*Arizona State University*
[10]*University of Giessen*

Abstract

We propose to measure inclusive η photoproduction in nuclei (^{2}H, ^{3}He, ^{4}He, ^{12}C, ^{58}Ni, ^{208}Pb) over the photon energy range k = 0.8-1.5 GeV. The experiment will be performed with the CEBAF Large Acceptance Spectrometer (CLAS) and the bremsstrahlung photon tagging system in Hall B. The neutral mesons will be detected via the 2γ decay mode. These measurements will provide important information on the ηN interaction and nuclear-medium modifications of N* resonances.

1. Scientific Motivation

Over the last fifteen years, significant progress has been made in understanding the pion-nucleus interaction. However, very little information exists on the interaction of the next simplest meson, the eta, with nucleons, and almost nothing is known about its interaction with nuclei. The study of the η meson shares many of the motivations of the study of the pion. Just as the pion studies have provided extensive information on the $\Delta(1232)$ and its dynamics within the nuclear medium, the investigation of the η, with its isospin selectivity, should enable us to obtain a similar understanding of the $S_{11}(1535)$ and other isospin-1/2 N* resonances. In addition, due to the lack of π beams, the production of η mesons in nuclei will provide important information on the η-nucleon and η-nucleus interactions. Reactions induced with photons are particularly suitable for these studies because photons probe the entire nuclear volume.

The current understanding of the photoproduction of η mesons is based on a rather sparse data set. Most of this data is 20 years old [1], with the exception of two more recent measurements [2,3]. The data base will soon improve, however, as extensive photoproduction measurements [4] are planned at CEBAF. These measurements will be complemented by an electroproduction experiment [5] at CEBAF to study the $S_{11}(1535)$ and $P_{11}(1710)$ resonances which are the only nucleon resonances of mass less than 2 GeV with significant η decay branches. The results of these upcoming experiments should improve our knowledge of the elementary (γ,η) process significantly.

Attempts to describe the elementary amplitudes involved in the (γ,η) reaction have focussed on several different theoretical approaches. In one approach [2,6,7], the process is described in terms of known nucleon resonances and a phenomenological background. This model contains a large number of parameters which must be determined from fits to the available data.

An effective Lagrangian method has been used by Benmerrouche and Mukhopadhyay [8]. This approach has fewer parameters to be fitted to the data. They found that the reaction was dominated by the excitation of the $S_{11}(1535)$ resonance, and they extracted a value for the helicity amplitude $A_{1/2}$ which is compatible with quark-model estimates [9-12].

Bennhold and Tanabe [13] developed an isobar model for η photoproduction on nucleons by using the $\pi N \rightarrow \pi N$, $\pi N \rightarrow \pi\pi N$, and $\pi N \rightarrow \eta N$ reactions to determine the hadronic vertices, and the pion photoproduction reactions to parameterize the electromagnetic vertices. The η

photoproduction amplitude was then used to estimate the cross sections for coherent and incoherent η production on several nuclei. The model was later extended [14] to include Born terms in the elementary production amplitude. The results of these studies indicate that coherent and incoherent nuclear cross sections are on the order of several 10 nb.

In a series of papers by Liu and collaborators [15-17], an isobar model was used to study the η interaction with hadrons. This model predicted an attractive ηN interaction and indicated the possible existence of bound ηN states in nuclei with $A \geq 12$. In the most recent of these papers [17], the authors conclude that the widths of these bound states may be rather large.

Very recently, Carrasco [18] performed a theoretical study of inclusive η photoproduction in nuclei. In this work the many-body calculations of the N*(1535) width of Ref. [17] for the case of bound η states was extended to the problem of η propagation through nuclei. The inclusive η photoproduction cross sections through the excitation of the N*(1535) resonance were calculated with a model which incorporates nuclear-medium modifications of the N*(1535) decay width, Fermi sea effects, and final-state interactions. The photon energy dependence of the cross sections per nucleon on ^{16}O and ^{208}Pb are shown in Fig. 1. The dot-dashed curves shown in the figure are the results of calculations with the impulse approximation. The dashed curves are the nuclear cross sections which were calculated taking into account changes in the N* width, Fermi motion, and Pauli blocking effects. The solid curves are the results of the full calculations which also include final-state interactions. As can be seen in the figure, η mesons can be produced below the production threshold on the free nucleon (k = 709 MeV) due to the Fermi motion of the nucleons in the nucleus.

The target mass dependence of the cross sections at k = 800 MeV calculated with this model is shown in Fig. 2. The cross section is found to increase as A^{α} with $\alpha \cong 0.6$. This behavior is similar to that found for π^0 photoproduction on nuclei in the Δ-resonance region where the A-dependence was described by $\sigma_A \propto A^{0.66}$ [19], and indicates that particles produced in the interior of the nucleus have a small chance of escaping. In fact, Carrasco reported [18] that, according to his calculations, about 40% of the η mesons are absorbed before leaving the ^{16}O nucleus, and about 65% are absorbed in the case of ^{208}Pb. The number of η mesons which are rescattered before leaving the nucleus is calculated to be about 9% for ^{16}O and 13% for ^{208}Pb.

Shown in Fig. 3 are the differential cross sections ($d^2\sigma/d\Omega dP_\eta$) calculated by Carrasco [18] for ^{16}O and ^{208}Pb at k = 800 MeV and $\theta = 25^\circ$ before (dashed curves) and after (solid curves)

final-state interactions. The inclusion of the final-state interactions has a greater effect on the magnitude of the cross sections than it does on the shape of the distributions.

The calculations discussed above show that both final-state interactions and nuclear-medium modifications are important in inclusive η photoproduction in nuclei at energies around the $S_{11}(1535)$ resonance. Additional theoretical work must be performed on the role of other resonances and background terms in order to have a complete description of the reaction. However, it is clear that measurements of the inclusive (γ,η) cross section will provide important information on the ηN interaction and the nuclear-medium modifications of the S_{11} response. In fact, since the cross sections for coherent and incoherent photoproduction of η mesons are predicted [13,14] to be quite small (several 10 nb), inclusive measurements may be the only feasible way to study the dynamics of the N*(1535) in the nuclear medium. These measurements are necessary if further theoretical progress is to be made in this area.

At present there is very little data available on inclusive η production in nuclei. Most of these experiments have been performed with pion beams [20-24]. Some of the results of this work are illustrated in Figs. 4-6 taken from Ref. [20]. Shown in Fig. 4 is an inclusive (π^+,η) spectrum taken on ^{12}C at a beam momentum of 680 MeV/c. Energy-integrated (π^+,η) inclusive cross sections plotted as a function of target mass are shown in Fig. 5 for three values of beam momentum. The dotted curves shown in the figure are the results of Glauber model calculations [25]. The ηN total cross section, which is the only unknown input in this calculation, was adjusted to obtain the best fit to the data. A good description of the mass dependence at all three beam momenta is obtained with $\sigma(\eta N) = 15$ mb. This should be compared to the πN total cross section of 34 mb at this energy. The ηN total cross sections are displayed as a function of pion beam momentum in Fig. 6. The solid curve shown in the figure is the prediction of the additive quark model [26]. The results of this calculation are in rather good agreement with the data. The πN total cross section, shown as the dashed curve for comparison, is clearly larger than the ηN cross sections over a wide momentum range. The η momentum range of the proposed experiment is indicated above Fig. 6.

It is important to point out a disadvantage in using pion beams to make these measurements. Pion absorption and scattering in the initial state introduces an uncertainty in the extracted ηN cross section which is not present in the photoproduction reaction. The effect of the pion initial-state interactions is illustrated in Fig. 5. We have added the solid line to the figure to show the A dependence of the cross section without initial-state or final-state interactions. This cross section

scales linearly with A. The difference between this line and the dotted curve for $\sigma_{\eta N} = 0$ mb is due to the π interaction in the initial state. In the case of the photoproduction reaction, any deviation from the linear dependence will be due to η absorption in the final state.

The inclusive (p,η) reaction on nuclei has been investigated in recent experimental [27] and theoretical [28] papers. The A dependence of the differential cross section measured [27] at a proton bombarding energy of 1 GeV is shown in Fig. 7. The solid and dashed curves are the predictions of a folding model [28] with and without η absorption, respectively. The result of the folding model calculation without η absorption (dashed curve) has a greater slope than the data. This suggests significant η absorption in the nucleus. However, the calculation with absorption (solid curve) underpredicts the data, and the fact that it increases more slowly with increasing A than the data indicates that η absorption is overestimated by the model. It has been suggested [27] that this is due to the fact that η absorption is evaluated with the assumption that all η mesons are produced at the center of the nucleus. The ηN absorption cross section used in the folding model calculations was estimated by detailed balance from the $\pi^- p \rightarrow \eta n$ reaction assuming that both reactions proceeds through the N*(1535) resonance. The resulting ηN total cross section (solid curve) is shown as a function of the kinetic energy of the η meson in the nucleon rest frame in Fig. 8. The dashed curve is the result of a coupled-channel analysis of Bhalerao and Liu [15]. The two results are in good agreement.

Recently, experiments were performed at the Mainz microtron (MAMI) to measure the photoproduction of η mesons from ^{1}H, ^{2}H, ^{12}C, ^{40}Ca, ^{93}Zr, and ^{nat}Pb in the photon energy range 600-790 MeV [29]. In these experiments the neutral mesons were detected with the Two Arm Photon Spectrometer (TAPS), which consists of BaF_2 arrays. The data are still being analyzed, and only very preliminary results are available. Shown in Fig. 9 are raw mass spectra taken on several of the targets. The hatched areas in the the figure are the π^0 and η peaks which stand well above the background.

This brief discussion of inclusive η production, though incomplete, shows that both the η energy spectrum and target mass dependence of the inclusive cross section are strongly influenced by final-state interactions, and are therefore sensitive to the features of the ηN interaction. Further progress in understanding the ηN interaction is impossible without much more extensive and precise data on inclusive η production in nuclei. The (γ,η) reaction is particularly well suited for these studies due to the absence of initial-state interactions.

We propose to measure differential cross sections for the inclusive (γ,η) reaction on ^{2}H, ^{3}He, ^{4}He, ^{12}C, ^{58}Ni, and ^{208}Pb over the photon energy range k = 0.8-1.5 GeV. The η momentum distributions and the target mass dependence of the inclusive cross section will provide information on the η-nucleon interaction. Comparisons with the data on η production from the proton [4] will yield information on the nuclear-medium modifications of the I = 1/2 N* resonances.

2. Experimental Procedure

The measurements will be performed with the CEBAF Large Acceptance Spectrometer (CLAS) in Hall B. The data on the ^{2}H target can be taken concurrently with experiment PR-89-045 [30]. The measurements on the ^{3}He, ^{4}He, and ^{12}C targets can be performed concurrently with experiment PR-91-014 [31]. Additional beam time is requested for the ^{58}Ni and ^{208}Pb target. The main features of the experiment will described in the following sections.

2.1 Beam

The reactions will be induced with tagged photons produced with the Hall B bremsstrahlung tagging system. Using an incident electron energy of 1.6 GeV, the tagged photons will have an energy range of 0.8 to 1.5 GeV. This energy range will span from the $S_{11}(1535)$ resonance to above the $P_{11}(1710)$ resonance. For the counting rate estimates, the tagged photon rate has been assumed to be 10^{7} photons/s.

2.2 Kinematics

The momentum as a function of laboratory angle for η mesons produced by photons with energies between 0.75 and 1.55 GeV is shown in Fig. 10. The dashed curves correspond to constant center-of-mass angles. It can be seen from this figure that the magic photon energy which produces recoilless η's is between 0.9 and 0.95 GeV. This is the energy range which one might expect to be most favorable for the production of bound states of the η meson in nuclei.

2.3 Neutral Meson Analysis

The neutral mesons will be detected with the CLAS via the two-photon decay. A typical event

is shown in Fig. 11. The energy E_γ, polar angle θ_γ, and azimuthal angle ϕ_γ will be measured for each photon. From this one gets the opening angle ψ between the two photons and the asymmetry parameter X, defined as

$$X = \frac{|E_{\gamma 1} - E_{\gamma 2}|}{E_{\gamma 1} + E_{\gamma 2}}.$$

The η mesons will be identified from the $\gamma\gamma$ invariant mass

$$M_{\gamma\gamma} = 2\sqrt{E_{\gamma 1} E_{\gamma 2}}\,\sin\left(\frac{\psi}{2}\right)$$

while the kinetic energy E_η and the polar production angle θ_η of the η are given by the expressions:

$$E_\eta = M_\eta \sqrt{\frac{2}{(1-\cos\psi)(1-X^2)}},$$

$$\cos\theta_\eta = \frac{E_{\gamma 1}\cos\theta_{\gamma 1} + E_{\gamma 2}\cos\theta_{\gamma 2}}{\sqrt{E_{\gamma 1}^2 + E_{\gamma 2}^2 + 2\,E_{\gamma 1}E_{\gamma 2}\cos\psi}}.$$

2.4 Acceptance

Since the 2γ decay mode will be used to detect the η mesons, the only detector components of the CLAS involved in the measurements are the shower calorimeters. Monte Carlo calculations were performed to determine the CLAS acceptance for these events. In the calculations discussed here we have assumed that the shower counter coverage will be from 8° to 45° in six sectors, with two additional calorimeter modules extending the coverage from 45° to 75° in two opposite sectors. We will consider the advantages of additional shower counter coverage in a later section.

Shown in Fig. 12 is the η momentum versus laboratory angle for events accepted by CLAS from a uniform distribution. The detection efficiency as a function of η production angle at P_η = 1.0 GeV/c and as a function of η momentum at θ_η = 0° are shown in Figs. 13 and 14, respectively. The detection efficiency peaks at about 30% at θ_η = 0° and P_η = 1.0 GeV/c, and decreases as the production angle increases or the η momentum decreases until it vanishes at about θ_η = 70° or P_η = 0.2 GeV/c.

The detection efficiency as a function of photon beam energy for photoproduction on a free proton is shown in Fig. 15. The efficiency increases from about 4% at threshold (k = 0.709 GeV) to almost 10% at k = 1.5 GeV.

2.5 Momentum Resolution

We have investigated the η momentum resolution expected in this experiment. This was done with Monte Carlo calculations which take into account the expected energy and angular resolutions of the calorimeters. The momentum resolution for 1-GeV η mesons is found to be approximately 6% (σ_P/P). A cut on the asymmetry parameter $X < 0.3$ improves the resolution to about 4% at the expense of 47% of the events.

2.6 Particle Identification

Monte Carlo calculations were also performed to investigate the particle identification which can be achieved with the CLAS. A simulated mass spectrum calculated for two coincident photons from photoproduction on a free proton at an incident energy of 1.2 GeV is shown in Fig. 16. The π^0 and η peaks are clearly discernible above the background which is shown as the dashed histogram in the figure. The main contribution to the background is from the detection of two coincident photons from different π^0s produced in the $\gamma N \rightarrow \pi^0\pi^0 N$ reaction. Other contributions to the background are from the detection of two coincident photons from different π^0s from the $3\pi^0$ decay of the η (≈32%), and from coincidences between the γ and one of the photons from the π^0 produced in the $\omega \rightarrow \pi^0\gamma$ decay (≈9%). The ω decay produces the background at large mass. The background has been suppressed in the mass spectrum displayed in Fig. 16 by excluding events in which more than two photons were detected in coincidence. The different processes contributing to the mass spectrum were weighted according to the cross sections [1] and branching ratios [32].

Two simulated mass distributions with different cuts to suppress the background are compared at incident photon energies of 0.8, 1.0, 1.2, and 1.4 GeV in Figs. 17, 18, 19, and 20, respectively. The upper panel of each figure shows a mass spectrum generated with a simple static cut on the opening angle between the two detected photons. The distribution in the lower panel of each figure was produced with the additional condition that only two photons are accepted. It can be seen from the figures that the two cuts together are quite effective at reducing the background at

all four energies. However, discriminating against events with more than two photons in coincidence may bias the data by excluding processes such as $\gamma N \rightarrow \eta\pi^0 N$. We will be able to check this by analyzing both distributions. Also, it should be pointed out that a dynamical opening angle cut can be applied to the data in the off-line analysis which should help to further suppress the background. The contributions to the background at large mass are not present in the spectra at incident photon energies of 0.8 and 1.0 GeV since the ω threshold is at 1.11 GeV.

2.7 Count Rate and Beam Time Estimates

The η mesons produced with monochromatic photons of energy k will be detected at a rate given by:

$$R(k) = \frac{N_A}{A} \cdot \sigma(k) \cdot N_\gamma(k) \cdot (\rho t) \cdot \varepsilon(k) \cdot BR$$

where N_A is Avogadro's number (6.022×10^{23}), A is the mass number of the nucleus, $\sigma(k)$ is the η photoproduction cross section, N_γ is the number of incident photons per second, (ρt) is the target thickness, $\varepsilon(k)$ is the detection efficiency, and BR is the branching ratio for the 2γ decay of the η (0.39).

In estimating the count rates, we have assumed a total tagged photon flux of 10^7 photons/s with an energy distribution which decreases as 1/k. Using energy bins of approximately 100 MeV results in seven energy bins going from 0.8 to 1.5 GeV for the 1.6-GeV incident electron energy. With these assumptions we arrive at about 1.9×10^6 photons/s in the 0.8-0.9-GeV bin and 1.1×10^6 photons/s in the 1.4-1.5-GeV bin.

The elementary η photoproduction cross section decreases from approximately 15 μb at 0.8 GeV to 1.2 μb at 1.5 GeV [1], and we have assumed that the total cross section scales as $A^{0.8}$. The results of our simulations shown in Fig. 15 indicate that the detection efficiency increases from about 4% at 0.8 GeV to 9% at 1.5 GeV. Also, we have assumed a target thickness of 1 gm/cm^2 for each of the targets.

Listed in Table 1 are the rates for the 0.8-0.9-GeV and 1.4-1.5-GeV energy bins for each of the targets calculated with the above assumptions. The counting rates decrease by a factor of about 10 as the photon energy is increased from 0.8 GeV to 1.5 GeV. At the calculated rates for the deuterium target, we would detect more than 4.1×10^5 η's at 0.8-0.9 GeV and 4.3×10^4 η's at

1.4-1.5 GeV in the 500 hours previously approved for running on this target [30]. In the 150 hours previously approved for each of the ^{3}He, ^{4}He, and ^{12}C targets [31], we will obtain a maximum of 120,000 (γ,η) counts at 0.8-0.9 GeV on ^{3}He and a minimum of 9200 at 1.4-1.5 GeV on ^{12}C. We request an additional 150 hours on each of the ^{58}Ni and ^{208}Pb targets in which we will acquire approximately 65,000 (γ,η) events in the low-energy bin on ^{58}Ni and about 5200 counts in the high-energy bin on ^{208}Pb.

2.8 Triggering

Since the η mesons will be detected via the 2γ decay mode, a neutral trigger will be needed for this experiment. The minimum opening angle between the two photons from the decay of η mesons in this experiment is 45°. Therefore, the two photons from an η decay will never hit the same calorimeter module, and neutral hits in two different modules can be used as the trigger in this experiment. It is worth pointing out here that this trigger will serve to suppress much of the background from π^0 events since the decay photons from these neutral mesons have much smaller opening angles.

The two other experiments [30,31] with which this one might run concurrently both request a single charged particle trigger. We estimate that the inclusion of this neutral trigger will increase the trigger rate by less than 10% and should have little effect on the other experiments.

2.9 Potential Future Development: Extended Shower Counter Coverage

We have investigated the effect that extended shower counter coverage would have on these measurements. The results are illustrated in Fig. 21 where the detection and background-suppression efficiencies, calculated for a photon beam energy of 1.2 GeV, are displayed as a function of the number of sectors extended from 45° to 75°. The detection efficiency (solid curve) increases from about 4% to 20% as the number of sectors extended to 75° increases from 0 to 6, while the background-suppression efficiency (dashed curve) increases from 47% to 73%.

3. Intranuclear Monte Carlo Calculations

We have performed intranuclear Monte Carlo calculations to predict the sensitivity of the differential cross sections to the ηN interactions. In these calculations, the η is created in a

quasifree production process, and the subsequent interaction of the η with the nuclear system is treated by a Monte Carlo calculation which follows the η through the nucleus. The momentum distribution of the bound nucleons is described by a density-dependent Fermi gas with a density distribution taken from electron scattering. The total η photoproduction cross section is taken from a parametrization of experimental data, and is assumed to be the same for production on the proton and neutron. The total scattering ($\eta N \rightarrow \eta N$) cross section is assumed to be 15 mb. The total absorption cross section is taken from a calculation by Bennhold and Tanabe [13].

The main features of the results of these calculations for inclusive η photoproduction are illustrated in Fig. 22 which shows η momentum distributions produced on ^{208}Pb by 1.2-GeV photons at 30 to 40° in the laboratory under various physical effects. Without final-state interactions the momentum distribution (dotted histogram) is dominated by the quasifree peak. Scattering of the outgoing η mesons (dot-dashed histogram) reduces the height of the quasielastic peak considerably and increases the yield at lower momentum. Turning on the η absorption (solid histogram) further reduces the quasifree peak and damps the scattering yield at low momentum.

The A dependence of the total cross section for inclusive η photoproduction at an incident photon energy of 1.2 GeV predicted by this model is shown in Fig. 23. The cross section scales as $A^{0.8}$. This scaling was found to be essentially independent of the incident photon energy over the range of interest in this experiment. The A dependence predicted by these calculations has a greater slope than the results of Carrasco's calculations at k = 0.8 GeV where the cross section was found to scale as $A^{0.6}$ [18]. The results reported by Carrasco are somewhat surprising when compared to the π^0 photoproduction measurements [19] where it was found that the cross section scales as $A^{0.66}$ which indicates surface production. This comparison suggests that the absorption is stronger for η mesons than for pions. However, earlier measurements of the ηN cross section with pion beams [20-24] indicate that it may be as much as a factor of two smaller than the πN cross section (see Fig. 6). Therefore, it appears that the η absorption may be overestimated in Carrasco's model.

Shown in Fig. 24 is the momentum distribution expected after 150 hours of running time on ^{12}C at k = 1.4 GeV and θ_η = 20-30°. The solid histogram shows the events generated with an intranuclear Monte Carlo calculation and the dashed histogram represents the events accepted and reconstructed by the CLAS.

The expected sensitivity of the proposed measurements to the ηN cross section is illustrated in Fig. 25. Shown in this figure is the A dependence of the ratio of the nuclear cross section per

nucleon to the deuteron cross section per nucleon calculated at k = 1.2 GeV and $0^\circ < \theta_\eta < 40^\circ$. Analyzing the data in this way will remove any dependence on the elementary production amplitudes. Also, many of the systematic errors associated with the cross section measurements will cancel. For the points shown in the figure, we have assumed that the remaining systematic uncertainty is ± 3% and the statistical uncertainties have been calculated from the count rate estimates. In the calculations shown in this figure, we have assumed that the scattering cross section σ_{scat} and the absorption cross section σ_{abs} are constant and that $\sigma_{abs}/\sigma_{scat} = 2$. Calculations were then performed for different values of $\sigma_{\eta N} = \sigma_{abs} + \sigma_{scat}$. The data points were calculated with $\sigma_{\eta N}$ = 45 mb and the solid, dashed, and dot-dashed curves show the results for $\sigma_{\eta N}$ = 0, 42, and 48 mb, respectively. It can be seen from the figure that we should be able to determine $\sigma_{\eta N}$ to about ± 3 mb.

4. Relation to Other Experiments

4.1 Experiments at CEBAF

This proposal can be thought of as an extension of two other experiments planned at CEBAF to study the photoproduction [4] and electroproduction [5] of η mesons from the proton. Indeed, the results of these experiments will be important in the analysis of our data. As pointed out earlier, a comparison of our results with those obtained on the proton will allow us to extract information on the ηN interaction and nuclear-medium modifications of the N* resonances.

We have indicated several times in the discussion of the experimental technique that the measurements proposed here are compatible with the kaon photoproduction experiments on deuterium [30] and ^{3}He, ^{4}He, and ^{12}C [31]. The only component of the experimental design which will be affected by this experiment is the trigger, as discussed above.

4.2 Experiment at MAMI

The quasifree photoproduction of η mesons from ^{2}H, ^{12}C, ^{40}Ca, ^{93}Zr, and ^{nat}Pb has recently been measured at MAMI over the photon energy range from 600 to 790 MeV [29]. The experiment proposed here will complement these measurements at MAMI and extend them to much higher energies.

5. Theoretical Support

A couple of theorists have already expressed interest in this experiment. Prof. C. Bennhold at George Washington University has done extensive work on the photoproduction of η mesons off nucleons and the coherent and incoherent production on nuclei and is interested in extending this work to the inclusive process.

Prof. J. B. Seaborn at the University of Richmond, with a background in pion photoproduction, has already assisted in the development of this proposal and will continue to work closely with the experimental group. He is currently on sabbatical leave at Mainz and has begun work on η photoproduction.

6. Future Directions

A natural extension of this proposal would be to perform similar measurements for the η' mesons to extract information on the η'-nucleon interaction. In the chiral limit of QCD, the η and η' mesons are predicted to have very different properties. One might therefore expect the behavior of these two mesons to be distinct. It has been suggested [33] that a comparison of the interactions of the ηN and η'N systems may provide a test of QCD and our understanding of these mesons. We have not investigated the feasibility of this experiment in detail, but will begin soon to do so.

References

[1] See compilation by H. Genzel, P. Joos, and W. Pfeil, *Photoproduction of Elementary Particles, Landolt-Bornstein*, New Series I/8 (Springer, New York, 1973), p. 278; compilation by R. Baldini *et al.*, *Total Cross Sections for Reactions of High Energy Particles*, New Series I/12b (Springer, New York, 1988), p. 361.

[2] S. Homma *et al.*, J. Phys. Soc. Japn. **57**, 828 (1988).

[3] S. A. Dytman *et al.*, Bull. Am. Phys. Soc. **35**, 1679 (1990).

[4] B. G. Ritchie *et al.*, CEBAF Experiment Proposal PR-91-008 (unpublished).

[5] S. A. Dytman *et al.*, CEBAF Experiment Proposal PR-89-039 (unpublished).

[6] F. Tabakin, S. A. Dytman, and A. S. Rosenthal, *Excited Baryons 1988,* (World Scientific, Singapore, 1989) p. 168.

[7] H. R. Hicks *et al.*, Phys. Rev. **D7**, 2614 (1973).

[8] M. Benmerrouche and Nimai C. Mukhopadhyay, Phys. Rev. Lett. **67**, 1070 (1991).

[9] R. P. Feynman, M. Kislinger, and F. Ravndal, Phys. Rev. **D3**, 2706 (1971).

[10] R. Koniuk and N. Isgur, Phys. Rev. **D21**, 1868 (1980).

[11] F. E. Close and Z. Li, Phys. Rev. **D42**, 2194 (1990).

[12] M. Warns *et al.*, Phys. Rev. **D42**, 2215 (1990).

[13] C. Bennhold and H. Tanabe, Nucl. Phys. **A530**, 625 (1991); Phys. Lett. **243B**, 13 (1990).

[14] L. Tiator, S. S. Kamalov, and C. Bennhold, presented at the National Conference on Physics of Few-Body and Quark-Hadronic Systems, Kharkov, Ukraine, June, 1992.

[15] R. S. Bhalerao and L. C. Liu, Phys. Rev. Lett. **54**, 865 (1985).

[16] Q. Haider and L. C. Liu, Phys. Lett. **172B**, 257 (1986).

[17] H. C. Chiang, E. Oset, and L. C. Liu, Phys. Rev. **C44**, 738 (1991).

[18] R. C. Carrasco, Mainz preprint MKPH-T-92-16 (1992).

[19] J. Arends *et al.*, Nucl. Phys. **A454**, 579 (1986).

[20] J. C. Peng, in *Production and Decay of Light Mesons*, edited by P. Fleury (World Scientific, Singapore, 1988), p. 102;

[21] O. Guisan *et al.*, Nucl. Phys. **B32**, 681 (1971).

[22] V. V. Barmin *et al.*, Sov. J. Nucl. Phys. **28**, 780 (1979).

[23] V. D. Apokin *et al.*, Sov. J. Nucl. Phys. **35**, 219 (1982).

[24] V. V. Arkhipov *et al.*, Sov. J. Nucl. Phys. **39**, 76 (1984).

[25] K.S. Kolbig and B. Margolis, Nucl. Phys. **B6**, 85 (1968).

[26] L.O. Abrahamian *et al.*, Phys. Lett. **44B**, 301 (1973).

[27] E. Chiavassa *et al.*, Z. Phys. **A342**, 107 (1992).

[28] W. Cassing *et al.*, Z. Phys. **A340**, 51 (1991).

[29] H. Stroeher, private communication.

[30] B. A. Mecking *et al.*, CEBAF Experiment Proposal PR-89-045 (unpublished).

[31] C. E. Hyde-Wright *et al.*, CEBAF Experimental Proposal PR-91-014 (unpublished).

[32] Particle Data Group, Phys. Rev. **D45**, 1 (1992).

[33] N. Isgur, private communication.

Table 1. Count rate estimates.

Target	R (0.8-0.9 GeV) [s^{-1}]	R (1.4-1.5 GeV) [s^{-1}]
^{2}H	0.23	0.024
^{3}He	0.22	0.022
^{4}He	0.20	0.021
^{12}C	0.16	0.017
^{58}Ni	0.12	0.012
^{208}Pb	0.092	0.0096

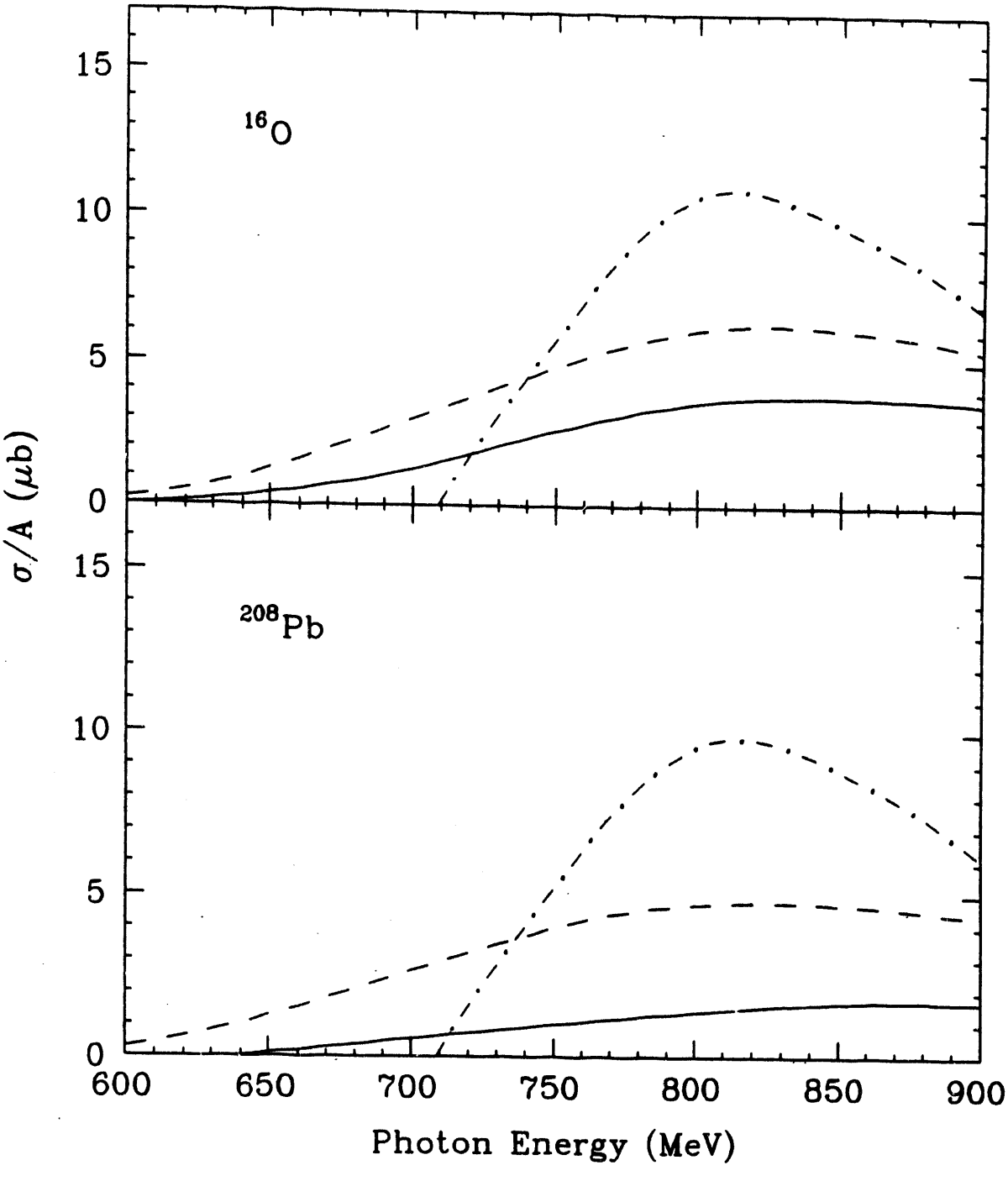

Fig. 1. Inclusive η photoproduction cross section per nucleon on ^{16}O and ^{208}Pb as a function of incident photon energy. The dot-dashed curves are the impulse approximation results. The dashed curves are the results of calculations which include Fermi sea effects and nuclear-medium modifications of the S_{11} width. The solid curves are the results of the complete calculations which also include final-state interactions. Figure reproduced from Ref. [18].

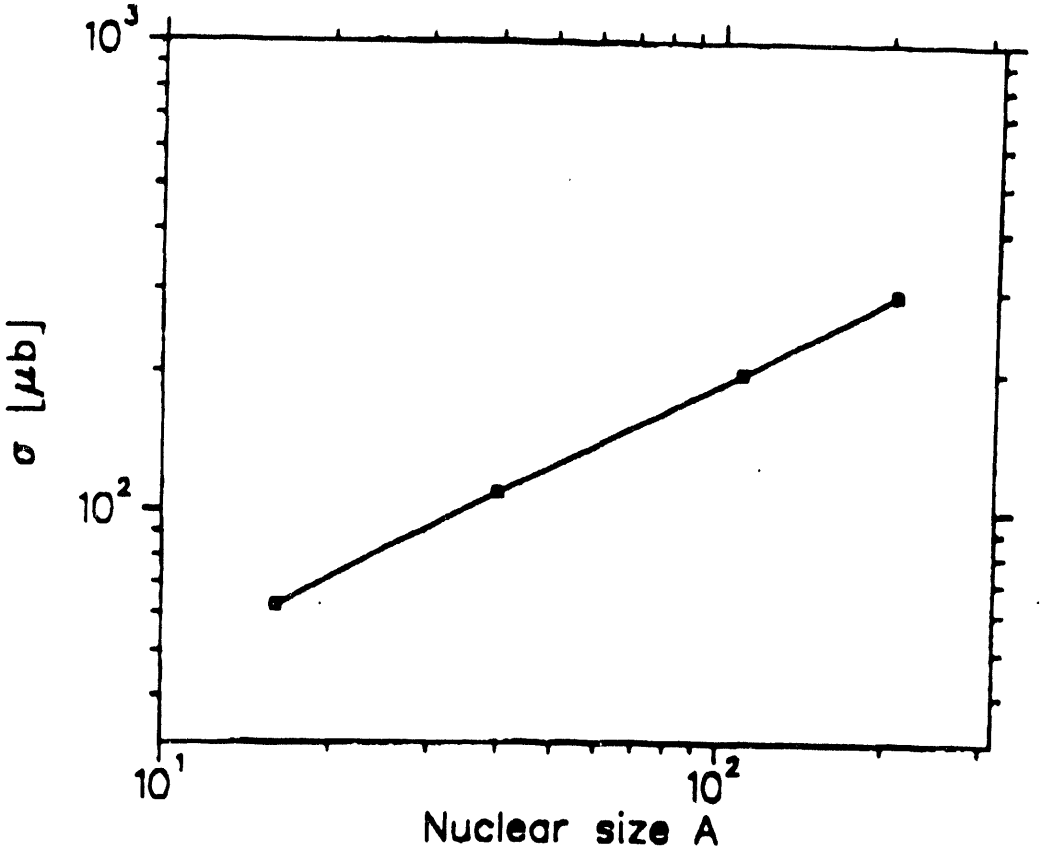

Fig. 2. Dependence of the total cross section for inclusive η photoproduction at k = 800 MeV on the nuclear mass number A. Figure taken from Ref. [18].

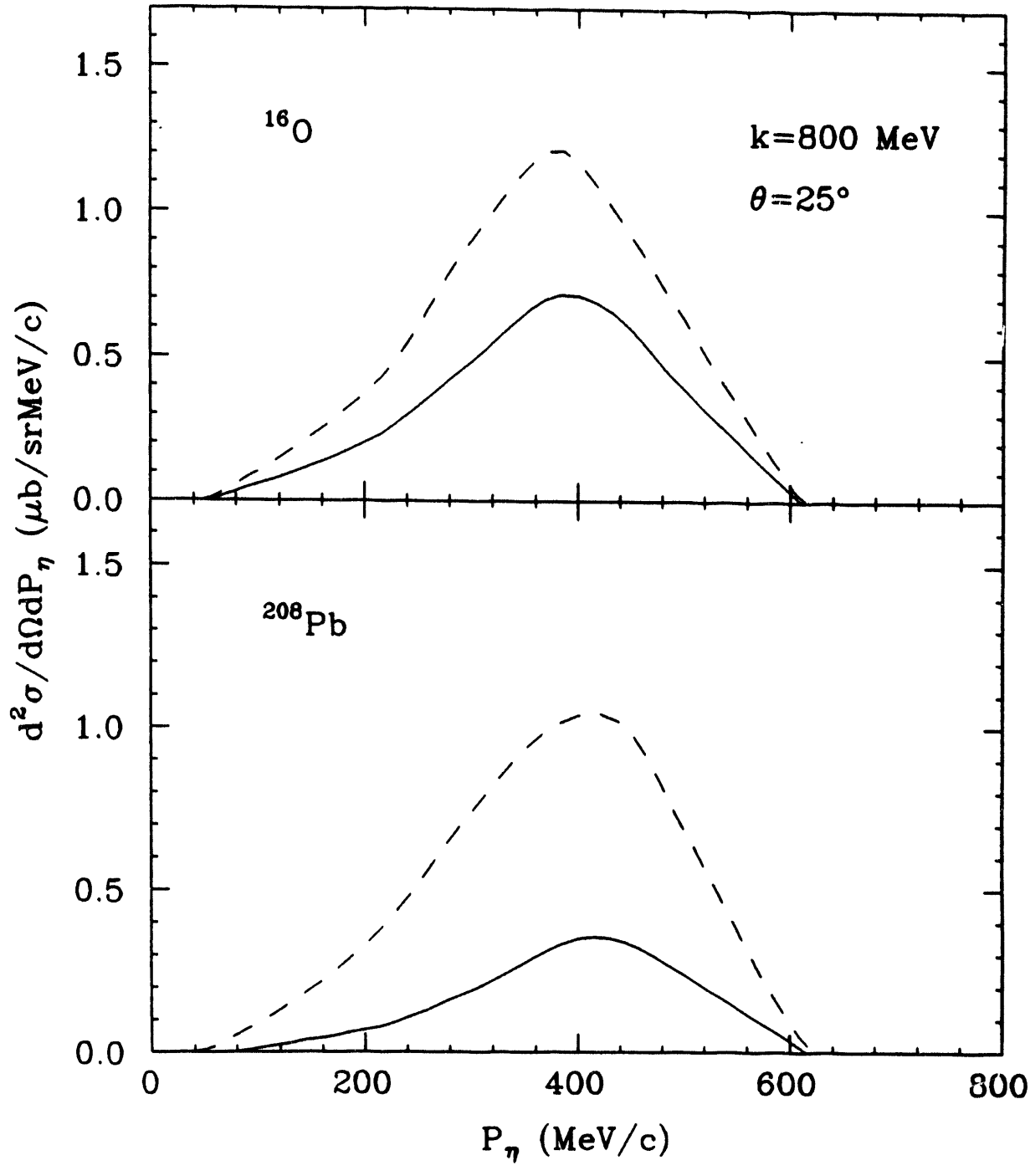

Fig. 3. Differential cross sections for the photoproduction of η mesons in ^{16}O and ^{208}Pb at a photon energy k = 800 MeV and a laboratory angle θ = 25°. The solid and dashed curves are the results of calculations with and without final-state interactions, respectively. Figure reproduced form Ref. [18].

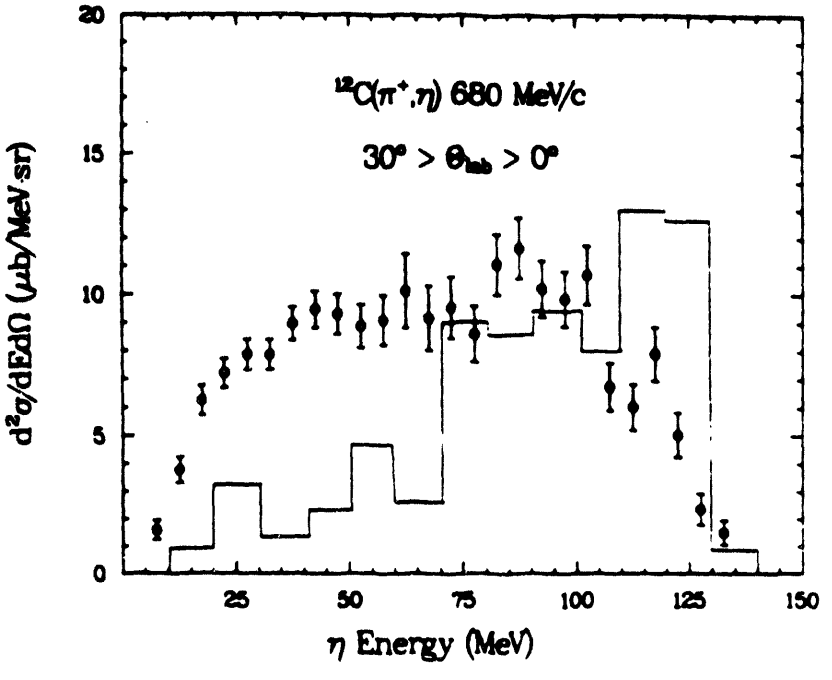

Fig. 4. Inclusive (π^+,η) energy spectrum on ^{12}C at a beam momentum of 680 MeV/c taken from Ref. [20]. The solid curve is a preliminary attempt to reproduce the spectrum.

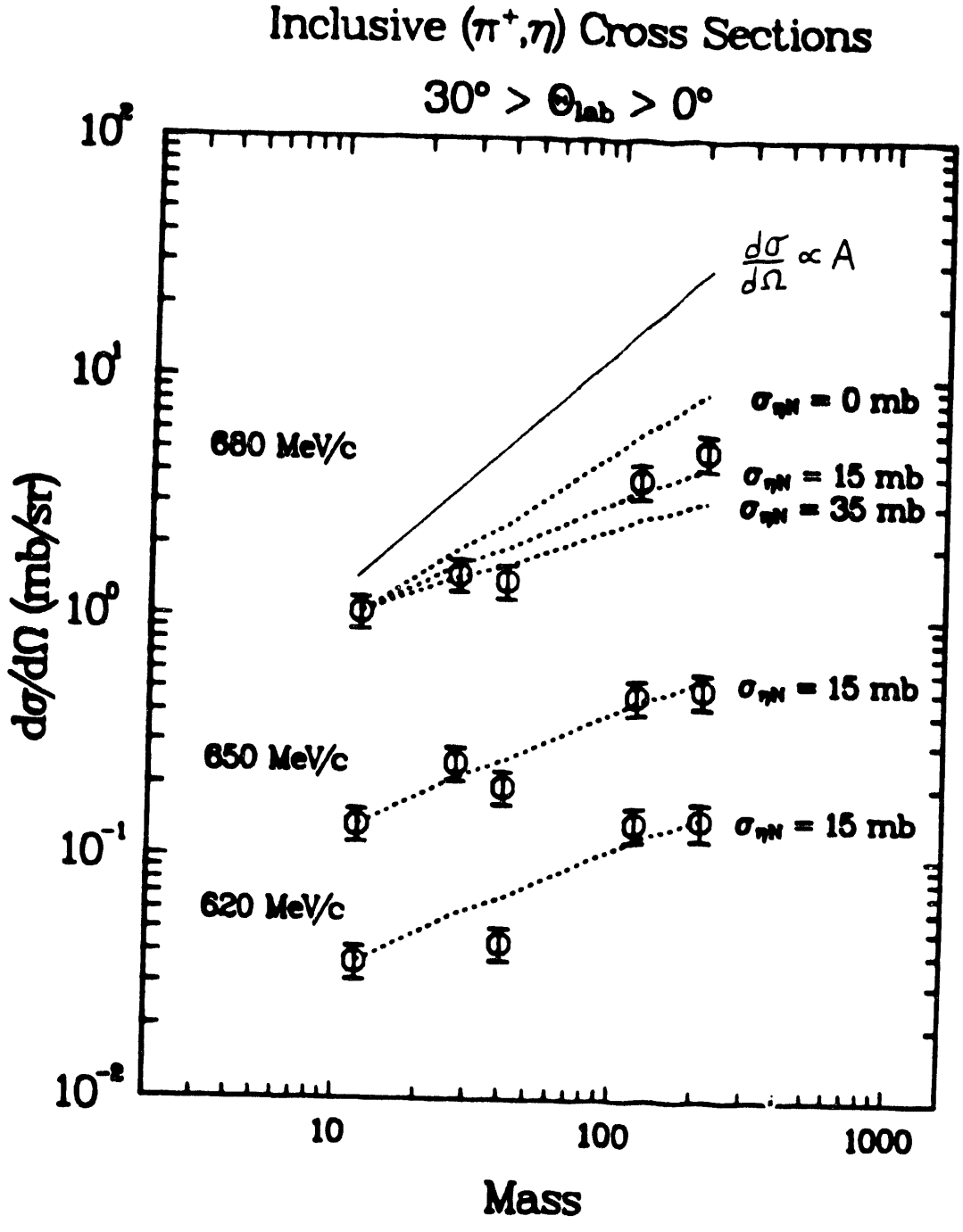

Fig. 5. Target mass dependence of inclusive (π^+,η) cross sections taken from Ref. [20]. The dashed curves are the results of Glauber calculations [25] using various ηN total cross sections. We have added the solid curve to the figure to represent the cross section without final-state or initial-state interactions.

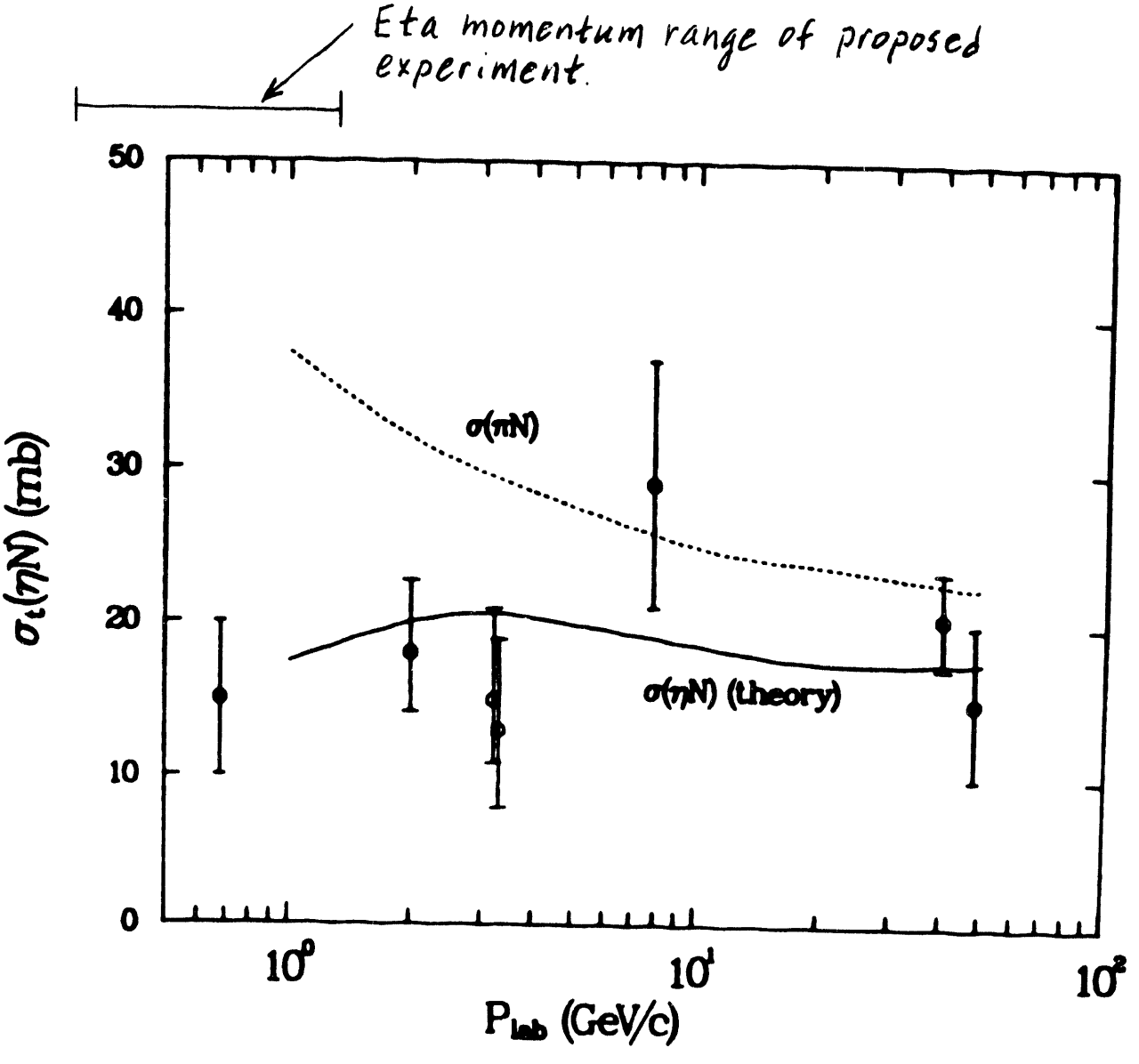

Fig. 6. Eta-nucleon total cross sections as a function of the pion beam momentum taken from Ref. [20]. The solid curve is the prediction of the additive quark model [26] for the ηN total cross sections. The πN total cross section is shown as the dashed curve for comparison. The η momentum range of the proposed experiment is indicated above the figure.

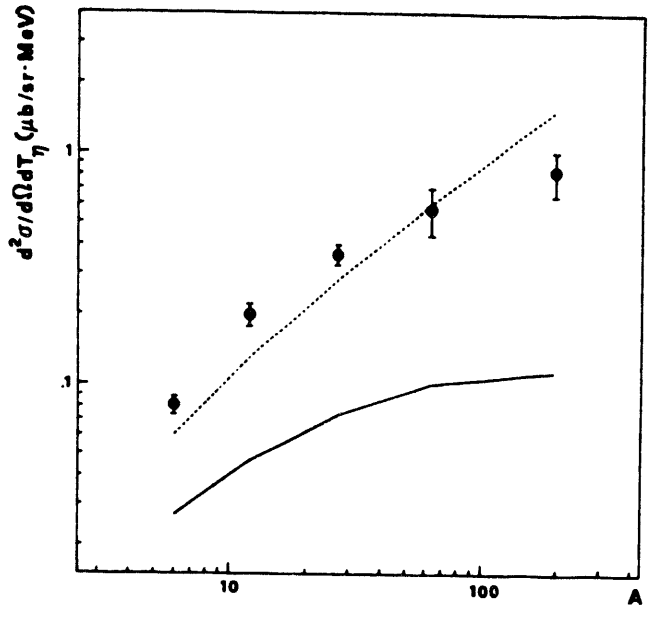

Fig. 7. Differential cross sections for the inclusive A(p,η) reaction at a proton energy of 1 GeV as a function of target mass number A, taken from Ref. [27]. The solid and dashed curves are predictions of the folding model [28] with and without η absorption, respectively.

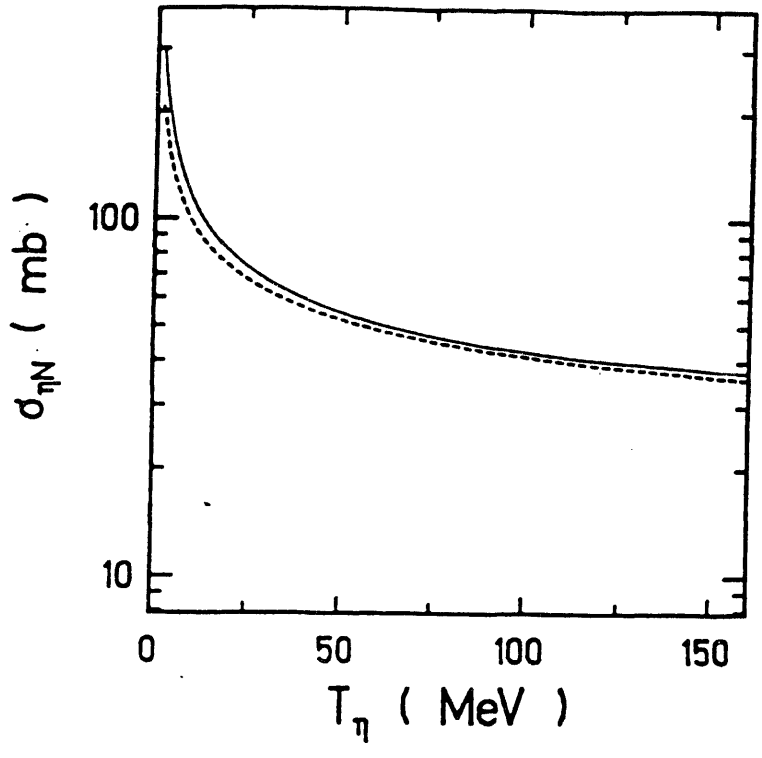

Fig. 8. The total cross section $\sigma_{\eta N}$ (solid curve) as a function of the kinetic energy of the η meson in the nucleon rest frame. The dashed curve is the result of a coupled-channel analysis of Bhalerao and Liu [15]. The figure is taken from Ref. [28].

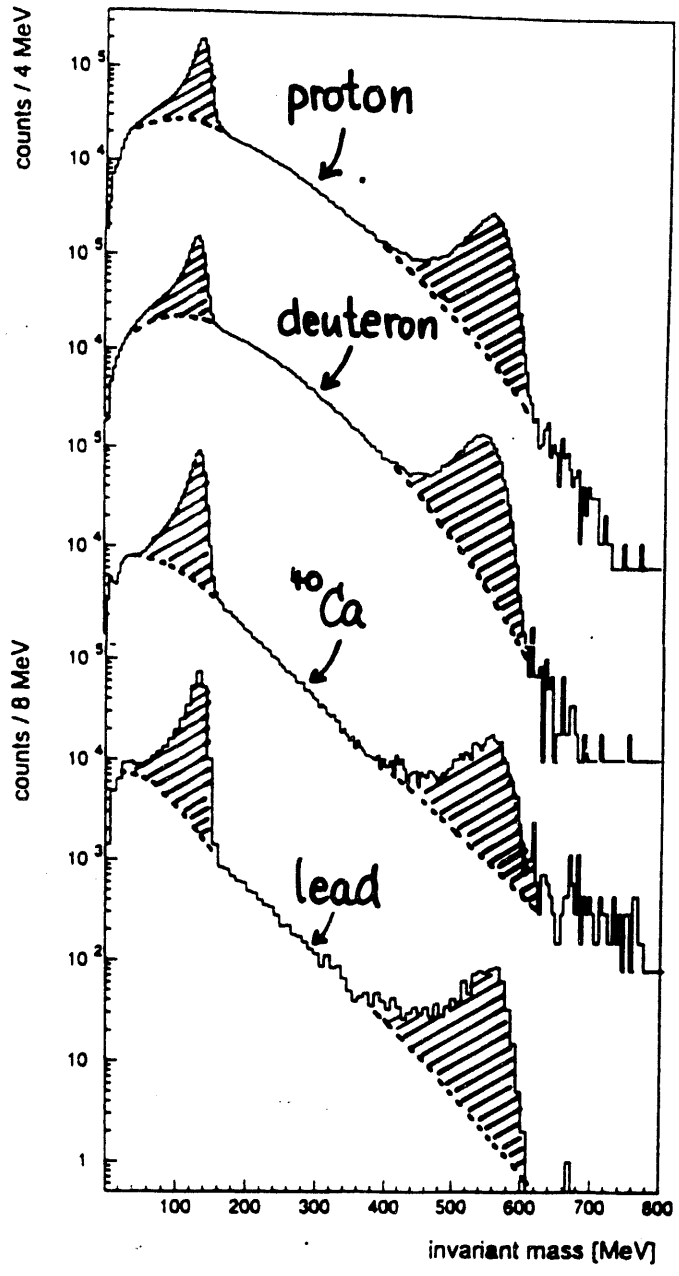

Fig. 9. Invariant mass spectra for photoproduction on ^{1}H, ^{2}H, ^{40}Ca, and ^{nat}Pb targets with incident photons in the energy range 600-790 MeV taken from Ref. [29].

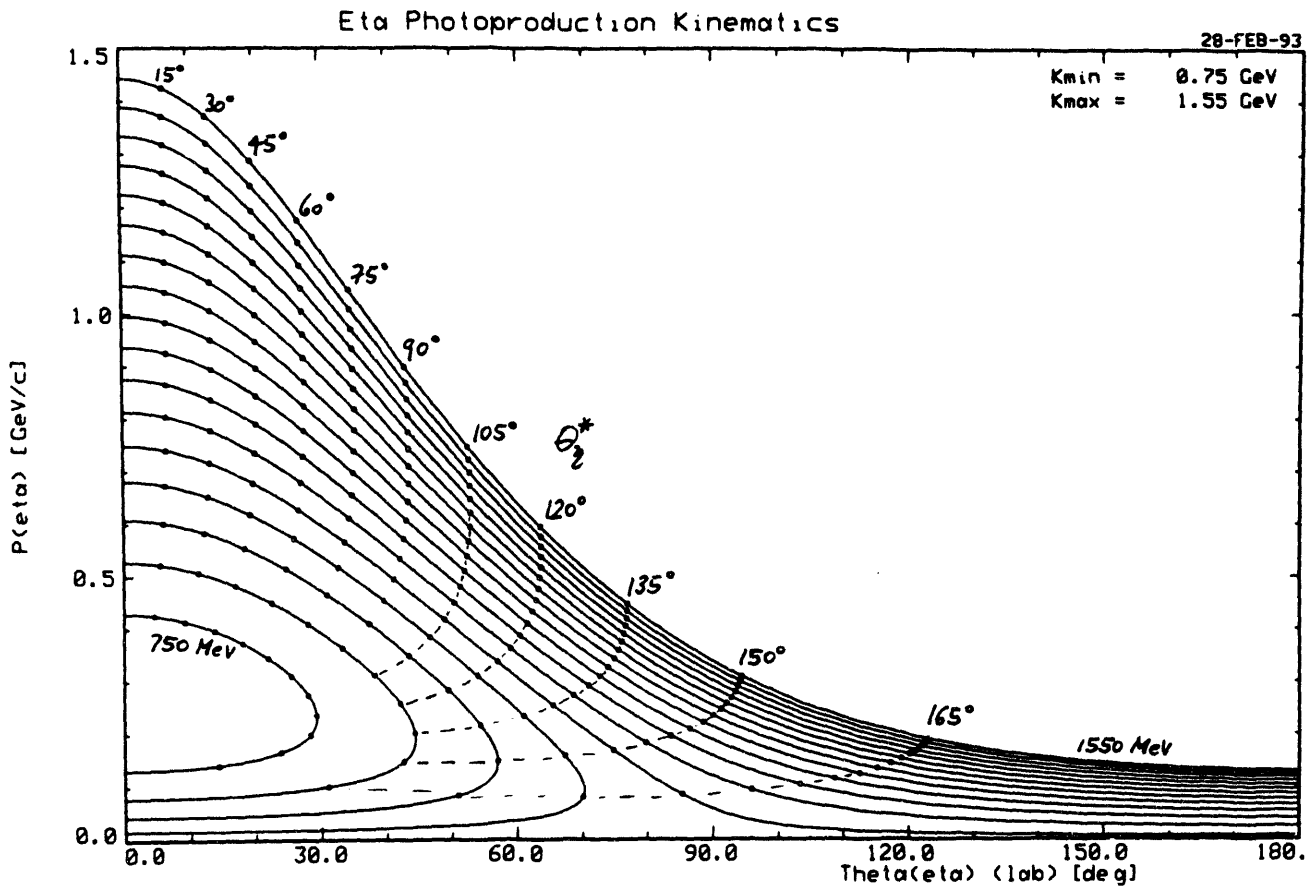

Fig. 10. Eta photoproduction kinematics for incident photon energies between 0.75 and 1.55 GeV.

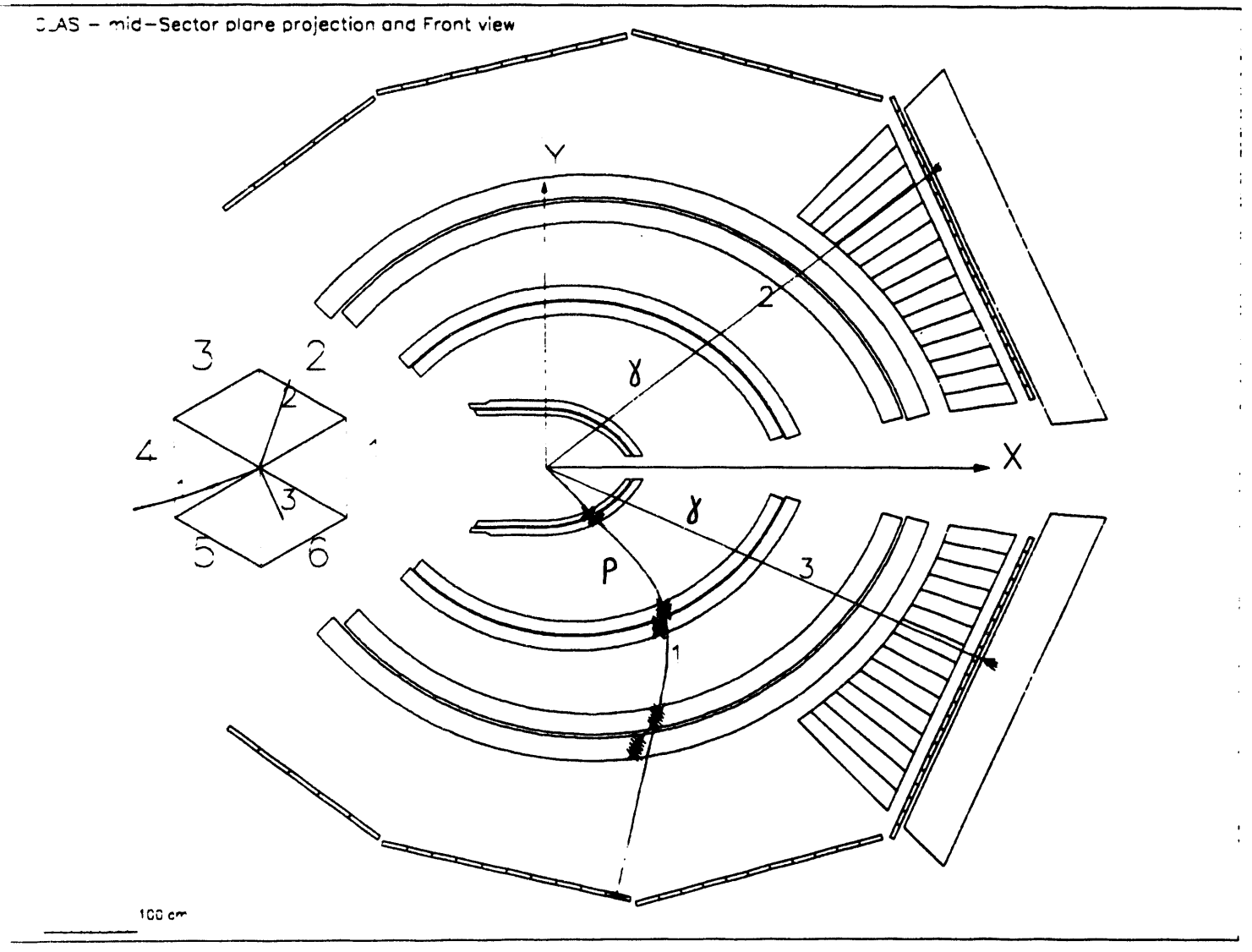

Fig. 11. A typical η photoproduction event in the CLAS. Track 1 is a proton, and tracks 2 and 3 are photons from the 2γ decay of the η meson. The incident photon energy is 1.2 GeV.

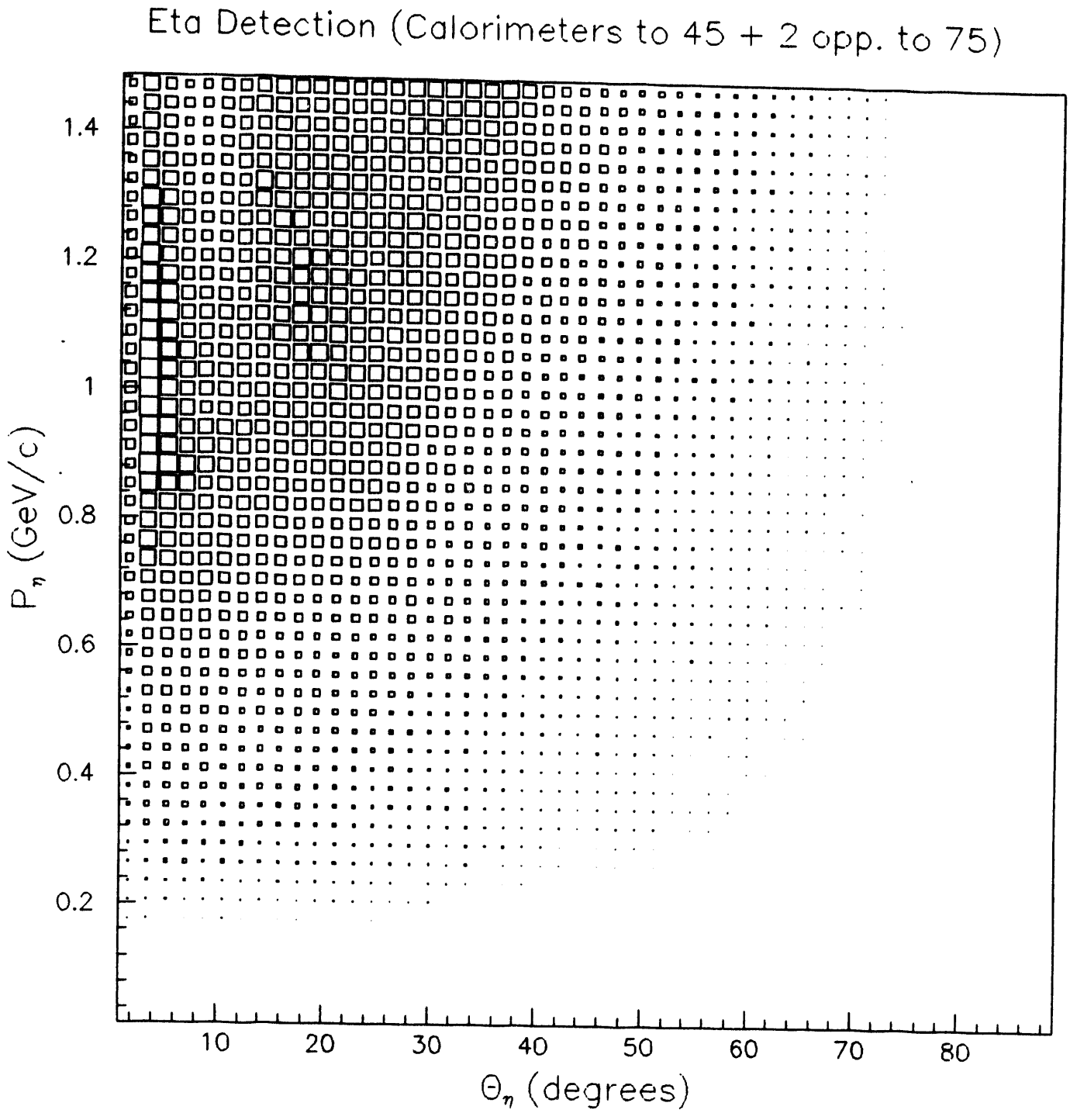

Fig. 12. Eta momentum versus laboratory angle for events accepted by CLAS from a uniform distribution in a Monte Carlo simulation assuming calorimeter coverage from 8° to 45° in six sectors with two additional 30° modules extending the coverage to 75° in two opposite sectors.

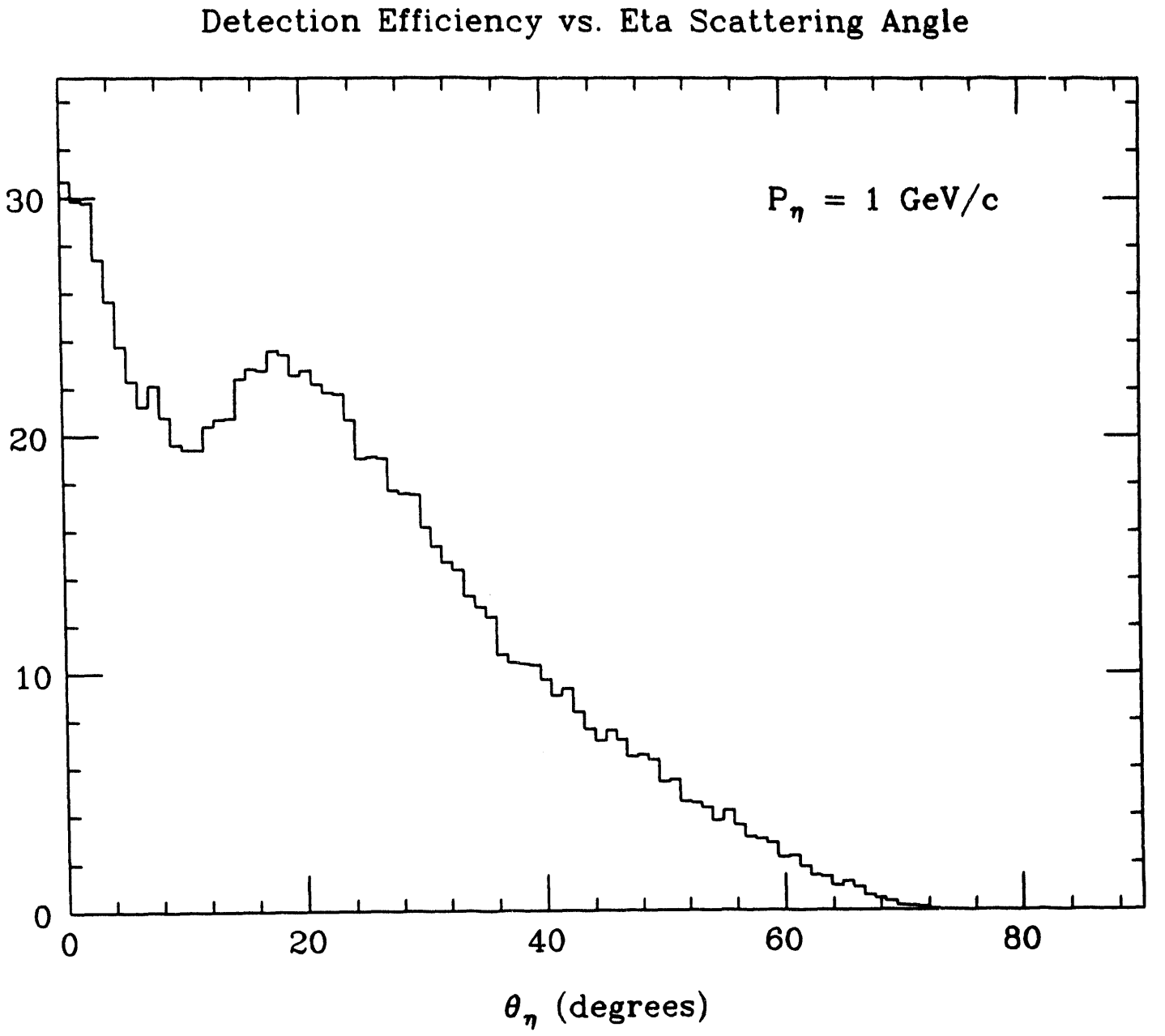

Fig. 13. Detection efficiency as a function of η laboratory angle at P_η = 1.0 GeV/c assuming calorimeter coverage from 8° to 45° in six sectors with two additional 30° modules extending the coverage to 75° in two opposite sectors.

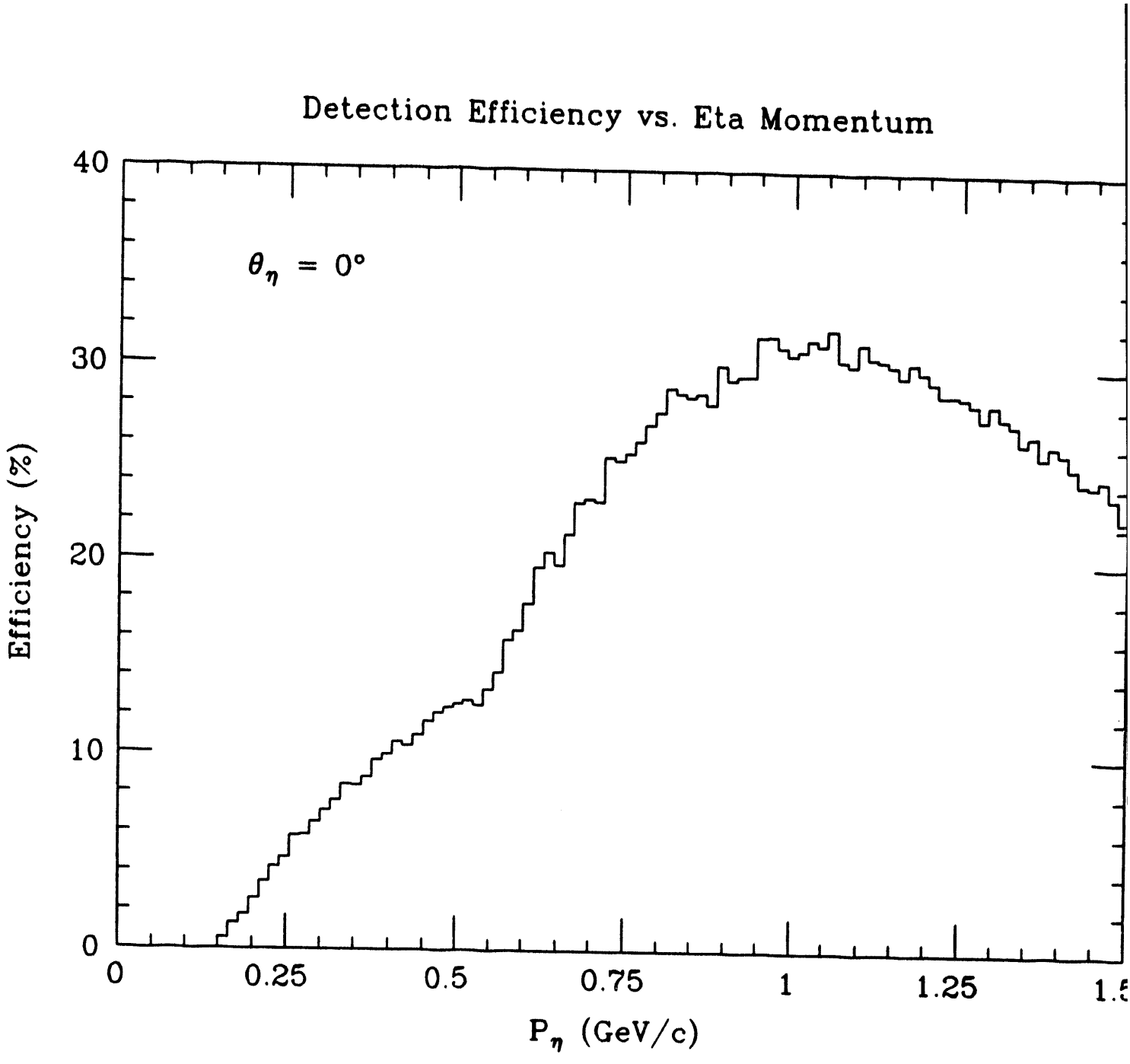

Fig. 14. Detection efficiency as a function of η momentum at $\theta_\eta = 0°$ assuming calorimeter coverage from 8° to 45° in six sectors with two additional 30° modules extending the coverage to 75° in two opposite sectors.

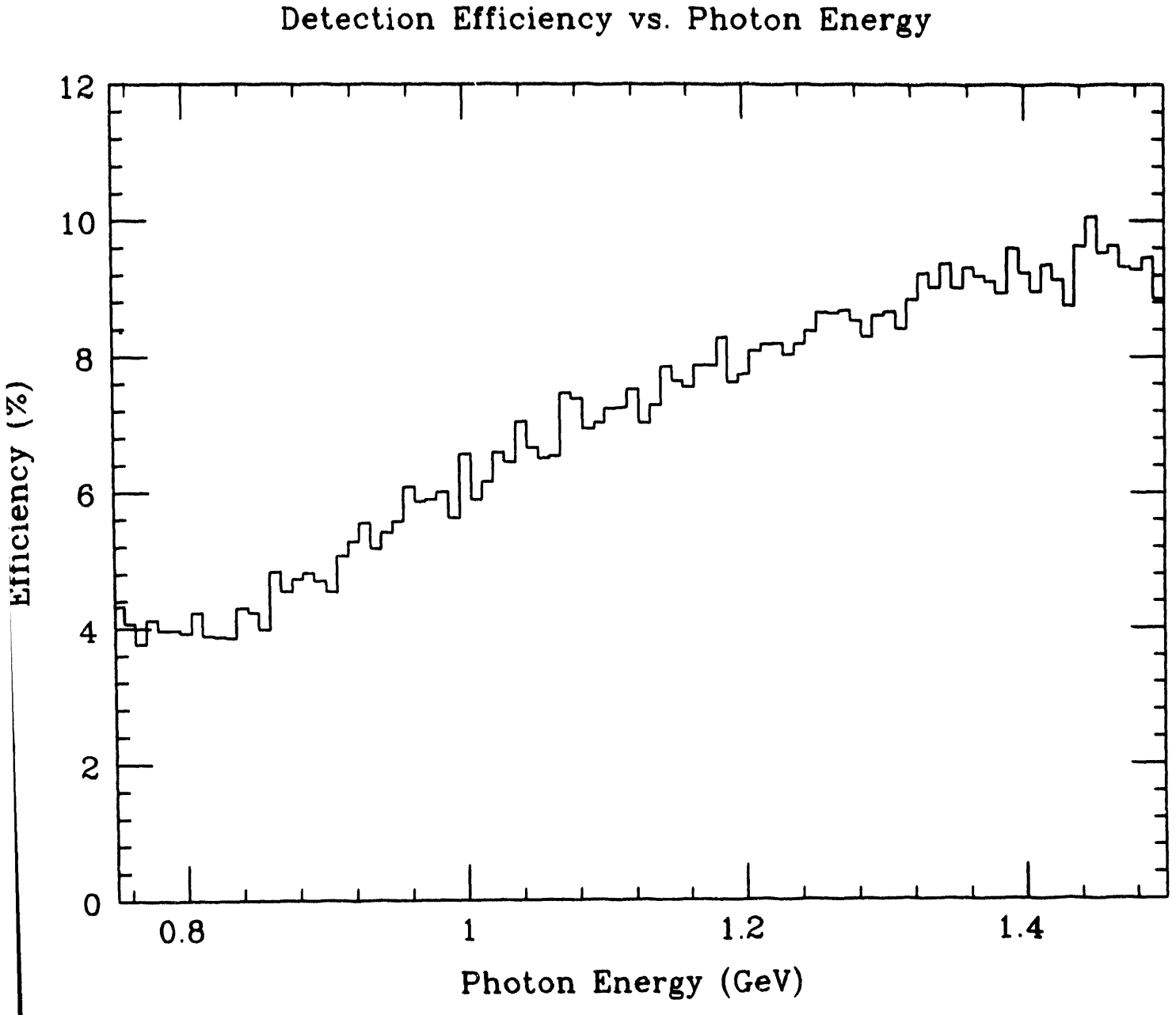

Fig. 15. Detection efficiency as a function of incident photon energy for production on the free proton assuming calorimeter coverage from 8° to 45° in six sectors with two additional 30° modules extending the coverage to 75° in two opposite sectors.

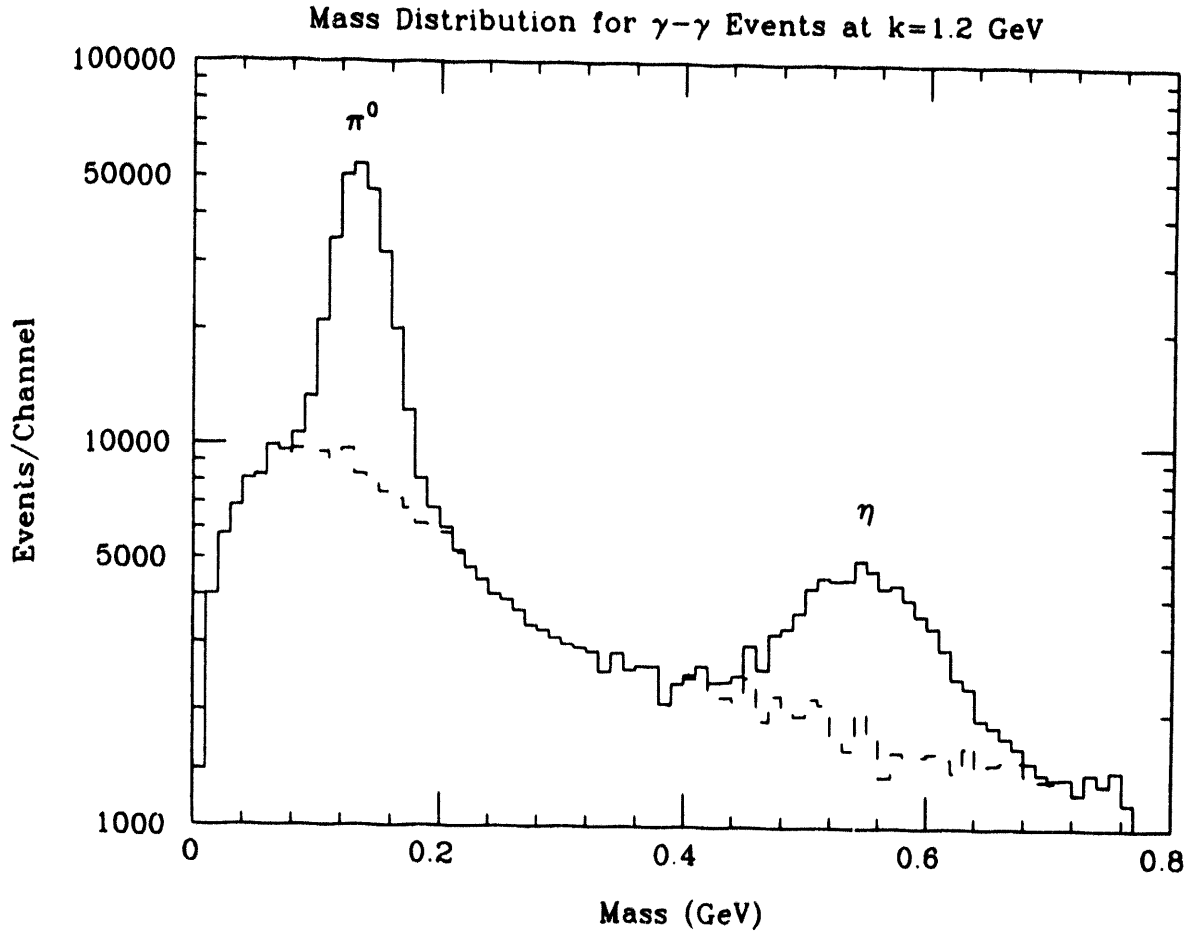

Fig. 16. Simulated mass spectrum for γ-γ events from photoproduction at k = 1.2 GeV. Most of the background (dashed histogram) is from the detection of two coincident photons from different π^0s produced in the $\gamma N \rightarrow \pi^0\pi^0 N$ reaction and the $3\pi^0$ decay of the η meson. The background at large mass is from coincidences between the γ and one of the photons produced in the $\omega \rightarrow \pi^0\gamma$ decay. The background has been suppressed by discriminating against events with more than two photons detected in coincidence.

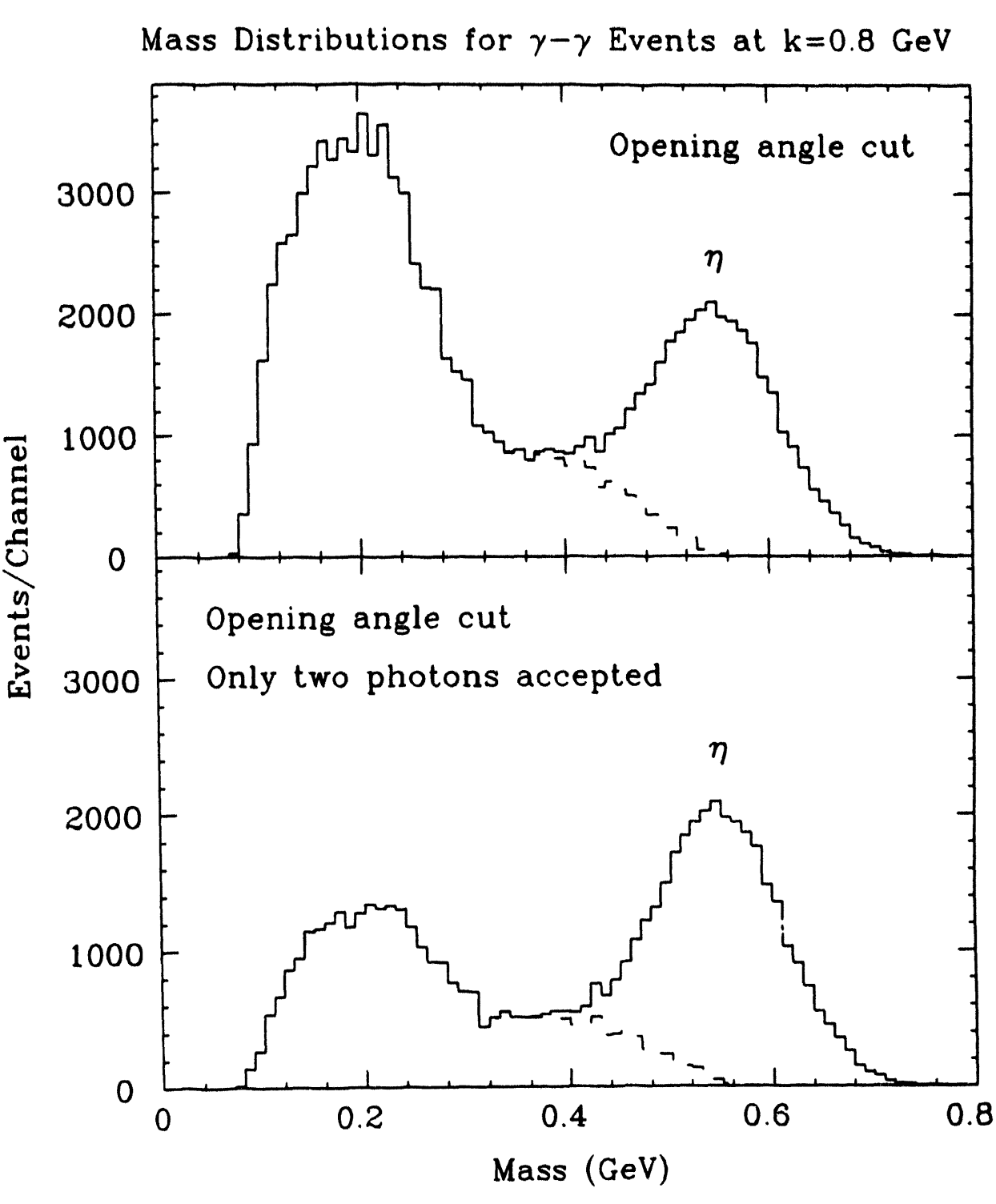

Fig. 17. Simulated mass distributions for γ-γ events from photoproduction at k = 0.8 GeV. The upper distribution was generated with a simple cut on the opening angle to suppress the background. The lower distribution was produced with the additional condition that only two photons are detected.

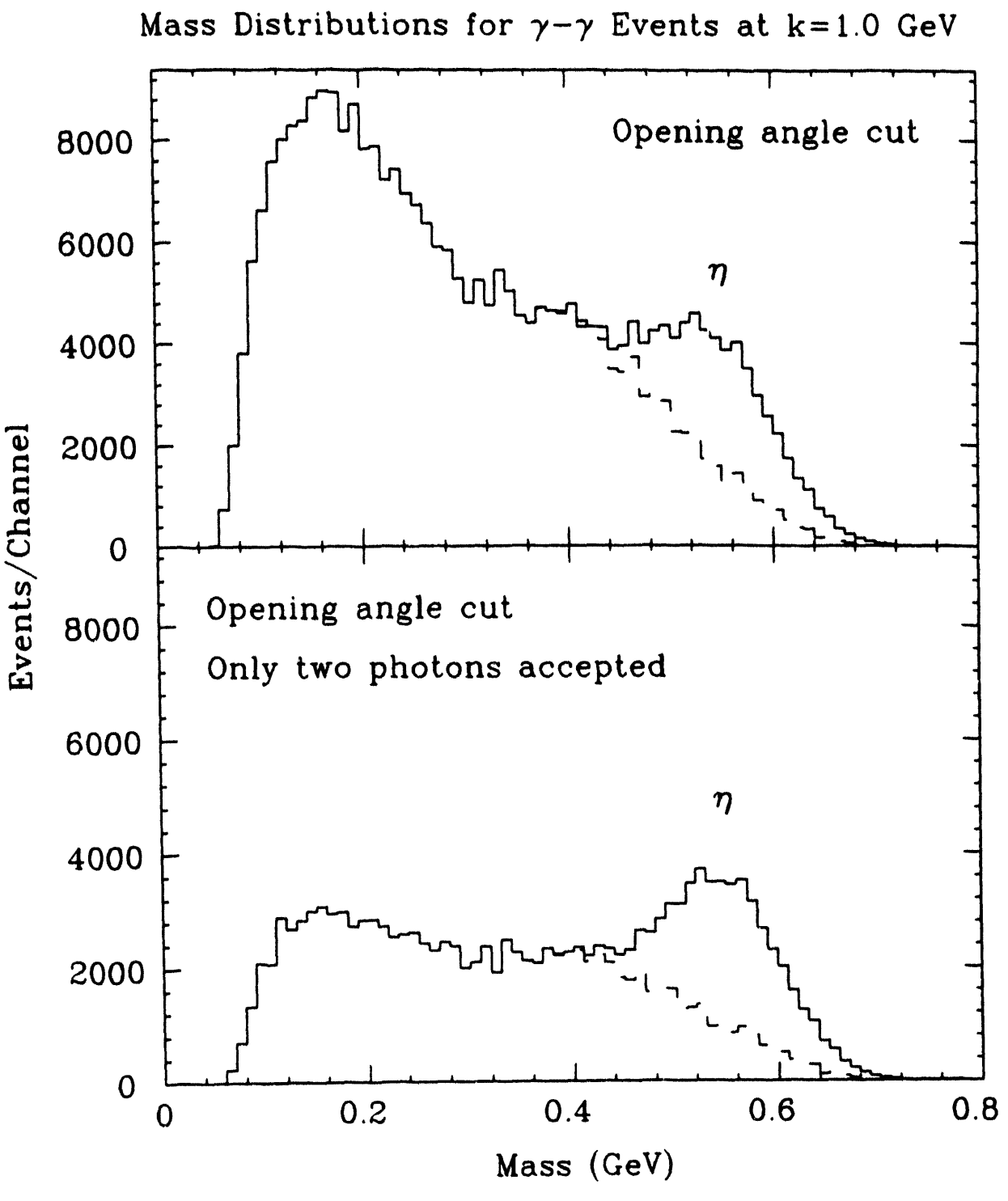

Fig. 18. Same as Fig. 17 except at k = 1.0 GeV.

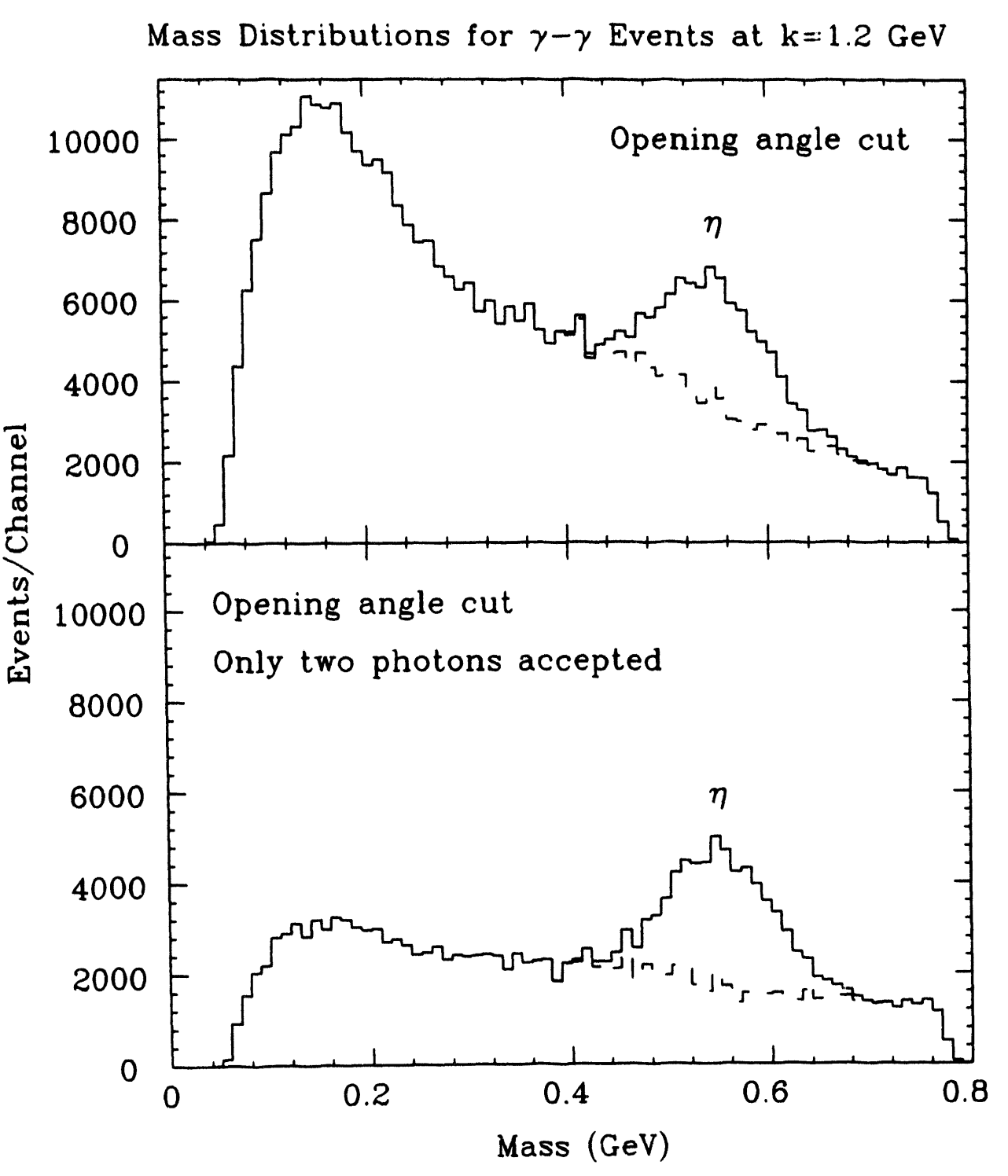

Fig. 19. Same as Fig. 17 except at k = 1.2 GeV.

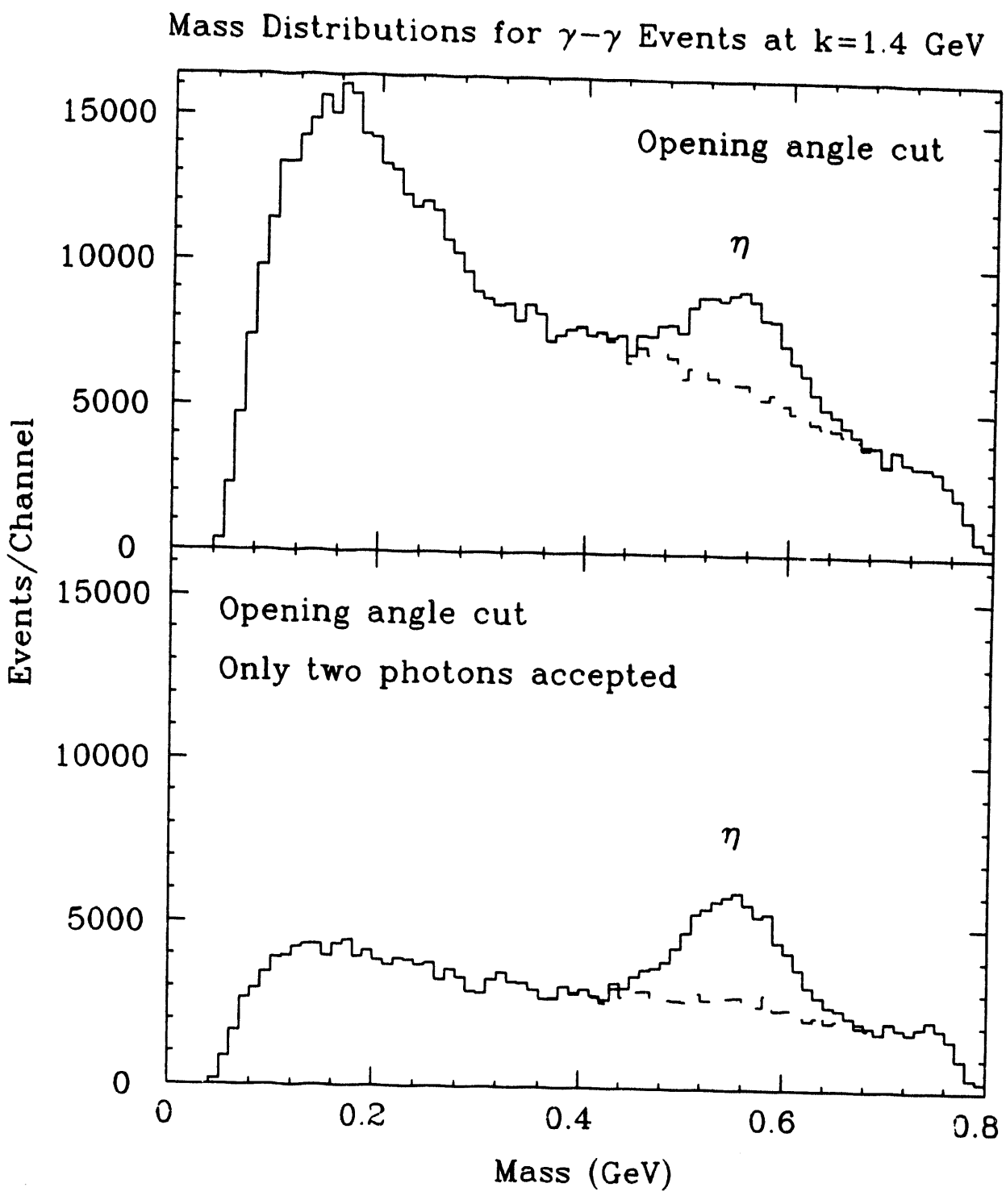

Fig. 20. Same as Fig. 17 except at k = 1.4 GeV.

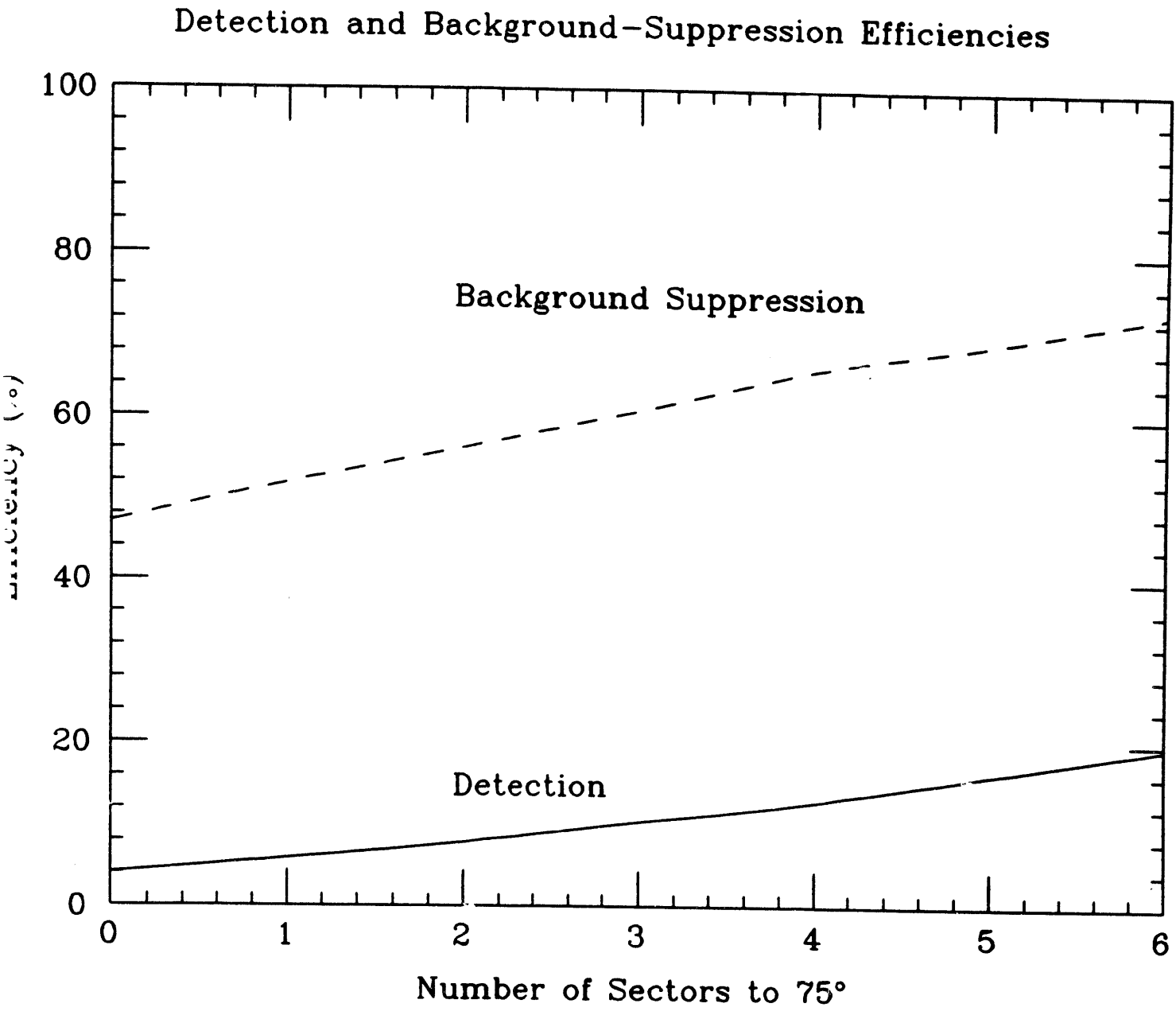

Fig. 21. Detection and background-suppression efficiencies as a function of the number of CLAS sectors with calorimeter coverage extended from 45° to 75°. The efficiencies were determined from Monte Carlo calculations for photoproduction on the free proton at k = 1.2 GeV.

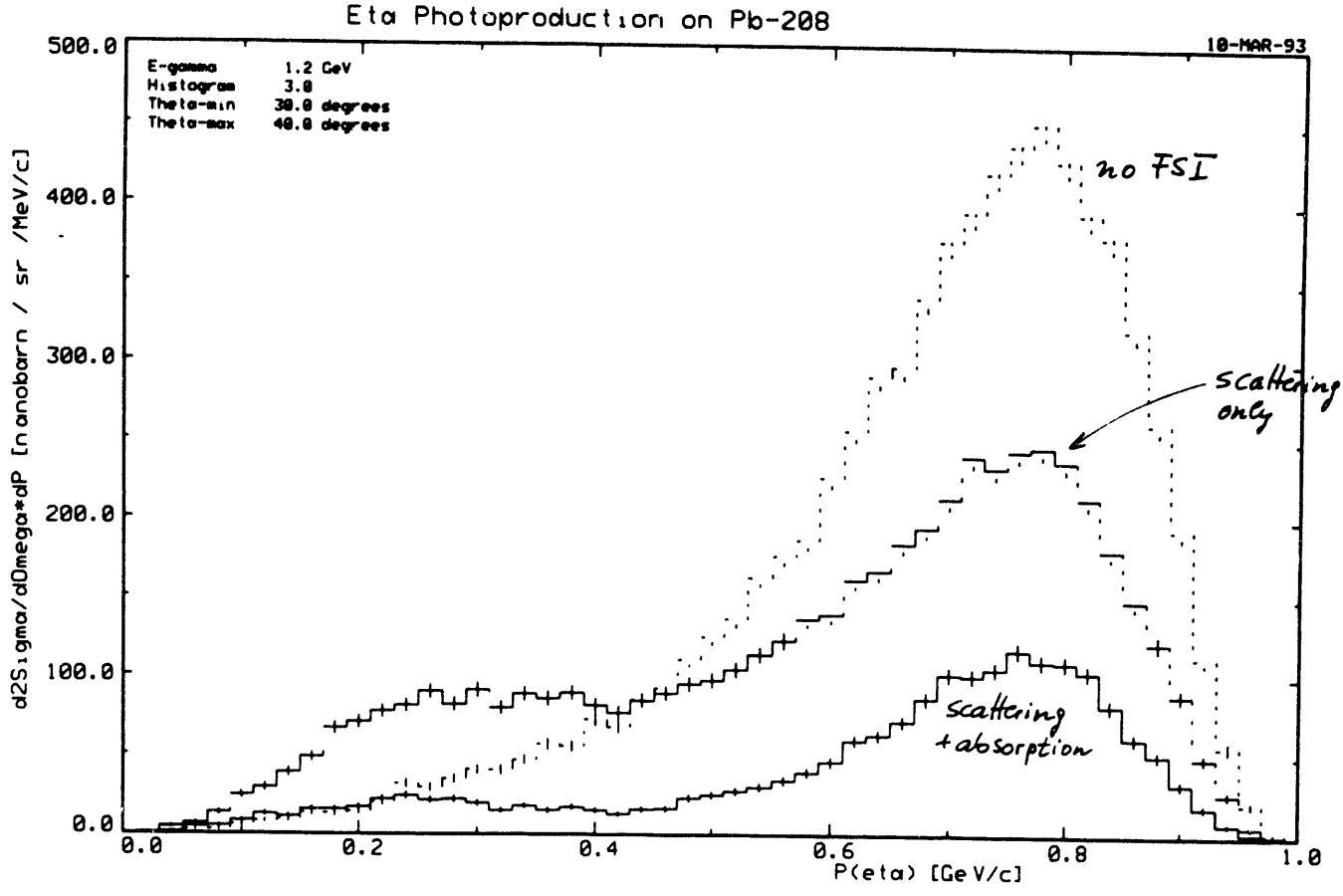

Fig. 22. Momentum distributions for η photoproduction on ^{208}Pb at k = 1.2 GeV and θ_η = 30-40° simulated with intranuclear Monte Carlo calculations. The dotted histogram represents quasifree production with no final-state interactions. The dashed histogram shows the effect of η scattering in the nucleus. The solid histogram is the expected distribution taking into account scattering and absorption.

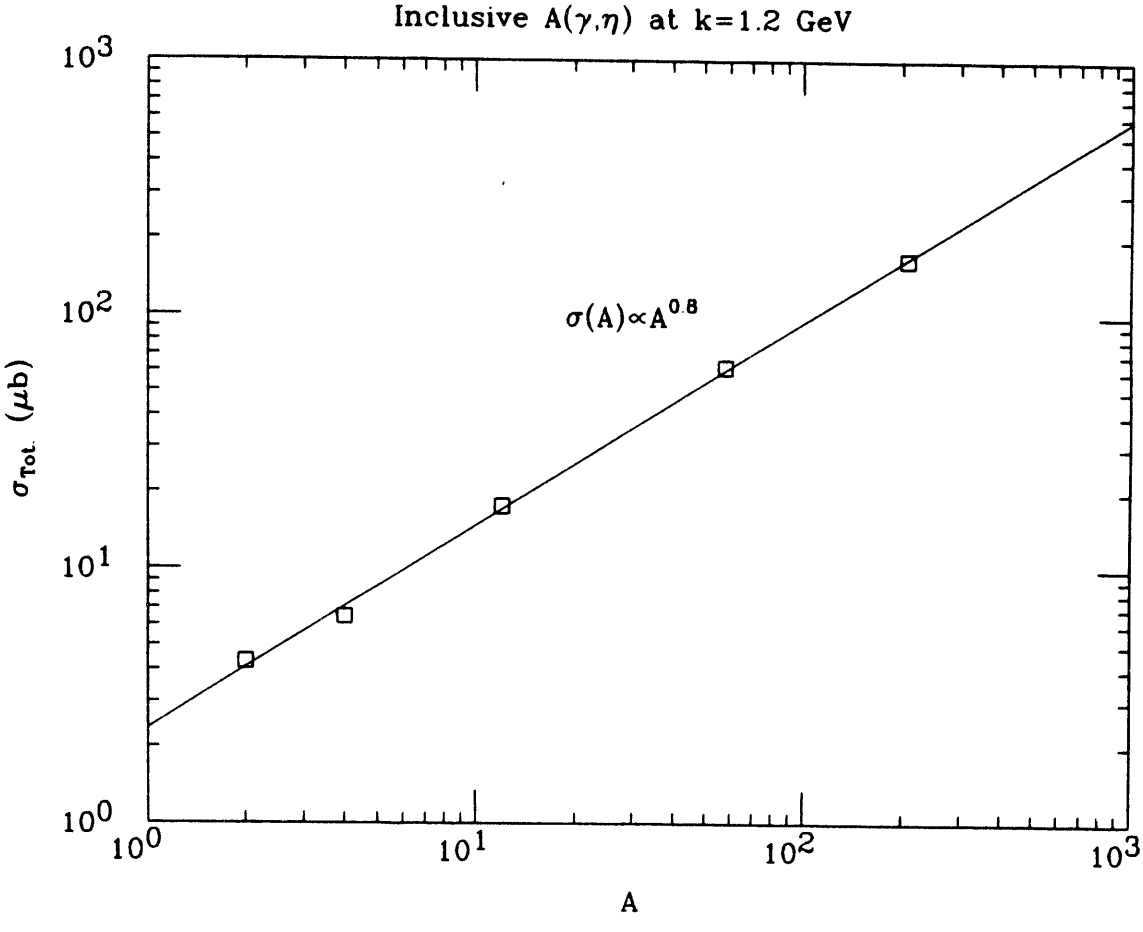

Fig. 23. The A dependence of the total η photoproduction cross sections calculated with an intranuclear Monte Carlo code at k = 1.2 GeV. The cross section scales as $A^{0.8}$.

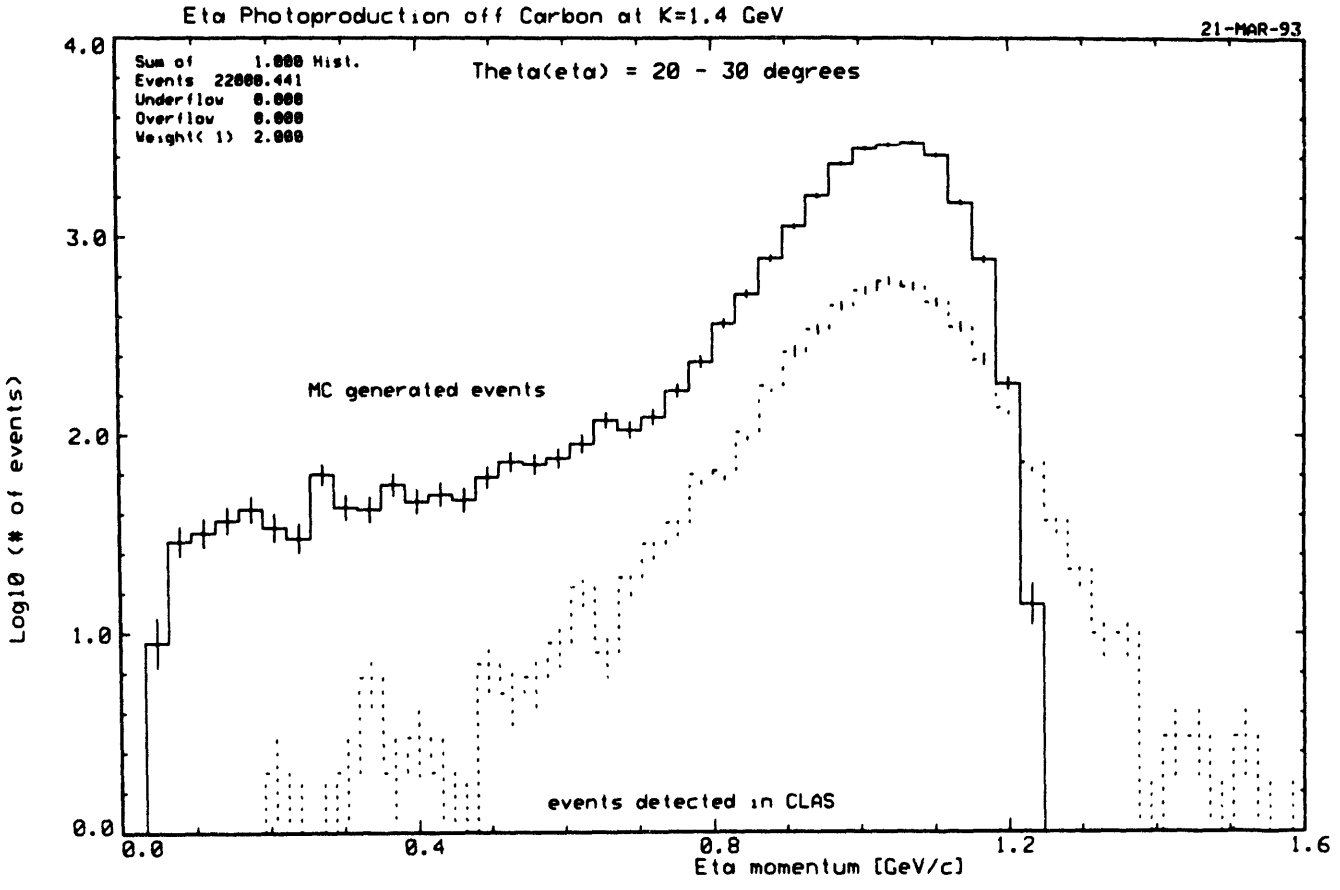

Fig. 24. Simulated momentum distributions expected after 150 hours of running time on ^{12}C at k = 1.4 GeV and θ_η = 20-30°. The solid histogram shows the events generated with an intranuclear Monte Carlo calculation. The dashed histogram represents the events accepted and reconstructed by the CLAS.

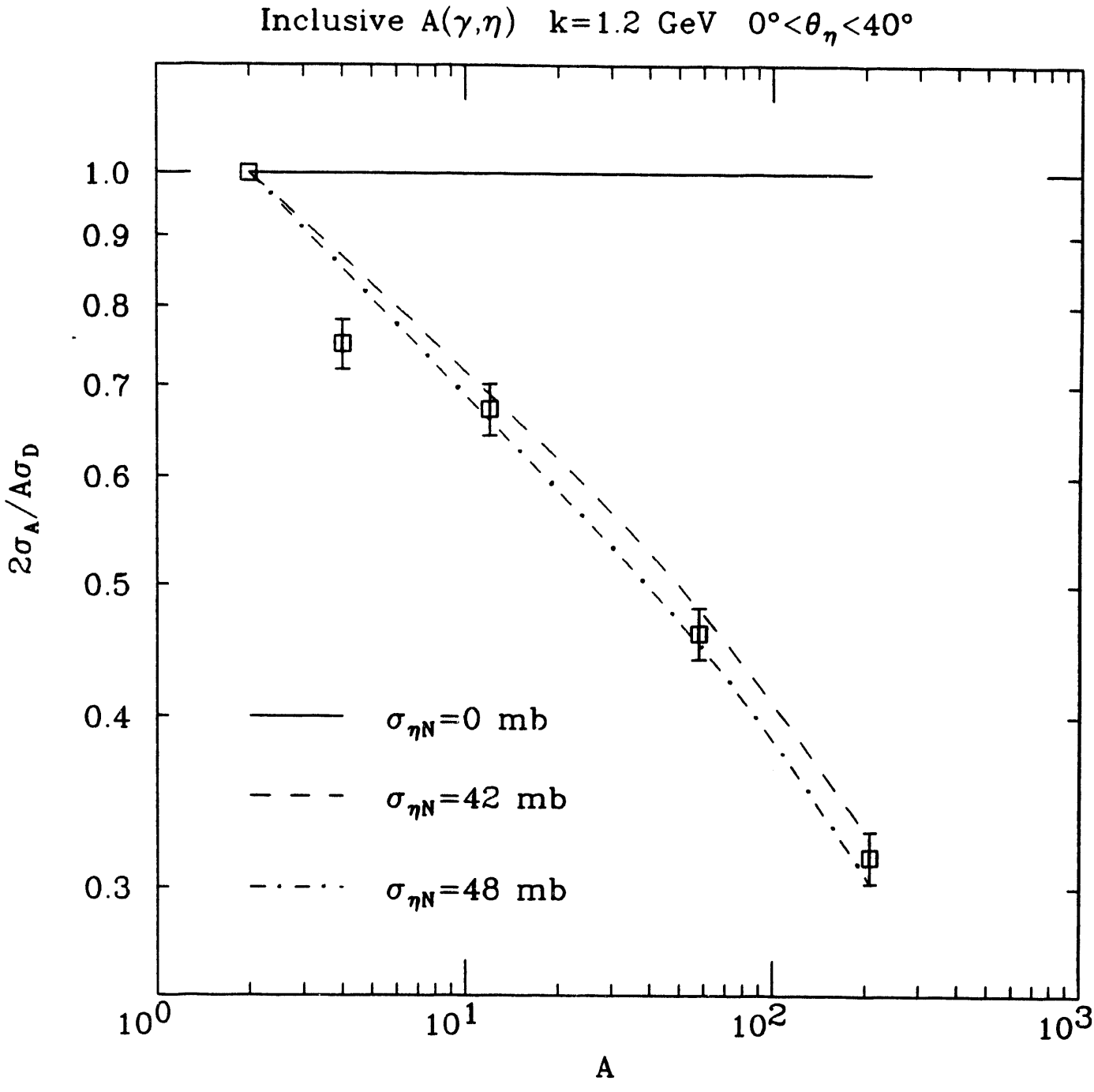

Fig. 25. The A dependence of the ratio of the nuclear cross section per nucleon to the deuteron cross section per nucleon calculated with an intranuclear Monte Carlo cascade code for inclusive η photoproduction at k = 1.2 GeV and $0° < \theta_\eta < 40°$. The solid, dashed, and dot-dashed curves show the results obtained with total ηN cross sections of 0, 42, and 48 mb, respectively.

Photoproduction of η' Mesons in Nuclei

Vineyard, McKeever, Sabloff, Gilfoyle, Major, Mecking, Rubin, and Seaborn

1. Scientific Motivation

Since the η' is a member of the pseudoscalar meson nonet, one might expect that the properties of the η' meson should be well understood within quark models as simple $q\bar{q}$ systems. However, there is significant evidence that suggests that the η' meson is not a simple $q\bar{q}$ state. As pointed out by Lenz [1], the primary problem is to understand the mass of the η'.

The η and η' mesons are usually considered to be mixed SU(3) states

$$|\eta> = \cos\theta\,|\eta_8> + \sin\theta\,|\eta_1>$$

$$|\eta'> = -\sin\theta\,|\eta_8> + \cos\theta\,|\eta_1>$$

where the quark content of the singlet and octet states are given by

$$|\eta_1> = \frac{1}{\sqrt{3}}\,|u\bar{u} + d\bar{d} + s\bar{s}>$$

$$|\eta_8> = \frac{1}{\sqrt{6}}\,|u\bar{u} + d\bar{d} - 2s\bar{s}>.$$

The mixing angle θ has been determined from the Gell-Mann-Okubo mass formula [2] to be about $-10°$. However, measurements of the $\gamma\gamma$ decay widths of the η and η' mesons yield a mixing angle of $-18.4° \pm 2°$ [3], nearly twice the value obtained from the quadratic mass formula.

Another problem has to do with the octet mass sum rule [4]. When this sum rule is applied to the η and η' masses it is violated by almost 50%. On the other hand, when the sum rule is applied to the masses of the ω and ϕ, the vector meson nonet counterparts of the pseudoscalar etas, it is satisfied to about the one percent level.

These discrepancies have led to the suggestion that there are exotic components in the η' wavefunction. The most convincing experimental evidence for this has come from a study of J/ψ decays into vector and pseudoscalar mesons [5]. In this work, measured branching ratios were fit to a simple model of J/ψ decays which was then used to calculate the strange- and nonstrange-

quark content of the η and η' mesons. The authors concluded that (35 ± 18) % of the η' wavefunction can be attributed to an additional component. Other theoretical investigations have come to similar conclusions about gluonium admixtures in the η-η' system [6,7].

It has been suggested [1,8] that this problem with the η' is connected to fundamental properties of the strong interaction, and that a comparison of the interaction parameters of the η'N system with those of the other members of the pseudoscalar nonet, in particular the η, is important to search for signals of this unusual structure. WE plan to use the CLAS to measure differential cross sections for the (γ,η') reaction on ^{2}H, ^{12}C, ^{58}Ni, and ^{208}Pb at photon energies beween 1.45 and 2.25 GeV. The η' momentum distributions and the target mass dependence of the cross section will provide information on the η'N interaction. These measurements will complement the (γ,η) experiments [9] to be performed at CEBAF and a comparison of the two data sets should shed some light on the η' puzzle.

2. Experimental Procedure

2.1 Beam

The reactions will be induced with tagged photons produced with the Hall B bremsstrahlung tagging system. Using an incident electron energy of 2.4 GeV, the tagged photons will have an energy range of 1.45 to 2.25 GeV. The threshold for η' photoproduction on a free proton is 1.44 GeV. For the counting rate estimates, the tagged photon rate has been assumed to be 10^7 photons/s.

2.2 Acceptance

The η' mesons will be detected with the CLAS via the $\eta' \rightarrow \rho^0\gamma \rightarrow \pi^+\pi^-\gamma$ decay (branching ratio ≈ 20%). A typical event is shown in Fig. 1. Tracks 1, 2, and 3 are the photon, π^+, and π^-, respectively, from the decay of the η', and track 4 is the recoil proton.

Monte Carlo calculations were performed to determine the CLAS acceptance for these events.

In the calculations discussed here we have assumed that the magnet will be at one-half the full operating field and that the shower counter coverage will be from 8° to 45° in six sectors, with two additional calorimeter modules extending the coverage from 45° to 75° in two opposite sectors. Shown in Fig. 2 is the acceptance as a function of η' momentum and production angle in the laboratory for events accepted by CLAS from a uniform distribution. The acceptance peaks at about 16% at forward angles and high momentum, and decreases as the production angle increases or the η' momentum decreases. The acceptance as a function of photon beam energy for photoproduction on a free proton is shown as the solid histogram in Fig. 3. The acceptance decreases slowly as the energy increases over the range of interest. The average acceptance is 12.6%. For comparison, the results obtained with calorimeter coverage from 8° to 45° in all six sectors is shown as the dashed histogram in Fig. 3. In this case, the average acceptance is 10.7%.

2.3 Particle Identification

Monte Carlo calculations were also performed to investigate the particle identification the can be achieved with the CLAS. A simulated $\pi^+\pi^-\gamma$ mass spectrum for photoproduction on a free proton at an incident energy of 1.6 GeV is shown in Fig. 4. The region of the spectrum around the η' peak is relatively free of background. The broad background at lower mass is due to the decay of lighter mesons. The only meson heavier than the η' produced in this experiment that can decay into $\pi^+\pi^-\gamma$ is the ϕ. However, because the ϕ photoproduction cross section is smaller than that of the η' [10], and because it decays into $\pi^+\pi^-\gamma\gamma$ only about 5% of the time, it introduces a relatively small background under the η' peak.

2.7 Count Rate and Beam Time Estimates

The η' mesons produced with monochromatic photons of energy k will ɔe detected at a rate given by:

$$R(k) = \frac{N_A}{A} \cdot \sigma(k) \cdot N_\gamma(k) \cdot (\rho t) \cdot \varepsilon(k) \cdot BR$$

where N_A is Avogadro's number (6.022×10^{23}), A is the mass number of the nucleus, $\sigma(k)$ is the η' photoproduction cross section, N_γ is the number of incident photons per second, (ρt) is the target thickness, $\varepsilon(k)$ is the detection efficiency, and BR is the branching ratio for the $\eta' \rightarrow \rho^0\gamma \rightarrow \pi^+\pi^-\gamma$ decay (0.20).

In estimating the count rates, we have assumed a total tagged photon flux of 10^7 photons/s. The elementary η' photoproduction cross section is approximately 1 μb over the energy range of 1.45 to 2.25 GeV [10], and we have assumed that the total cross section scales as $A^{0.8}$. The results of our simulations shown in Fig. 3 indicate that the acceptance is approximately 12% over the entire energy range. Also, we have assumed a target thickness of 1 gm/cm^2 for each of the targets.

Listed in Table 1 are the total count rates for each of the targets calculated with the above assumptions. Also listed in the table are the number of η' mesons we would expect to detect in 150 hours of beam for each target. These numbers seem to be sufficient for this experiment.

References

[1] F. Lenz, Nucl. Phys. **B279**, 119 (1987).

[2] Particle Data Group, Rev. Mod. Phys. **56**, 1 (1984); Phys. Lett. **239B**, 1 (1990).

[3] W. Bartel *et al.*, Phys. Lett. **158B**, 511 (1985).

[4] F. E. Close, *An Introduction to Quarks and Partons*, (Academic Press, New York, 1979).

[5] R. M. Baltrusaitis *et al.*, Phys. Rev. **D32**, 2883 (1985).

[6] J. F. Donoghue and H. Gomm, Phys. Lett. **121B**, 49 (1983).

[7] S. C. Chao *et al.*, Phys. Lett. **172B**, 253 (1986).

[8] N. Isgur, private communication.

[9] M. F. Vineyard *et al.*, CEBAF Proposal PR-93-008 (unpublished).

[10] A. Baldini *et al.*, *Total Cross Sections for Reactions of High Energy Particles*, New Series I/12b (Springer, New York, 1988), p. 361.

Table 1. Count rate estimates.

Target	R (1.45-2.25 GeV) [s^{-1}]	Counts in 150 hours
^{2}H	0.13	70,200
^{12}C	0.088	47,520
^{58}Ni	0.064	34,560
^{208}Pb	0.050	27,000

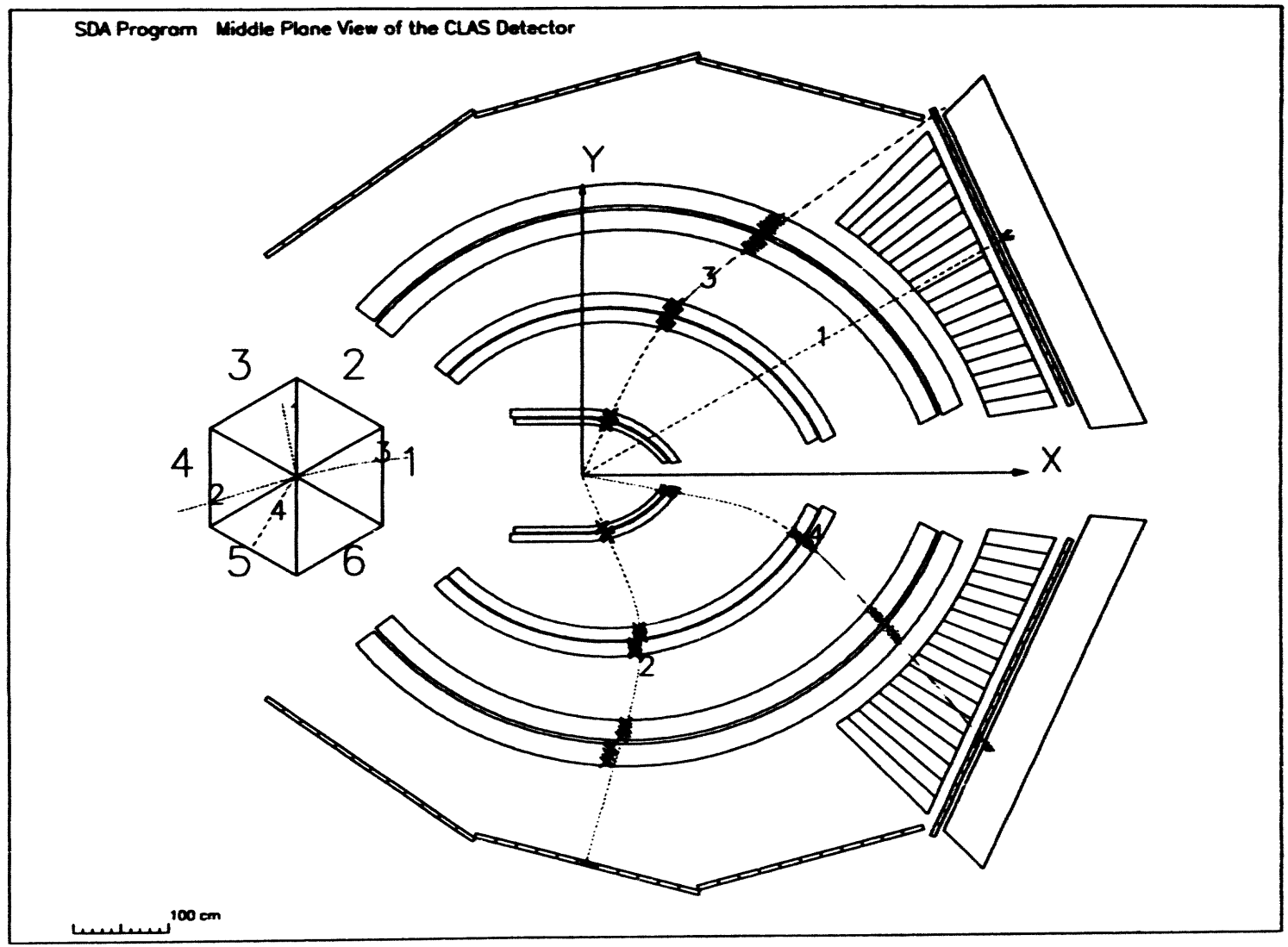

Fig. 1. A typical η' photoproduction event in the CLAS. Tracks 1, 2, and 3 are the photon, π^+, and π^-, respectively, from the η' decay, and track 4 is the recoil proton.

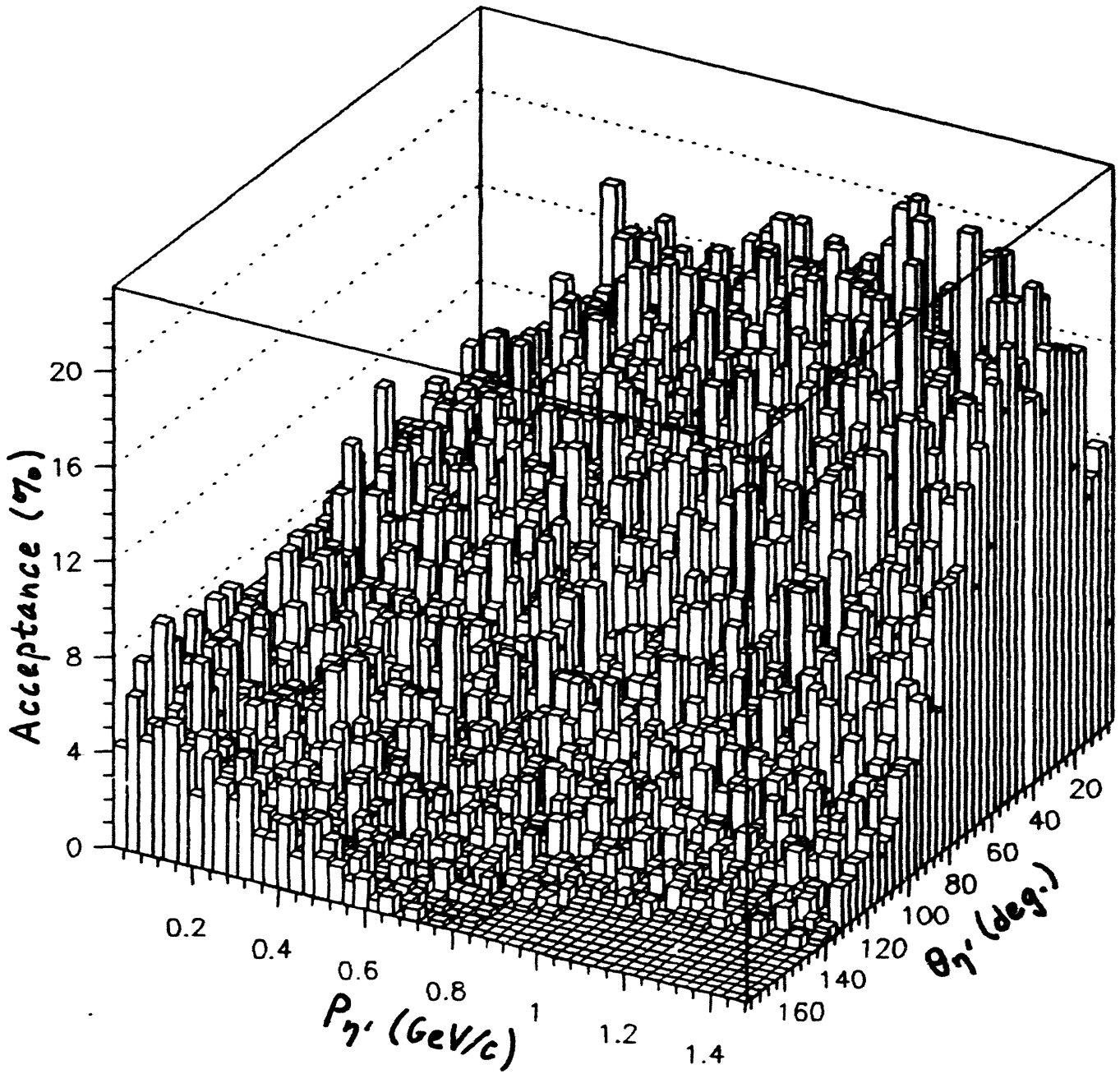

Fig. 2. The acceptance as a function of η' momentum and production angle in the laboratory.

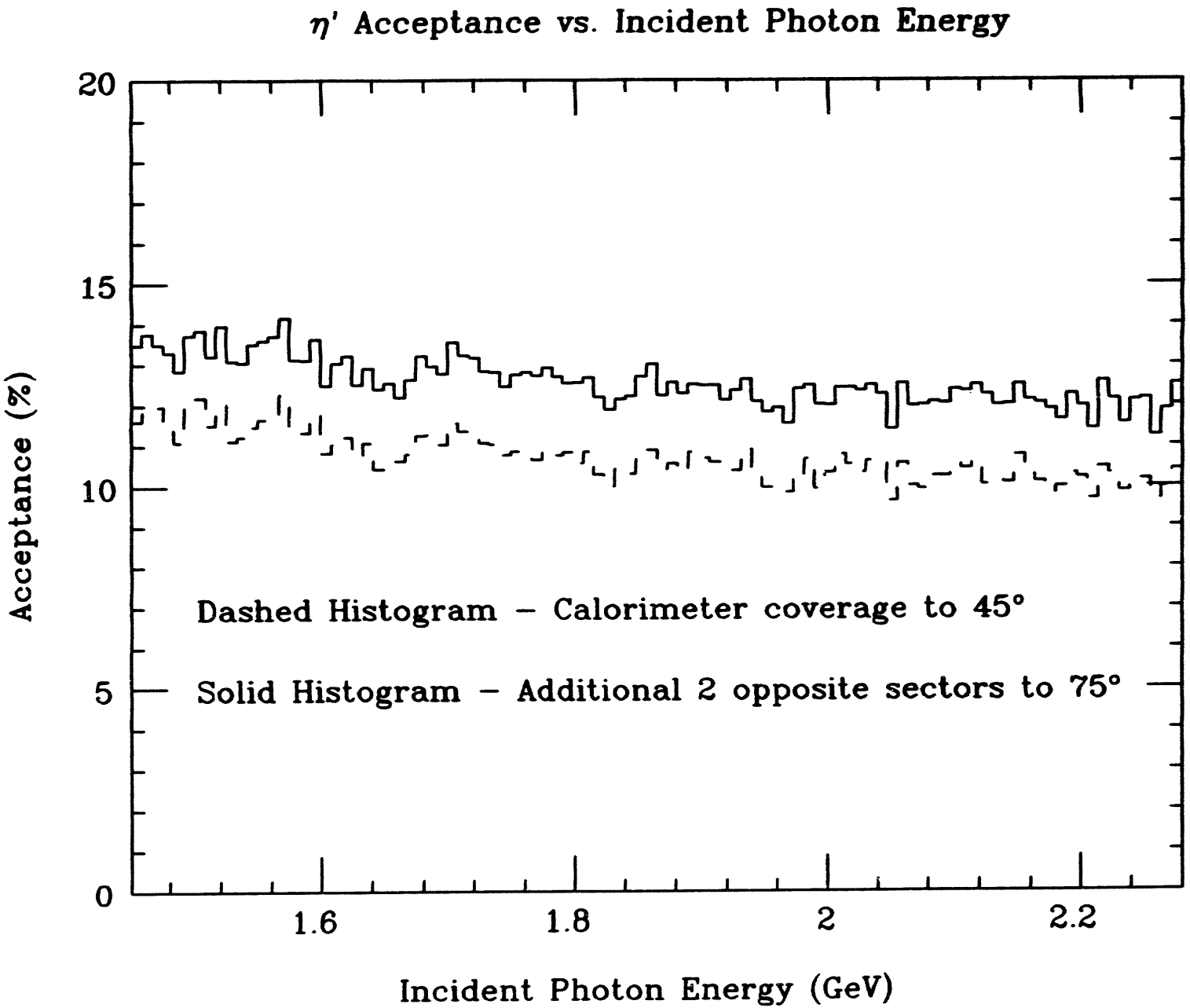

Fig. 3. The acceptance as a function of incident photon energy.

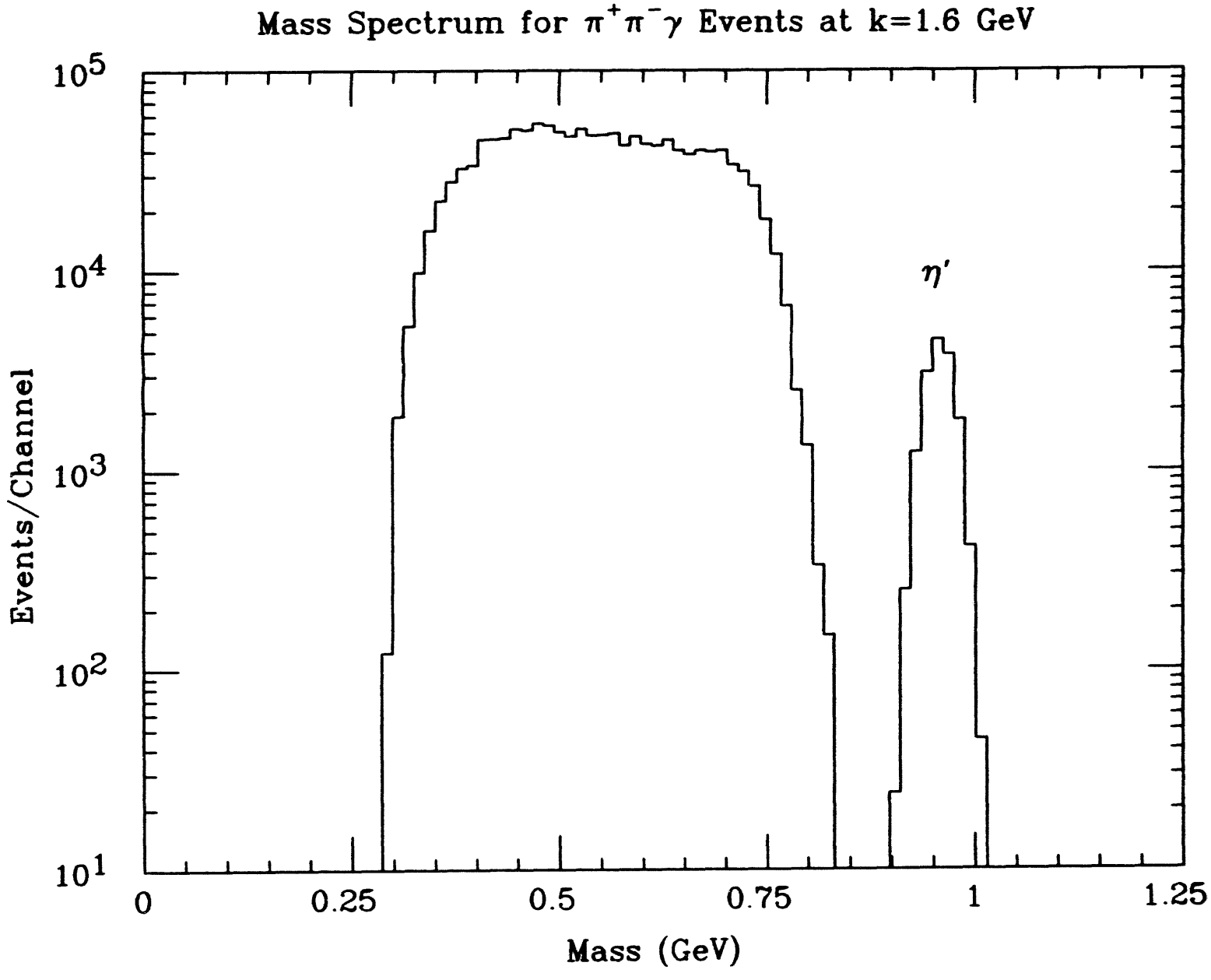

Fig. 4. Simulated $\pi^+\pi^-\gamma$ mass spectrum for photoproduction at k = 1.6 GeV.

Photoproduction of the f_0 Scalar Meson

Gilfoyle, Major, Rubin, Seaborn, and Vineyard

The structure of the $f_0(975)$ scalar meson has been a continuing source of controversy for more than two decades now[1-7]. The standard model predicts the existence of a nonet of $q\bar{q}$ objects, the $^3P_0$ nonet, that is complementary to the observed $^3P_2$ nonet. The f_0 is a candidate for the $s\bar{s}$ member of the $^3P_0$ nonet and can be viewed as an $l=1$ orbital excitation of the ω. However, there are a number of flaws with this classification. The width of the f_0 differs dramatically from expectations. A variety of models predict $\Gamma(f_0 \rightarrow \pi\pi) \approx 500\text{-}1000$ MeV whereas the measured value is about 30 MeV[5]. The f_0 is also a partner to the nearly degenerate $a_0(980)$ in the $^3P_0$ nonet. The naive classification of the these particles implies a difference in mass of about 200 MeV while their observed masses are nearly identical (974 MeV for the f_0 versus 983 MeV for the a_0). Treating the f_0 and a_0 as a (ρ,ω)-like doublet (where the a_0 is the $l=1$ orbital excitation of the ρ) can resolve the problem of the mass difference between the f_0 and the a_0, but it leads to other contradictions. This approach predicts the ratio $\Gamma(f_0 \rightarrow \pi\pi)/\Gamma(a_0 \rightarrow \eta\pi)$ should have a value of 4. The observed value is close to 1/2[5]. In addition this model does not explain the coupling of the f_0 to the $K\bar{K}$ decay channel. If the f_0 and a_0 were truly a (ρ,ω)-like doublet then the ratio $\Gamma(f_0 \rightarrow K\bar{K})/\Gamma(f_0 \rightarrow \pi\pi)$ would be approximately equal to $p_K/3p_\pi$. In reality the f_0 is so strongly coupled to the $K\bar{K}$ decay channel that the $\pi\pi$ mass distribution from the f_0 decay displays a typical Breit-Wigner shape with a dramatic cutoff at the $K\bar{K}$ mass threshold[5]. The comparison of the f_0 with its presumed partner in the $^3P_2$ nonet, the $f_2(1270)$, also leads to consistencies. The coupling to the $\gamma\gamma$ decay channel can be calculated on the basis of the $f_2(1270)$ data, but the result is not consistent with the observed $\gamma\gamma$ coupling of the f_0. The decay widths of the J/Ψ into various channels also show the f_0 does not behave as the analog to the $f_2(1270)$[5].

A number of models have been put forward to resolve these paradoxes. One that has received

considerable attention is the notion that the f_0 is $K\bar{K}$ molecule. Weinstein and Isgur have used a non-relativistic potential model to investigate the $qq\bar{q}\bar{q}$ system[5]. Their results show the formation of such states to rare in general and when they do form the quarks form clusters of color singlets which are considerably smaller than the intercluster separation. They form a weakly bound 'meson molecule'. The best candidates for such a configuration are the f_0 and the a_0. The narrow decay width of each scalar meson can be accounted for since the weakly-bound mesons seldom come close enough to one another to exchange or annihilate quarks and hence decay. The strong coupling to the KK decay channel is also no surprise since the f_0 is itself a weakly bound $K\bar{K}$ state in this model. One consequence of this model that will become important later is that the f_0 is considerably larger in size than the usual $q\bar{q}$ system.

Another theoretical investigation of the $q^2\bar{q}^2$ system by Jaffe uses the MIT bag model to predict the existence of such states in the particle spectrum[2]. This approach predicts a different spectrum of states and that the $q^2\bar{q}^2$ system will be comparable in size to the usual $q\bar{q}$ system.

Other workers have tried to reconcile the discrepancies in the $q\bar{q}$ picture of the f_0 by including the effect of the nearby $K\bar{K}$ mass threshold in their models and analyses[6,8]. These investigations predict a different spectrum of states than either approach cited above and, of course, a size consistent with the usual $q\bar{q}$ system.

With the array of alternative explanations for the anomalous behavior of the f_0 cited above, the question becomes one of distinguishing among these choices. One experiment at the Continuous Electron Beam Accelerator Facility (CEBAF) has already been approved to address these questions by examining the electroproduction of the f_0 using a proton target and measuring the $f_0 \rightarrow K\bar{K}$ decay channel[9]. Presumably by determining the Q^2 and t dependence of the cross section one can distinguish between the large, weakly-bound 'meson molecule' and the more compact $q\bar{q}$ configuration. However, the direct production of $K\bar{K}$ pairs may make it difficult to extract the f_0 cross section from the background and even if successful, the experiment does not discriminate between the $q\bar{q}$ and the $q^2\bar{q}^2$ pictures.

A different experimental signature has been proposed by Alexandrou and Sato using the production of the f_0 from a nuclear target[10]. This technique relies on geometric arguments to differentiate between the three alternatives described above ($K\bar{K}$,$q\bar{q}$, and $q^2\bar{q}^2$). They calculate the total cross section and the inelastic cross section, σ_{total} and $\sigma_{inelastic}$, respectively, for the f_0N scattering process using the three hypotheses. If the f_0 is either a $K\bar{K}$ molecule or a $q^2\bar{q}^2$ state the total cross section should be about twice the expectation for a $q\bar{q}$ state. Furthermore, the ratio of the inelastic to total cross section or $r=\sigma_{inelastic}/\sigma_{total}$ will be large compared to the $q\bar{q}$ expectation for the $K\bar{K}$ molecule. If the f_0 is a $q^2\bar{q}^2$ state then r will be much smaller than the $q\bar{q}$ expectation. Hence, a determination of σ_{total} and $\sigma_{inelastic}$ will discriminate among the different models. The authors propose using the nucleus as a 'laboratory' to determine the total and inelastic cross sections. The A-dependence of the inclusive reaction $\gamma A \rightarrow f_0 X$ and the exclusive reaction $\gamma A \rightarrow f_0 N(A-1)$ will enable one to extract the desired cross sections. This A-dependance for the inclusive and exclusive cross sections is shown in Figures 1 and 2[10]. In Figure 1 the ratio of the inclusive cross section is normalized to the corresponding cross section in the impulse approximation and plotted versus A. The curves labelled A and B in the figure are a product of a calculation assuming a $K\bar{K}$ molecular picture with different assumptions about the amounts of σ_{total} and $\sigma_{inelastic}$. The curve labelled C is for the $q^2\bar{q}^2$ hypothesis. The last two curves (labelled D and E) are produced using the $q\bar{q}$ hypothesis with different assumptions about the amounts of σ_{total} and $\sigma_{inelastic}$. The inclusive cross section is strongly dependent on the amount of $\sigma_{inelastic}$, but only weakly dependent on the size of σ_{total}. Hence, one can extract the f_0N inelastic cross section. In Figure 2 the ratio of the exclusive cross section to the appropriate impulse approximation cross section is plotted versus A. The A dependence of the $q^2\bar{q}^2$ and $K\bar{K}$ molecule hypotheses is shown in curves A and B, respectively. This exclusive cross section is only weakly dependent on $\sigma_{inelastic}$, but is sensitive to the size of the total cross section. Hence, the total cross section can be extracted here and one would have the means to distinguish among the different models.

To test the feasibility of this approach we have begun investigating the photoproduction of the f_0 and detecting its decay with the CEBAF Large Acceptance Spectrometer (CLAS). The invariant mass spectrum extracted from the $K\bar{K}$ decay channel of the f_0 provides a comparatively clean signal with few background processes to interfere. However, the amount of direct production of $K\bar{K}$ pairs is largely unknown and the peak in the invariant mass spectrum is distorted because the centroid of the f_0 mass distribution lies below the $K\bar{K}$ mass threshold. This effect is demonstrated in Figure 3 where the invariant mass spectrum for decay via the $K\bar{K}$ channel is compared with decay via the $\pi\pi$ mode[5]. The $\pi\pi$ mode clearly shows a more prominent peak whose cross section will be easier to extract. These difficulties have lead us to consider the $\pi\pi$ decay channel of the f_0. That investigation is underway.

References

[1] D.Robson, Nucl. Phys., **B130**, 328(1977).

[2] R.J.Jaffe, Phys. Rev., **D15**, 267(1977).

[3] N.N.Achasov, S.A.Devyanin, and G.N.Shestakov, Sov. Phys. Usp. **27** (3), 161(1984).

[4] F.Lenz, Nucl. Phys., **B279**, 119(1987).

[5] J.Weinstein and N.Isgur, Phys. Rev., **D41**, 2236(1990).

[6] D.Morgan and M.R.Pennington, Phys. Lett., **B258**, 444(1991).

[7] B.S.Zou and D.V.Bugg, Phys. Rev., **D48**, R3948(1993).

[8] N.A.Tornquist, Phys. Rev. Lett., **49**, 624(1982).

[9] "Measurements of the Electroproduction of Λ(gnd), Λ(1520), and f_0(975) via the K^+K^-p and $K^+\pi^-p$ REactions", CEBAF Proposal PR-89-043, H.Funsten and L.Dennis, contact persons.

[10] C.Alexandrou and T.Sato, Phys. Rev., **C36**, 732(1987).

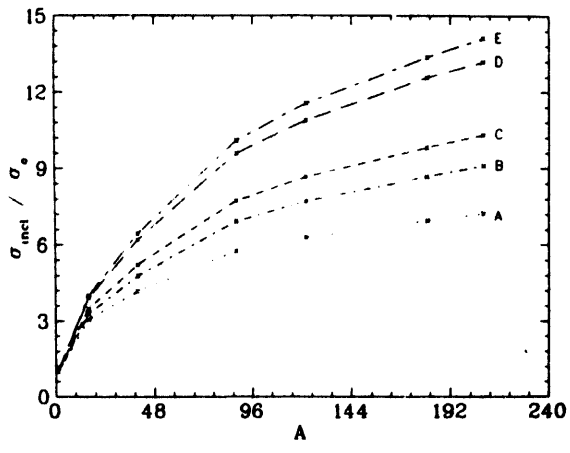

Figure 1. The inclusive cross section versus A is shown for the reaction $\gamma A \rightarrow f_0 X$. The cross section is normalized to the cross section calculated in the impulse approximation. Curves A and B represent the A-dependence of the $K\bar{K}$ molecular picture, curve C represents the $q^2\bar{q}^2$ model, and curves D and E were calculated using the $q\bar{q}$ model.

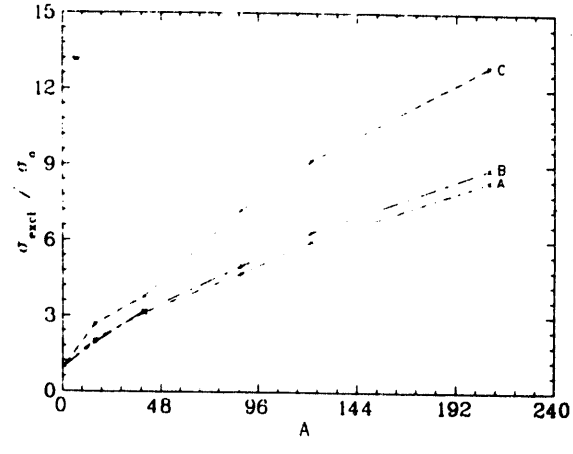

Figure 2. The exclusive cross section versus A is shown for the reaction $\gamma A \rightarrow f_0 N(A-1)$. The cross section is normalized to the cross section calculated in the impulse approximation. Curve A represents the A-dependence of the $q^2\bar{q}^2$ model, curve B represents the $K\bar{K}$ molecular picture, and curve C was calculated using the $q\bar{q}$ model.

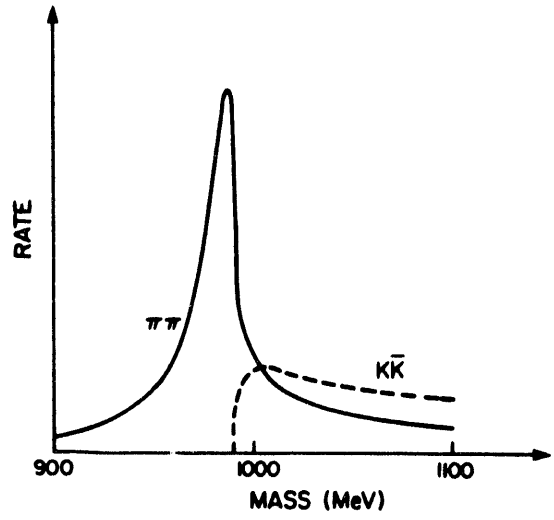

Figure 3. A schematic plot is shown of the rate of production of $\pi\pi$ versus the rate of production of $K\bar{K}$ from the decay of the f_0 is shown.

CLAS Drift Chamber Gas System Progress

Major, Christo, Kline, Mawicke, Woods, Anderson, and Mestayer

A prototype system for the CLAS (CEBAF Hall B) detector was completed and tested during 1992-1993. At an input rate of up to 2 liter/sec, it filters, mixes and delivers to a $1m^3$ dummy chamber a 50:50% combination of Argon and Ethane at a pressure of 0.5 Torr above atmospheric. Neither the hardware nor specific design features are limited to those gas choices; e.g Helium may be used rather than Argon. The mass ratio may also be changed arbitrarily. This prototype also recirculates any desired fraction of the mix which has passed through the drift chamber, using electronic mass flow controllers and buffer tanks to provide fresh gas as replacement for the fraction exhausted from the system. Control of the recirculation loop is achieved by using a differential pressure transducer and proportioning solenoid valve to maintain constant pressure excess inside the chamber, with respect to ambient atmospheric pressure.The flow rate through the upstream mass flow controllers only determines the average net flow through the chambers; it is decoupled from the main pressure control system by a mixed gas buffer volume.

Figure 1 is a schematic of the working prototype, displayed to correspond to the reality that all filtering, mixing and metering hardware is located on one instrument rack (left page), while all recirculation equipment is on a second rack (right page).While the diagram is intended for use by the gas system operator and is not an engineering blueprint, it displays all essential components and implies those not shown (see Fig. 1 Legend). The prototype operates as intended, with a characteristic response time to a step function pressure overload of about 10 seconds. Out-of-limit pressure changes, excessive concentrations of Oxygen, or temperature excursions beyond preset (+/- 5C) limits trigger automatic isolation of the chamber via electrically actuated valves. Protection of the chamber's gas bag during such an episode is ensured by over-and under-pressure bubblers. Upon chamber isolation, the recirculation pump also stops and a status light is activated. Manual

flow control is provided as an option in case of power loss. Oxygen and water vapor concentrations are limited to 50 ppm by passive traps and filters, and Oxygen has been further reduced to 10 ppm with a DeOxo catalytic device which uses Hydrogen to produce water which is then trapped. In other tests at CEBAF, a DO muon drift chamber with a total drift time of 1000 ns displayed a 45% change in pulse height with 3200 ppm of O_2 in the gas. To keep such effects to 1% and maintain high efficiency for long drift paths (consistent with a 9% resolution on dE/dx) we conclude that O_2 content must be kept *below* 70 ppm. Although the full scale detector will certainly have more and larger gas leaks than the prototype, the experience referred to above indicates that we can achieve this.

This prototype serves as the basis for the conceptual design, now essentially completed, of the full scale CLAS gas system. Combined input flow will be 16 - 20 liter/min, assuming two volume changes per day of the 60,000 liter (~ 2000 ft^3) detector and recirculation of 80% of the chamber throughput. A 20 x 30 ft metal building to serve as a gas shed will be located on the graded area between experimental Halls B and C and close to the former. Present plans include at least nine gas lines connecting this shed with Hall B; six for input and return from the three detector regions, one for exhaust, and one each for Nitrogen flow and Helium bags. One - half inch stainless lines are specified for delivery of gas to the hall, and 1 - inch diameter lines for recirculation and exhaust. Some copper or Nylon may be used in the gas shed on mixing panels, and for exhaust lines. A 10 ft x 20 ft section of the gas shed will be partitioned for housing electronics and instrumentation, including the monitor for a cctv camera located in the experimental hall. The remaining 20 ft x 20 ft space will house mixing, metering, and monitoring equipment and transducers. Groups other than the drift chamber group may wish to use space in this facility. Potential needs include a Freon cleaning and recirculation system, a Nitrogen system, and a cryogenics target gas system.

Efforts to estimate yearly gas costs, and to control this operating expense, are hindered by the difficulty in locating a reasonably priced source of Ethane. Our best estimate (December 1993) is

that gas costs will be $49,000 per year. Operating manpower is expected to be 1 FTE during the first year of operation, and 1/2 to 3/4 FTE thereafter.

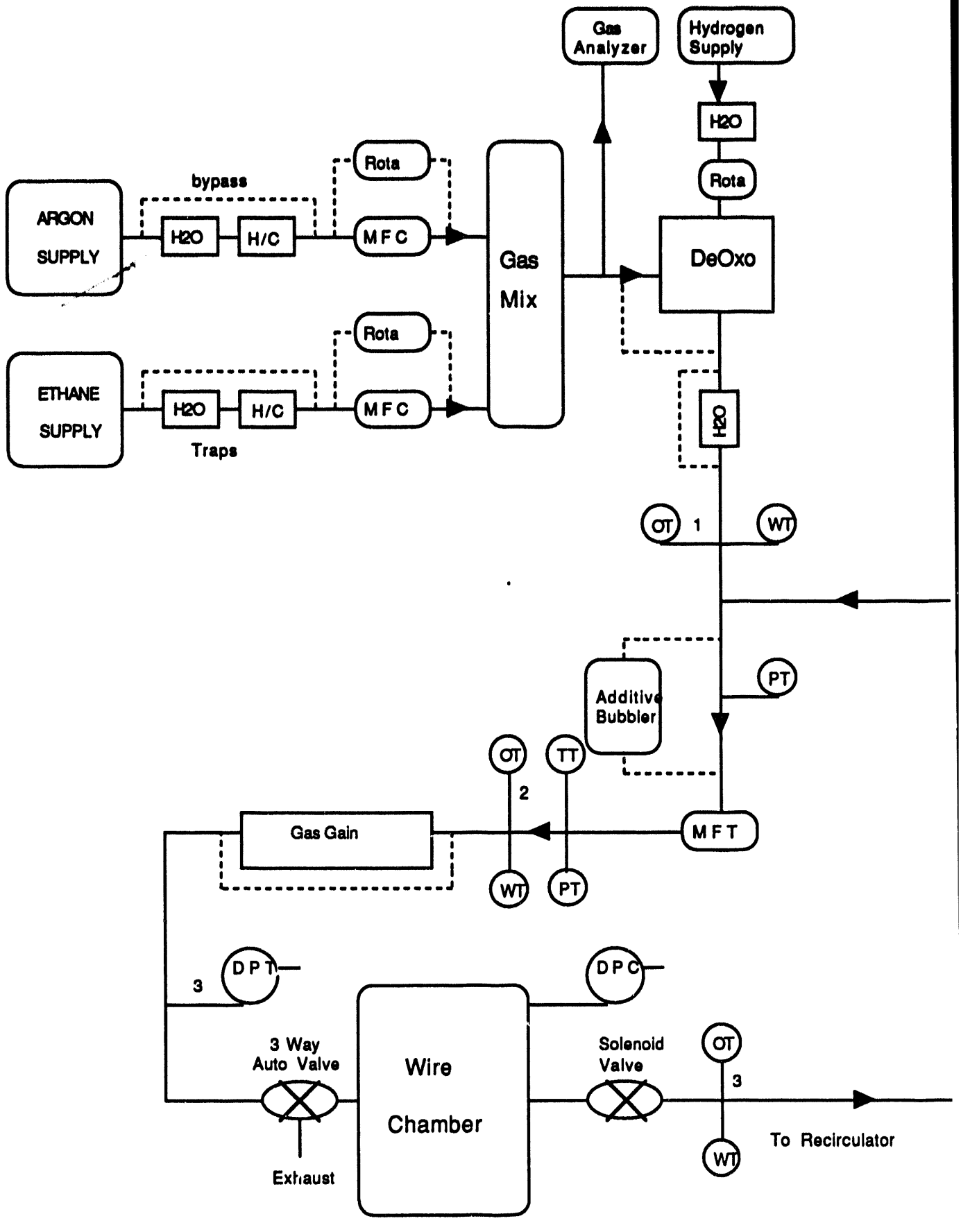
Gas Analyzer
Hydrogen Supply
H2O
Rota
bypass
ARGON SUPPLY
H2O
H/C
MFC
Rota
Gas Mix
DeOxo
ETHANE SUPPLY
H2O
H/C
MFC
Traps
Rota
H2O
OT
1
WT
PT
Additive Bubbler
OT
TT
2
Gas Gain
MFT
WT
PT
DPT
3
DPC
3 Way Auto Valve
Wire Chamber
Solenoid Valve
OT
3
To Recirculator
WT
Exhaust

U.R. Prototype Gas System For CLAS

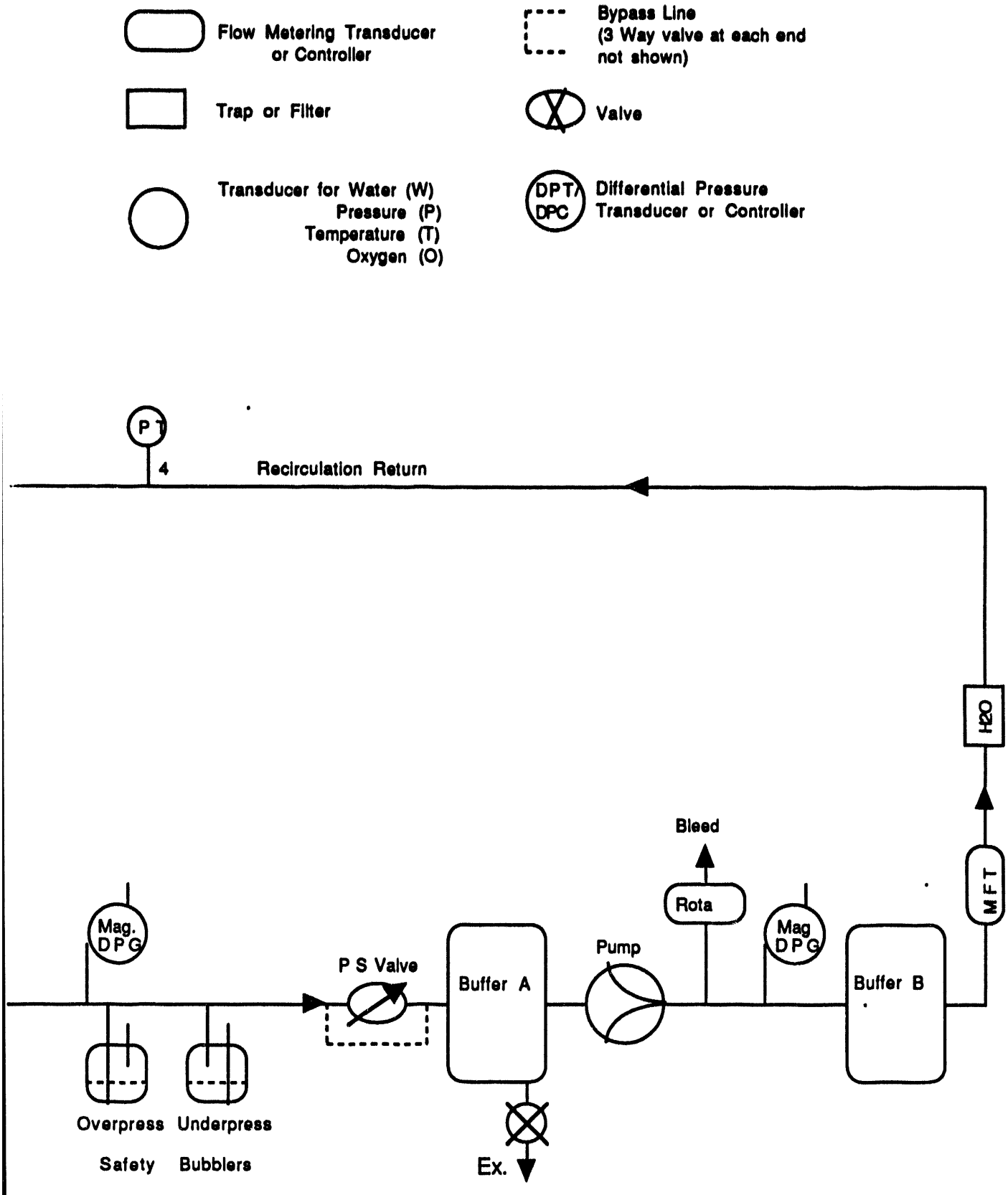

CLAS Slow Controls System

Vineyard and Bonneau

Part of the UR group's contribution to the CLAS collaboration is the development of the slow controls system. This system is being constructed within the framework of the CEBAF Online Data Acquisition (CODA) system. CODA is designed to run on an Ultrix (DEC/RISC) host, connected via ethernet to multiple intelligent front end crates, FASTBUS and VME. CAMAC crates are interfaced through VME. Slow controls is defined to include everything necessary to control and/or monitor the detectors, magnets, beamline, power supplies, etc. Following the experience of large high energy physics experiments, slow controls and data acquisition will be kept as separate as possible, operating as separate processes using separate CPU's and I/O crates. The CODA slow controls system passes information to and from the user through a graphical user interface. Currently this user interface is created with a software system called DataViews.

The initial work on the slow controls system has been focussed on the prototype gas system for the drift chambers which has been developed by the UR group. The instruments included in the gas system are listed in Table 1 along with the quantities measured and the type of interface or output information available. A VME crate with a Motorola 167 single-board computer and an Xycom 64-channel ADC is used to interface with the gas system instrumentation. A real-time operating system, VxWorks, is run on the crate CPU to provide the basis for real-time control. A driver has been written for the Xycom ADC to read all the analog signals provided by the instruments (see Table 1). Views for the graphical user interface have been created with DataViews to display this information. A black and white version of the main view which shows the location of the various transducers is shown in Fig. 1. Selecting the icon of one of the transducers will display another view through which information is presented. A software driver is also being developed to communicate with the MKS 147 Gas Flow Controller through an RS-232 interface.

During the next year, this system will be converted to the Experimental Physics and Industrial Control System (EPICS) which is currently being incorporated into the CODA system. EPICS is a state-of-the-art distributed real-time data acquisition and process control software package developed and maintained by a collaboration between Los Alamos Laboratory, Argonne National Laboratory, CEBAF, and several industrial partners. It supports a large number of channels conveniently and efficiently and is based on open-system concepts. The EPICS operator interface includes one or more UNIX workstations which communicate over ethernet with one or more intelligent I/O controllers, called IOCs. EPICS supports VME, VXI, and CAMAC IOCs. This software package also includes logic and alarm handling.

Over the next three years, the slow controls system will be expanded to include the many other CLAS components.

Table 1. Prototype Gas System Instrumentation

- MKS 147 Gas Flow Controller
  - only active control in system
  - controls and reads flow rate in liters/min
  - 4 channels
  - RS-232 interface
  - 0-2 V analog output

- GOW-MAC Thermal Conductivity Gas Analyzer
  - measures % ethane (by volume)
  - 0-1 V analog output

- Panadry Hygrometer
  - measures dew point in °C which is converted to ppm H_2O
  - 0-2 V analog output

- Illinois Instruments 2550 Oxygen Analyzer
  - measures ppm oxygen
  - 0-100 mV analog output

- MKS PDR-5B Power Supply and Readout
  - reads pressure
  - 5 channels
  - 0-1 V analog each channel

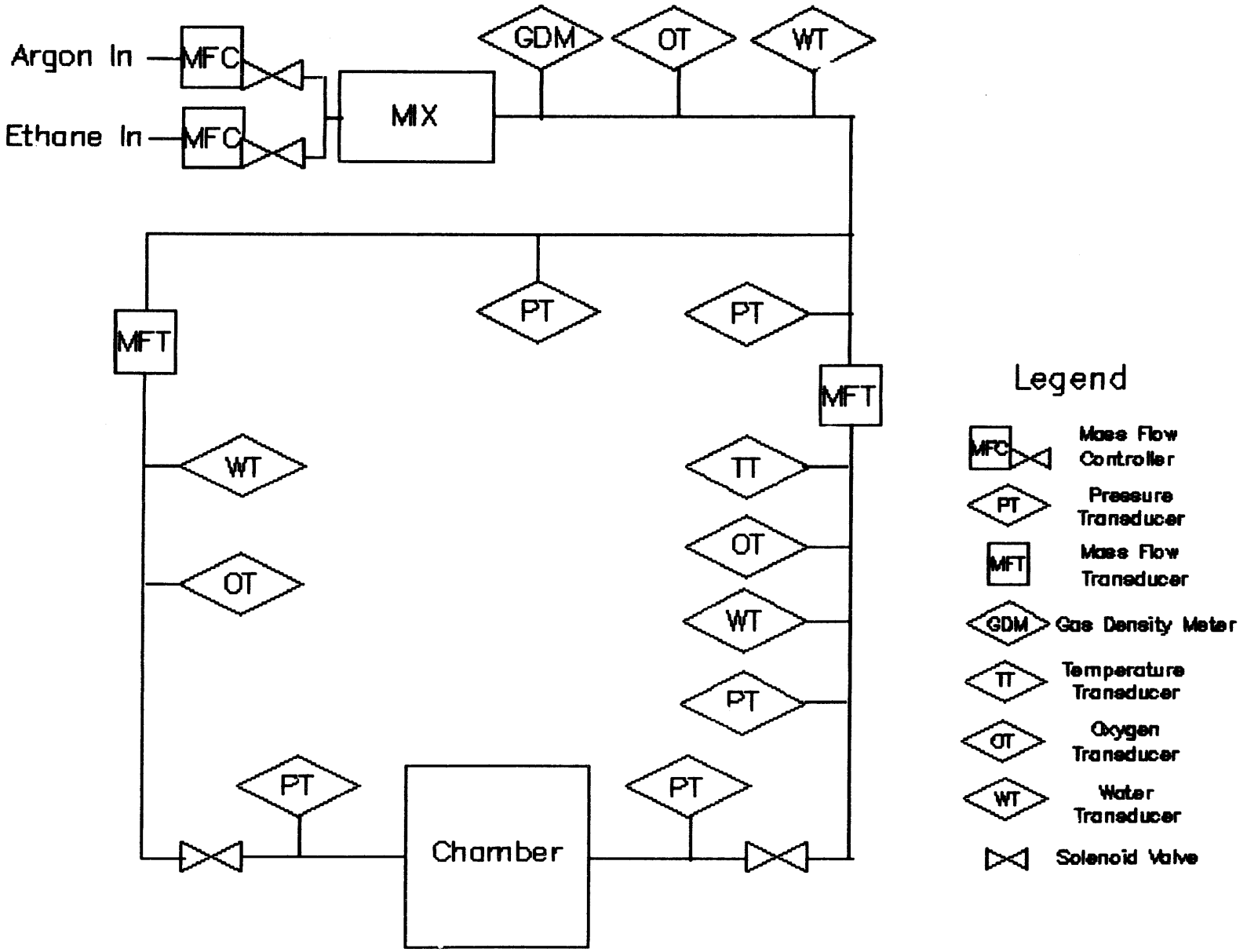

Fig. 1. Main view of the graphical user interface for the prototype gas system.

CLAS Drift Chamber Software Development

Gilfoyle and Mestayer

The software demands of the CEBAF Large Acceptance Spectrometer (CLAS) are considerable. It is expected to generate more than 5000 bytes/event at a data rate of up to 1500 events/s. The disposition of these events will be determined by a triggering system based on hits in the scintillation counters and the outermost drift chambers, the energy deposited in the shower counters, and by identifying desirable track candidates in the drift chambers. Higher level trigger decisions can be made after further analysis of the events. Thus, the data acquisition system must be capable of pattern recognition to identify a track candidate from the hit pattern in the drift chambers and scintillators and to quickly fit the track to enable the users to separate true events from any background. Both topics are the subject of current work [1,2,3].

To provide a testing ground for both software and hardware we are currently building a prototype of the most forward angle portion of the Region 3 drift chambers (see Figure 1). This nosecone prototype is the first of its kind that reproduces the geometry of the drift chambers that will be part of the final detector and will be one of the last steps in the drift chamber development before construction of the final drift chambers begins. It will consist of the sixteen most forward angle sense wires in the twelve layers of wires that make of the region 3 drift chambers. It will also contain the associated sense and guard wires. It is anticipated that the nosecone prototype will be ready for testing in the winter of 1993-1994.

One of the essential needs of the nosecone prototype is a data acquisition and analysis system for the cosmic rays that will provide ionizing radiation needed to test the detectors components. There exists now a software package at CEBAF that runs under VMS that has been used for several years for these same purposes, but with other drift chambers. Because of the impending need for a function data acquisition and analysis package (*i.e.*, in the next few months at the time of this writing) we have decided to modify this existing code (entitled 'TRACK') for use with the nosecone prototype.

At this time the modification of 'TRACK' is well underway. Figure 2 is plot of the new sense wire positions and the hex-cell geometry associated with each wire along the midplane of the drift chamber. The various parts of TRACK's rudimentary database has been modified so that the

electronics-channel-to-wire-number and the associated electronics parameters (pedestals, gains, etc.) are now consistent with the nosecone prototype geometry. Various and sundry parameters and software 'cuts' that were 'hardwired' into the code have been removed or adapted to the new configuration. The capability to write out events read in by TRACK into a file in the CLAS event format has been added. This will enable other software developers to test their analysis packages with real events once the nosecone prototype begins operation. The code compiles without error, links with the correct libraries, and runs.

The initial testing of the code is demonstrated in Figures 2 and 3. In Figure 2 is shown a single track from a computer-generated event that moves along the midplane of the detector. The circles centered on different sense wires represent the distance of closest approach to the wire by the track and were used to generate simulated the drift times that will be the quantities measured during the operation of the drift chambers. These drift times were then written into an event file that could be read by TRACK and analyzed. Figure 3 is the output of TRACK after it has analyzed one of the simulated events. One sees that the geometry is faithfully reproduced as is the track through the detector. Upon close examination one may also observe there is a small discrepancy between the size of the distance-of-closest-approach circles in Figure 2 and Figure 3. The source of this inconsistency is under investigation.

Before the nosecone prototype begins operation a number of goals must be accomplished. Several minor bugs like the one mentioned above must be fixed. More complete testing using simulated events must be performed. Finally, testing the data acquisition portion of the software has not begun because there is currently no testing equipment available. These tests will be done during the winter of 1993-1994.

References

[1] **Conceptual Design Report, CEBAF End Station B, (1990).**

[2] B.Niczyporuk, **Track Fitting in an Inhomogeneous Magnetic Field,** CLAS NOTE-91-001(1991).

[3] R.Brun and M.Hansroul, GEANT User's Guide, PHYS 320-1.

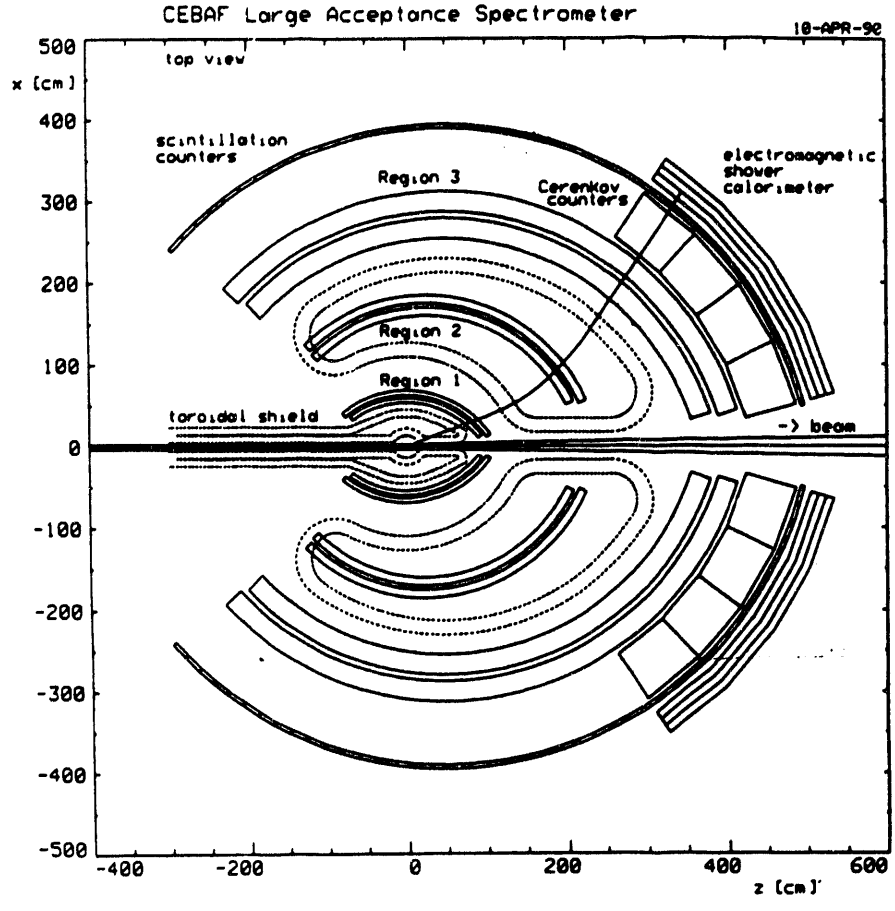

Figure 1. Midplane slice of the CLAS detection system (viewed from the top). The dotted lines show the projection of the magnet coil contours on the midplane. The Cerenkov counters and the electromagnetic calorimeter extend to 45°. The trajectory of a 1 GeV/c particle is shown.

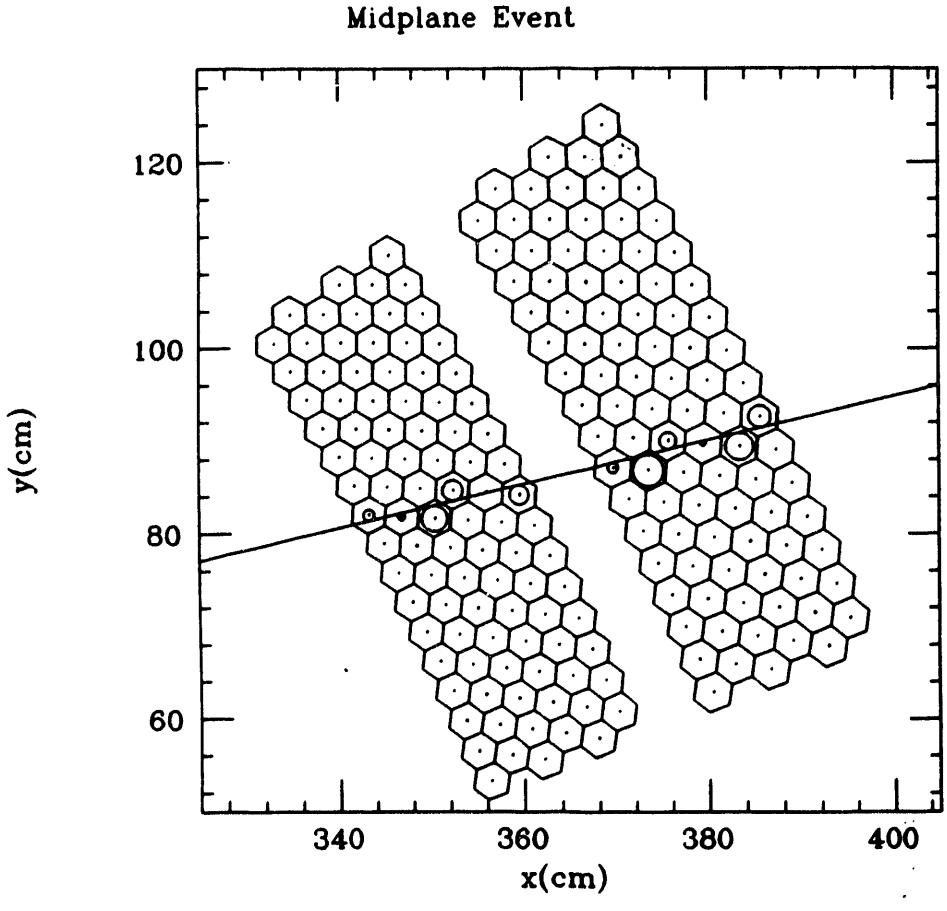

Figure 2. Midplane wire positions and hex-cell geometry for the nosecone prototype. The track is from a simulated event used for testing purposes. The circles represent the distance of closest approach of the particle to the wires that have fired after its passage.

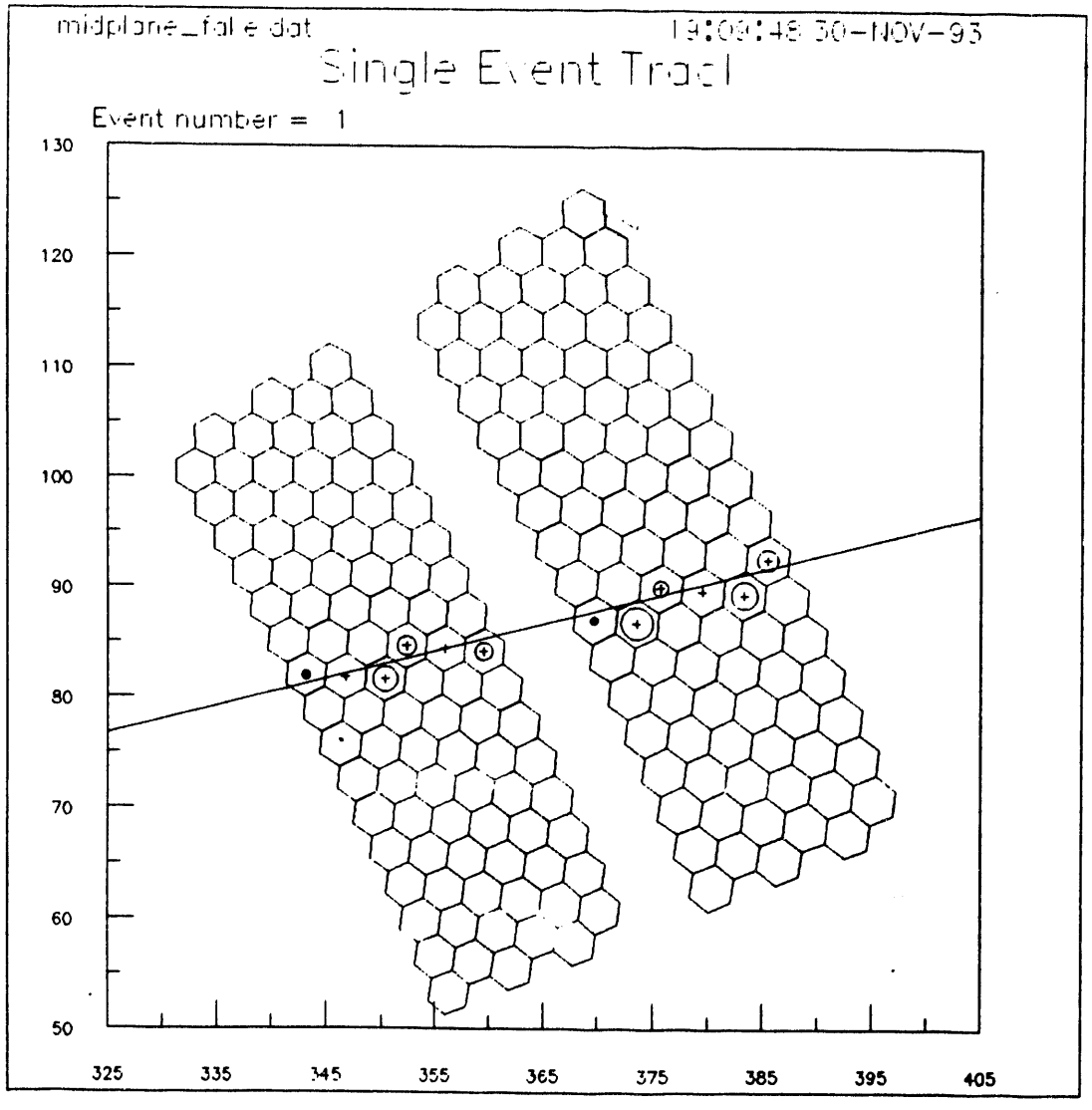

Figure 3. Event plot generated with TRACK. The simulated event shown in Figure 2 was read from a file by TRACK and analyzed to produce the reproduction of the event shown here.

Accepted for publication in Physical Review C

Light-Particle Correlations with Evaporation Residues in the $^{40}Ca+^{12}C$ Reaction at E(^{40}Ca)=450 MeV

M. F. Vineyard,[1] S. E. Atencio,[1] J. F. Crum,[1] G. P. Gilfoyle,[1]
B. G. Glagola,[2] D. J. Henderson,[2] D. G. Kovar,[2,*] C. F. Maguire,[3] J. F. Mateja,[4]
R. G. Ohl,[1] F. W. Prosser,[5] J. H. Rollinson,[1] and R. S. Trotter[1]

[1]*Department of Physics, University of Richmond, VA 23173*
[2]*Physics Division, Argonne National Laboratory, Argonne, IL 60439*
[3]*Department of Physics and Astronomy, Vanderbilt University, Nashville, TN 37235*
[4]*Division of Educational Programs, Argonne National Laboratory, Argonne, IL 60439*
[5]*Department of Physics, University of Kansas, Lawrence, KS 66045*

ABSTRACT

Proton and α-particle correlations with evaporation residues were measured over the complete angular range in the interaction of a 450-MeV ^{40}Ca beam with a ^{12}C target. Comparisons of the data with predictions of the statistical model and expectations for complete fusion from the kinematics provide clear and consistent evidence of incomplete fusion due to pre-equilibrium emission of both protons and α particles from the ^{12}C target. However, there is conflicting evidence both for and against pre-equilibrium emission from the projectile.

PACS number(s): 25.70.Jj

*Present address: Division of Nuclear Physics, Department of Energy, Washington, D.C. 20585.

I. INTRODUCTION

The study of linear-momentum transfer in relatively-light, heavy-ion systems ($A_{projectile}+A_{target}\leq 60$) at bombarding energies around and above 10 MeV/nucleon has received considerable attention in recent years [1-10]. In these studies, the velocity distributions of evaporation residues are compared to that expected for a complete-fusion reaction in which the full linear momentum of the projectile is transferred to the compound nucleus. In studies of reactions involving asymmetric systems in which the projectile is lighter than the target, the velocity centroids of the heavy residues are found to be shifted to lower velocities than expected for full linear-momentum transfer. When the projectile is heavier than the target, the distributions are shifted to higher velocities than expected. For symmetric systems, a broadening of the velocity distributions rather than a shift in the centroids is observed. These results have been interpreted as evidence that some fraction of the evaporation residues arise from a composite nucleus, formed in a pre-equilibrium or incomplete-fusion process, that is moving at a different velocity than the complete-fusion compound nucleus due to the emission of pre-equilibrium particles. This behavior is qualitatively consistent with the picture that particle emission from (or breakup of) the projectile and/or target occurs (some fraction of the time) prior to fusion, and that the emission from the lighter reaction partner is dominant.

The origin of the pre-equilibrium emission of light particles associated with incomplete fusion is unknown and one of the interesting questions is whether the incomplete momentum transfer is the result of the emission of predominantly nucleons or of heavier particles. Several coincidence experiments [11-15] have been performed to investigate pre-equilibrium emission in these relatively-light systems. The results of three studies of rather asymmetric systems [11-13] indicate that pre-equilibrium α emission plays an important role. In a study of the $^{20}Ne+^{27}Al$ reaction at $E(^{20}Ne)=19.2$ MeV/nucleon, a pre-equilibrium α component was identified, however it was determined that it accounted for at most 1/3 of the momentum lost in the incomplete fusion process [14]. On the other hand, measurements for the $^{14}N+^{12}C$ system at $E(^{14}N)=12.9$ MeV/nucleon

yielded results for α-particle correlations and energy spectra consistent with evaporation [15].

In recent years, considerable progress has been made in the development of various theoretical descriptions of pre-equilibrium emission. Most of these models are based on either the Fermi jet approach [16-18], the Boltzmann master equation [19], or the Landou-Vlasov equation [20]. In general these models have provided reasonable descriptions of the rather sparse pre-equilibrium nucleon data that exist. However, these models are appropriate only to explain nucleon emission and it is possible that pre-equilibrium emission of composite particles is important (for which there are no promising models proposed). A much broader range of nucleon and cluster emission spectra gated on central collisions are needed to provide more severe tests of these models and future efforts in the description of pre-equilibrium particle emission. It is important to develop a quantitative understanding of pre-equilibrium particle emission so that it can be used to probe the very early stages of heavy-ion collisions.

In this paper we report on a detailed measurement of protons and α particles emitted in coincidence with evaporation residues for the $^{40}Ca+^{12}C$ system at E(^{40}Ca)=450 MeV. The energy spectra of the evaporation residues and the energy and angular distributions of the light particles are compared with predictions of the statistical model for complete fusion and equilibrium decay. The proton energy spectra are also compared with the predictions of a pre-equilibrium emission model [18].

The experimental procedure is described in Section II. In Section III the experimental results are presented. The results are discussed in the context of previous measurements and existing models in Section IV, and a summary is presented in Section V.

II. EXPERIMENTAL PROCEDURE

The experiment was performed with a pulsed, 450-MeV ^{40}Ca beam from the Argonne National Laboratory ATLAS facility. The time resolution of the beam pulses was better than 200 ps (FWHM) with a period of 82.5 ns. The beam was incident on a 100 $\mu g/cm^2$ carbon target mounted

in the ATLAS 91-cm scattering chamber. The heavy ions were detected at 4.5° in a large-solid-angle, time-of-flight detector system. This system consists of a parallel-plate avalanche counter for timing and position information and a Bragg-Curve Spectrometer [21] to obtain the energy and Z identification of the heavy ions. The detector was mounted on the vacuum extension box of the scattering chamber at a distance of 1.00 m from the target and subtended a solid angle of 5.5 msr. The timing information was used to aid in the separation of heavy ions from quasielastic and fusion events. An example of the Z resolution attained is shown in Fig. 1 where the energy is plotted as a function of the range of the heavy ions detected in the Bragg-Curve Spectrometer.

The light particles were measured at 23 in-plane angles with twelve telescopes consisting of surface-barrier ΔE detectors and lithium-drifted silicon E detectors. The distance of these telescopes from the target ranged from 19.5 to 41.0 cm and the solid angles varied from 0.577 msr at the most forward angles to 10.75 msr at the backward angles. Identification of the light particles was achieved using the rf beam timing of ATLAS and is illustrated in Fig 2. Shown in Fig. 2 is a two-dimensional spectrum of energy deposited in the ΔE detector versus time-of-flight (TOF) for light particles detected at -55° in coincidence with evaporation residues. The negative angle refers to the opposite side of the beam from the heavy-ion detector.

The energy calibration of the Bragg-Curve Spectrometer was derived using the alpha groups from a ^{228}Th source and a precision pulser. The slopes of the time-to-amplitude converters (TACs) used for the TOF measurements of the light particles were determined using a time calibrator. The pedestal (or t_0) for each TAC was obtained using the protons and alpha particles that penetrated the ΔE detectors. The energies of the light particles were then calculated from the TOF calibrations and the measured flight paths.

Signals from the ΔE detectors were used to trigger the electronics. As a result there are high-energy cut-offs in the proton spectra due to the fact that high-energy protons do not lose enough energy in the ΔE detectors to produce signals above the discriminator thresholds. The high-energy cut-off depends on the thickness of the ΔE detector and the discriminator threshold level, but is typically about 30 MeV.

III. EXPERIMENTAL RESULTS

A. Statistical-Model Calculations

The complete-fusion and equilibrium-decay process has been modeled with the Monte Carlo computer code PACE [22] to aid in the interpretation of the data. This calculation was performed with a total fusion cross section of 900 mb obtained from a surface-friction-model calculation by Frobrich [23] for the $^{16}O+^{40}Ca$ system. Discrete energy levels were used for the low excitation-energy region of each nucleus involved in the evaporation cascades. A level density parameter of a = A/8.5 MeV^{-1} was used at higher excitation energy. An "event" file was created that contained the history of 10^6 cascades. The history includes the mass, charge, and energy of the evaporation residues as well as the energies and angular momenta of the emitted light particles. The file was then scanned with the experimental detector positions and solid-angles to construct the energy and angular distributions of the evaporation residues and light particles.

For comparison, the calculation was also performed with the statistical-model code LILITA [24] for fewer cascades. The results of the two calculations were in good agreement.

B. Evaporation Residues

Approximately 75% of the evaporation residues detected were isotopes of K, Ca, or Sc. An energy spectrum of Sc residues is shown in Fig. 3. The solid curve is the PACE prediction for complete fusion normalized to the maximum value consistent with the data. The experimental energy distribution is shifted to higher energy than predicted by the PACE calculation indicating significant incomplete fusion due to pre-equilibrium emission from the ^{12}C target. This was observed for all residue Z groups. The shape of the spectra were found to be consistent with the assumption that contributions to incomplete fusion corresponding to pre-equilibrium emission from the ^{40}Ca projectile are negligible. By normalizing the PACE predictions to the maximum value consistent with the data, it is estimated that at most 35% of the evaporation residues arise from complete fusion. These results are consistent with the systematics established by Morgenstern et al.

[3] from the measurements of inclusive evaporation-residue velocity spectra.

C. α-Particle Correlations

The energy spectra of α particles measured at θ_α=-7°, -27°, -45°, -65°, -95°, +15°, +25°, +45°, +65°, and +75° in coincidence with evaporation residues with $12 \leq Z_{ER} \leq 24$ are shown in Fig. 4. Negative and positive angles refer to the opposite and same side of the beam as the heavy-ion detector, respectively. The vertical scale in the figure indicates the α-particle double-differential multiplicity ($d^2M_\alpha/d\Omega_\alpha dE_\alpha$) defined by

$$\frac{d^2M_\alpha}{d\Omega_\alpha dE_\alpha} = \frac{\frac{d^3\sigma}{d\Omega_\alpha d\Omega_{HI} dE_\alpha}}{\left(\frac{d\sigma}{d\Omega_{HI}}\right)_{\theta_{HI}}}$$

where $(d\sigma/d\Omega_{HI})_{\theta_{HI}}$ is the differential cross section of the evaporation residues measured at θ_{HI}=4.5°. The solid curves shown in the figure are the results of the PACE calculation for complete fusion and equilibrium decay. The agreement with the data at forward angles ($|\theta_\alpha| \leq 45°$) is quite reasonable except at the most forward angles on the opposite side of the beam. The experimental spectrum at -7° shows a large probability of α particles with energies between 25 and 65 MeV which is not predicted by the calculation. Also, the high-energy slope of the experimental spectra at -7° and -27° are steeper than predicted. At angles larger than 45° the calculations underpredict the experimental spectra.

Integrating over the α-particle energy spectra, we obtain the angular correlation (squares) shown in Fig. 5. The solid curve is the statistical-model prediction for complete fusion and equilibrium decay. The calculation provides a good description of the data at angles around 45° on both sides of the beam, however it underpredicts the data at the more forward and backward angles.

The angular correlations of α particles with residues of K, Ca, and Sc are shown in Fig. 6. The solid curves shown in the figure are the results of the statistical-model calculation for complete

fusion and equilibrium decay. From this figure it can be seen that the discrepancies between the data and the calculation become more pronounced with increasing Z of the evaporation residues.

D. Proton Correlations

Although the experiments were primarily designed for α-particle correlations with heavy ions, protons were also detected in these measurements. The energy spectra of protons measured at θ_p=-7°, -45°, -95°, -140°, -170°, +25°, +45°, +75°, +120°, and +150° in coincidence with evaporation residues with $12 \leq Z_{ER} \leq 24$ are shown in Fig. 7. The solid curves are the results of the PACE calculation for complete fusion and equilibrium decay. The agreement between the data and the predictions at forward angles is poor. The experimental spectra at -7° and +25° show an enhanced yield at low energies. Also, the high-energy slopes of the forward-angle spectra are steeper than predicted. The agreement between the data and the calculations improves at larger angles and is fairly good at -95° and +75° as shown in the figure. However, at backward angles the statistical model underpredicts the experimental spectra.

The angular correlation obtained by integrating the proton energy spectra (squares) is compared with the PACE prediction for complete fusion and equilibrium decay (solid curve) in Fig. 8. Tne calculation overpredicts most of the data at forward angles and underpredicts the data at backward angles. The overprediction of the data at forward angles may, at least in part, be due to the high-energy cut-offs in the proton energy spectra.

The angular correlations of protons with residues of K, Ca, and Sc are shown in Fig. 9. The solid curves shown in the figure are the results of the statistical-model calculation for complete fusion and equilibrium decay. As in the case of the α correlations, the discrepancies between the data and the calculation become more pronounced with increasing Z of the evaporation residues.

IV. DISCUSSION

There is clear and consistent evidence from the data of pre-equilibrium emission of both α

particles and protons from the target. The evaporation-residue energy spectra (Fig. 3) are shifted to higher energy than predicted by PACE and expected from the reaction kinematics for complete fusion. This indicates that there is significant incomplete fusion due to pre-equilibrium emission from the target. Also, the α-particle and proton yields at backward angles are much larger than predicted by the statistical model. One would expect that any pre-equilibrium particles emitted from the target will be detected at large angles. In fact, due to the reverse kinematics employed in this reaction, nearly all of the statistical light particles fall in the forward hemisphere and, therefore, the light particles detected at backward angles in coincidence with evaporation residues are almost exclusively pre-equilibrium. It should also be pointed out that light particles evaporated from a reduced compound nucleus formed in an incomplete-fusion reaction due to pre-equilibrium emission from the target will be even more forward focussed since the reduced compound nucleus will be moving with a higher velocity than the complete-fusion compound nucleus.

From the comparisons of the PACE predictions for complete fusion with the data, there is conflicting evidence both for and against significant pre-equilibrium emission from the projectile. The shapes of the energy spectra of the evaporation residues are consistent with the assumption that pre-equilibrium emission from the projectile is negligible. These observations are compatible with the results of earlier inclusive measurements [1-10] of evaporation-residue velocity distributions which indicate that emission from the lighter reaction partner is dominant. The estimate that an upper limit of 35% of the evaporation residues arise from complete fusion is also in agreement with the systematics established by Morgenstern et al. [3] and supported by recent measurements [6-9]. This estimate was obtained by normalizing the PACE predictions for complete fusion to the maximum value consistent with the data with the assumption that pre-equilibrium emission from the projectile is negligible.

On the other hand, comparisons of the statistical-model predictions for complete fusion and equilibrium decay with the light-particle data suggests that there may be pre-equilibrium emission from the projectile. There appears to be beam-velocity components in the energy spectra at forward angles for both α particles (Fig. 4) and protons (Fig. 7). An α particle traveling with the beam

velocity would have an energy of 45 MeV, while a beam-velocity proton would have an energy of 11 MeV. Light particles traveling at the beam velocity are expected in the simplest pictures of incomplete-fusion due to pre-equilibrium emission from the projectile. Also, from a comparison of the experimental (squares) and calculated (solid curve) α-particle angular correlations shown in Fig. 5, it can be seen that the calculation underpredicts the data at forward angles as well as at backward angles. After subtracting the calculation from the data, we obtain the angular distribution of the apparent nonstatistical component shown as the diamonds in Fig. 5. This distribution is forward peaked and roughly symmetric around the beam which is also expected in the simplest pictures of incomplete-fusion due to pre-equilibrium emission from the projectile. There is also a second peak in the distribution centered around -70° which might be taken as evidence that some α particles escape from the projectile with a substantial transverse velocity component and not simply in the initial beam direction. Evidence for this type of process has been reported [25] for $^{12}C+^{197}Au$, ^{160}Gd, and ^{120}Sn reactions at E(^{12}C)=5.5 - 10 MeV/nucleon where it was found that the angular distributions for incomplete fusion peaked at significantly larger angles than those for complete fusion.

The proton differential multiplicities (squares) shown in Fig. 8 are overpredicted by the PACE calculation for complete fusion and equilibrium decay (solid curve) at most of the forward angles. As mentioned earlier, this may, at least in part, be due to the high-energy cut-offs in the proton energy spectra. If we assume that the shape of the calculation is correct and normalize it to the data at -55°, we obtain the dashed curve shown in the figure. Comparing the shape of the normalized calculation with the experimental distribution, an extra component is apparent. The angular distribution of this extra component was obtained by subtracting the renormalized calculation from the data and is shown as the diamonds in Fig. 8. As with the α correlations, this distribution is roughly symmetric around the beam direction and peaked at forward angles.

Another discrepancy between the data and the PACE calculation for complete fusion is that the high-energy slopes of the proton spectra measured at forward angles are steeper than the

predictions. A similar, although less dramatic, disagreement is seen for the α-particle spectra measured at forward angles on the opposite side of the beam from the heavy-ion detector. Statistical-model calculations for the formation of reduced compound nuclei that might be formed in a simple picture of incomplete fusion suggest that this is not a simple effect due to the presence of incomplete fusion.

Since nearly all of the light particles observed at backward angles ($\theta>65^{\circ}$ for α particles and $\theta>120^{\circ}$ for protons) in coincidence with evaporation residues are of pre-equilibrium origin, the large-angle spectra should provide a good test for pre-equilibrium-emission models. Shown in Fig. 10 are averaged proton energy spectra compared with the predictions of the nucleon-exchange-transport model for pre-equilibrium emission [18] (solid curves). The experimental distributions were obtained by averaging energy spectra taken at the same angle on either side of the beam to remove the experimental asymmetry and facilitate the comparison with the pre-equilibrium-emission model. The model overpredicts the high-energy portion of the energy spectra at forward angles. As one goes back in angle the agreement between the calculation and the data improves, and at 75° it is quite good. However, at backward angles the calculation overpredicts the spectra. Emission at backward angles is induced in the model by nucleons originating in the target and propagating through the projectile. Similar discrepancies between the predictions and data at backward angles have been observed previously [18].

V. SUMMARY

We have performed a detailed measurement of α particles and protons emitted in coincidence with evaporation residues produced in the $^{40}Ca+^{12}C$ reaction using a pulsed 450-MeV ^{40}Ca beam from the ATLAS facility. The evaporation residues were detected and Z-identified with a large-solid-angle, time-of-flight detector system. Energy spectra were obtained for each evaporation-residue Z group. These energy spectra are shifted to higher energy than expected for complete fusion indicating the presence of significant incomplete fusion due to pre-equilibrium emission

from the ^{12}C target. The shape of the evaporation-residue energy spectra are consistent with the assumption that incomplete fusion due to emission from the projectile is negligible. Comparisons of the evaporation-residue energy spectra with statistical-model predictions for complete fusion suggest that at most 35% of the evaporation residues arise from complete fusion.

Energy and angular distributions were generated for α particles and protons in coincidence with each evaporation-residue Z group. The light-particle yields at backward angles are much larger than predicted by the statistical model and expected from reaction kinematics for complete fusion and equilibrium decay, indicating the presence of considerable pre-equilibrium emission of both α particles and protons from the ^{12}C target. Comparisons of the forward-angle, light-particle data with statistical-model predictions for complete fusion also suggest that there may be pre-equilibrium emission from the projectile in contradiction with the results from the evaporation-residue energy spectra.

We have also compared the averaged proton energy spectra with the predictions of the nucleon-exchange-transport model for pre-equilibrium emission [18]. While the agreement between the calculation and the data is reasonable at 75°, the calculated proton spectra are harder than the data at forward angles and overpredict the yields at backward angles.

ACKNOWLEDGMENTS

We would like to thank Prof. R. Vandenbosch for performing calculations with the nucleon-exchange-transport model. This work was supported by the U.S. Department of Energy under Contract Nos. DE-FG05-88ER40459 and W-31-109-ENG-38.

REFERENCES

[1] H. Morgenstern, W. Bohne, K. Grabisch, D. G. Kovar, and H. Lehr, Phys. Lett. **113B**, 463 (1982); H. Morgenstern, W. Bohne, K. Grabisch, H. Lehr, and W. Stoffler, Z. Phys. **A313**, 39 (1983).

[2] Y. Chan, M. Murphy, R. G. Stokstad, I. Tserruya, S. Wald, and A. Budzanowski, Phys. Rev. **C27**, 447 (1983).

[3] H. Morgenstern, W. Bohne, W. Galster, K. Grabisch, and A. Kyanowski, Phys. Rev. Lett. **52**, 1104 (1984).

[4] G. Rosner, J. Pochodzalla, B. Heck, G. Hlawatsch, A. Miczaika, J. H. Rabe, R. Butsch, B. Kolb, and B. Sedelmeyer, Phys. Lett. **150B**, 87 (1985).

[5] G. S. F. Stephans, D. G. Kovar, R. V. F. Janssens, G. Rosner, H. Ikezoe, B. Wilkins, D. Henderson, K. T. Lesko, J. J. Kolata, C. K. Gelbke, B. V. Jacack, Z. M. Koenig, G. D. Westfall, A. Szanto De Toledo, E. M. Szanto, and P. L. Gonthier, Phys. Lett. **161B**, 60 (1985).

[6] C. Beck, D. G. Kovar, S. J. Sanders, B. D. Wilkins, D. J. Henderson, R. V. F. Janssens, W. C. Ma, M. F. Vineyard, T. F. Wang, C. F. Maguire, F. W. Prosser, and G. Rosner, Phys. Rev. **C39**, 2202 (1989).

[7] M. F. Vineyard, J. S. Bauer, C. H. Gosdin, R. S. Trotter, D. G. Kovar, C. Beck, D. J. Henderson, R. V. F. Janssens, B. D. Wilkins, G. Rosner, P. Chowdhury, H. Ikezoe, W. Kuhn, J. J. Kolata, J. D. Hinnefeld, C. F. Maguire, J. F. Mateja, F. W. Prosser, and G. S. F. Stephans, Phys. Rev. **C41**, 1005 (1990).

[8] M. F. Vineyard, J. S. Bauer, J. F. Crum, C. H. Gosdin, R. S. Trotter, D. G. Kovar, C. Beck, D. J. Henderson, R. V. F. Janssens, B. D. Wilkins, C. F. Maguire, J. F. Mateja, F. W. Prosser, and G. S. F. Stephans, Phys. Rev. **C45**, 1784 (1992).

[9] M. F. Vineyard, J. F. Mateja, C. Beck, S. E. Atencio, L. C. Dennis, A. D. Frawley, D. J. Henderson, R. V. F. Janssens, K. W. Kemper, D. G. Kovar, C. F. Maguire, S. J. Padalino, F. W. Prosser, G. S. F. Stephans, M. A. Tiede, B. D. Wilkins, and R. A.

Zingarelli, Phys. Rev. **C47**, 2374 (1993).

[10] G. P. Gilfoyle, M. S. Gordon, R. L. McGrath, G. Auger, J. M. Alexander, D. G. Kovar, M. F. Vineyard, C. Beck, D. J. Henderson, P. A. DeYoung, and D. Kortering, Phys. Rev. **C46**, 265 (1992).

[11] H. Morgenstern, W. Bohne, W. Galster, and K. Grabisch, Z. Phys. **A324**, 443 (1986).

[12] H. Ikezoe, N. Shikazono, Y. Tomita, Y. Sugiyama, and K. Ideno, Nucl. Phys. **A462**, 150 (1987).

[13] P. Gonthier, H. Ho, M. N. Namboodiri, L. Adler, J. B. Natowitz, S. Simon, K Hagel, R. Terry, and A. Khodai, Phys. Rev. Lett. **44**, 1387 (1980); P. L. Gonthier, H. Ho, M. N. Namboodiri, J. B. Natowitz, L. Adler, S. Simon, K Hagel, S. Kniffen, and A. Khodai, Nucl. Phys. **A411**, 289 (1983).

[14] K. A. Griffioen, E. A. Bakkum, P. Decowski, R. J. Meijer, and R. Kamermans, Phys. Rev. **C37**, 2502 (1988).

[15] J. Gomez del Campo, D. E. DiGregorio, J. A. Biggerstaff, Y. D. Chan, D. C. Hensley, P. H. Stelson, D. Shapira, and M. E. Ortiz, Phys. Rev. **C35**, 137 (1987).

[16] S. Leray, G. La Rana, C. Ngo, M. Barranco, M. Pi, and X.Vinas, Z. Phys. **A320**, 383 (1985).

[17] K. Mohring, W. J. Swiatecki, and M. Zielinska-Pfabe, Nucl.. Phys. **A440**, 89 (1985).

[18] J. Randrup and R. Vandenbosch, Nucl. Phys. **A474**, 2129 (1987); S. J. Luke, R. Vandenbosch, and J. Randrup, to be published in Phys. Rev. C.

[19] M. Blann, Phys. Rev. C31, 295 (1985); M. Blann, Phy. Rev. **C32**, 1231 (1985).

[20] C. Gregoire, B. Remaud, F. Scheuter, and F. Sebille, Nucl. Phys. **A436**, 365 (1985).

[21] M. F. Vineyard, B. D. Wilkins, D. J. Henderson, D. G. Kovar, C. Beck, C. N. Davids, and J. J. Kolata, Nucl. Instr. and Meth. **A255**, 507 (1987).

[22] PACE is the modification of the code JULIAN described by A. Gavron, Phys. Rev. **C21**, 230 (1980).

[23] P. Frobrich, Phys. Rep. **116**, 337 (1984).

[24] J. Gomez del Campo and R. G. Stokstad, Oak Ridge National Laboratory Technical Report No. ORNL-TM-7295 (1981).

[25] I. Tserruya, V. Steiner, Z. Fraenkel, P. Jacobs, D. G. Kovar, W. Henning, M. F. Vineyard, and B. G. Glagola, Phys. Rev. Lett. 60, **14** (1988).

FIGURE CAPTIONS

FIG. 1. Two-dimensional spectrum of energy versus range of heavy ions detected in the Bragg-Curve Spectrometer for $^{40}Ca+^{12}C$ at $E(^{40}Ca)=450$ MeV and $\theta_{HI}=4.5°$. A gate on the two-dimensional energy versus time-of-flight spectrum was used to exclude quasielastic events from this spectrum.

FIG. 2. Two-dimensional spectrum of energy deposited in the ΔE detector versus time-of-flight (TOF) for light particles detected at -55° in coincidence with evaporation residues detected at 4.5° for $^{40}Ca+^{12}C$ at $E(^{40}Ca)=450$ MeV. The negative angle refers to the opposite side of the beam from the heavy-ion detector. The fold-over exhibited in the spectrum is due to the fact that the high-energy particles are not stopped in the ΔE detector.

FIG. 3. Energy spectrum of Sc residues detected at 4.5° for $^{40}Ca+^{12}C$ at $E(^{40}Ca)=450$ MeV. The solid curve is the result of a PACE [22] calculation for the complete-fusion equilibrium-decay process.

FIG. 4. Energy spectra of α particles detected in coincidence with evaporation residues ($12\leq Z_{ER}\leq 24$) observed at 4.5°. Negative and positive angles refer to the opposite and same side of the beam as the heavy-ion detector, respectively. The solid curves are the results of PACE [22] calculations for the complete-fusion and equilibrium-decay process.

FIG. 5. Angular correlation of α particles with evaporation residues ($12\leq Z_{ER}\leq 24$) detected at 4.5° (squares). The solid curve is the result of the complete-fusion and equilibrium-decay calculation performed with the code PACE [22]. The diamonds indicate the angular distribution of pre-equilibrium (PE) α particles obtained by subtracting the calculation from the data.

FIG. 6. Angular correlations of α particles with residues of K, Ca, and Sc detected at 4.5°. The

solid curves are the results of PACE [22] calculations for the complete-fusion and equilibrium-decay process.

FIG. 7. Energy spectra of protons detected in coincidence with evaporation residues ($12 \leq Z_{ER} \leq 24$) observed at 4.5°. Negative and positive angles refer to the opposite and same side of the beam as the heavy-ion detector, respectively. The solid curves are the results of PACE [22] calculations for the complete-fusion and equilibrium-decay process.

FIG. 8. Angular correlation of protons with evaporation residues ($12 \leq Z_{ER} \leq 24$) detected at 4.5° (squares). The solid curve is the result of the complete-fusion and equilibrium-decay calculation performed with the code PACE [22]. The dashed curve is the calculation normalized to the data at θ_p=-55°. The diamonds indicate the angular distribution of pre-equilibrium (PE) protons obtained by subtracting the renormalized calculation from the data.

FIG. 9. Angular correlations of protons with residues of K, Ca, and Sc detected at 4.5°. The solid curves are the results of PACE [22] calculations for the complete-fusion and equilibrium-decay process.

FIg. 10. Averaged energy spectra of protons detected in coincidence with evaporation residues ($12 \leq Z_{ER} \leq 24$) observed at 4.5°. The spectra were obtained by averaging the energy spectra taken at the same angle on either side of the beam. The solid curves are the results of calculations with the nucleon-exchange transport model for pre-equilibrium emission [18].

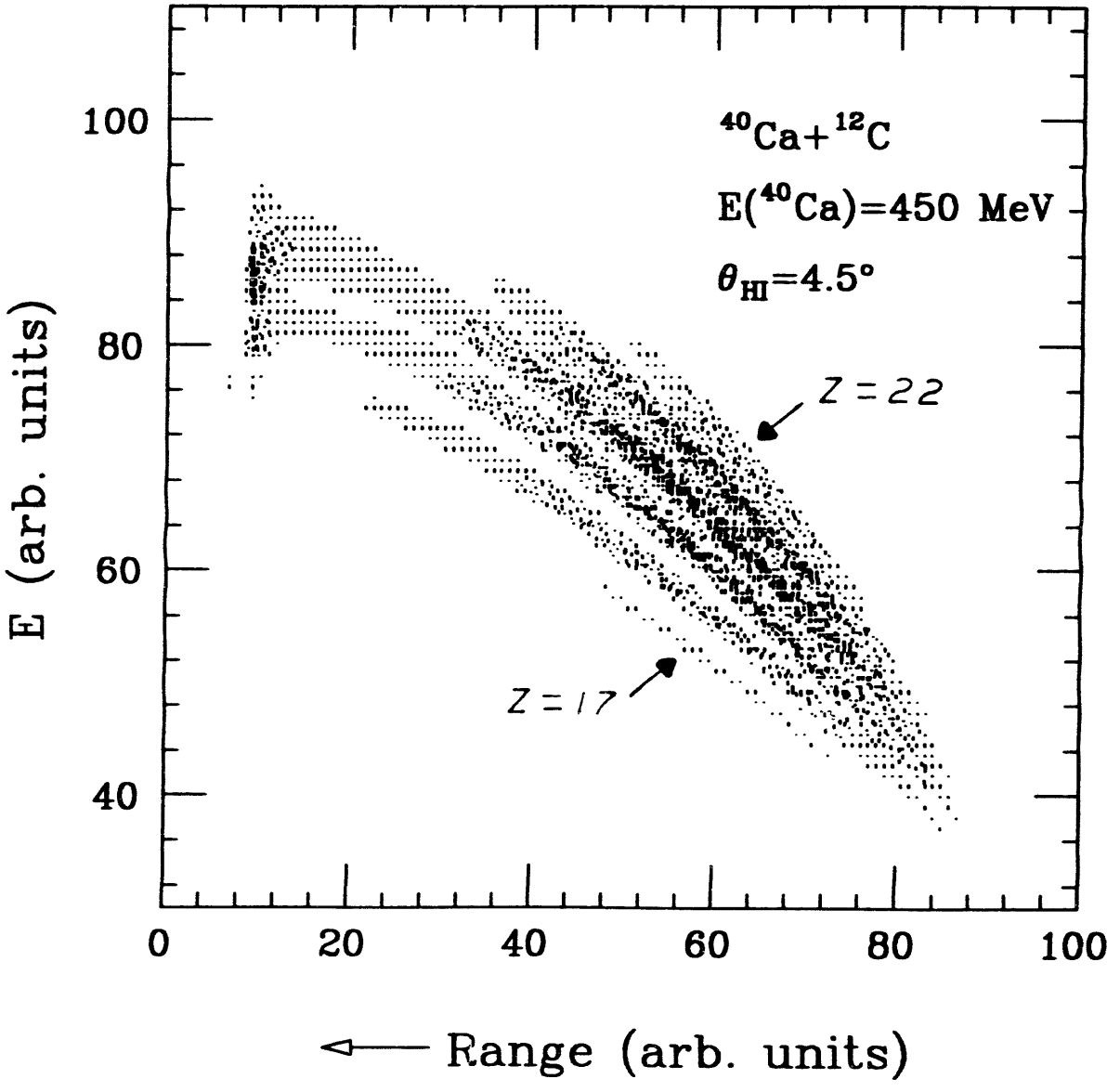
$^{40}Ca+^{12}C$
E(^{40}Ca)=450 MeV
θ_{HI}=4.5°
Z = 22
Z = 17
E (arb. units)
100
80
60
40
0
20
40
60
80
100
Range (arb. units)

Fig 1

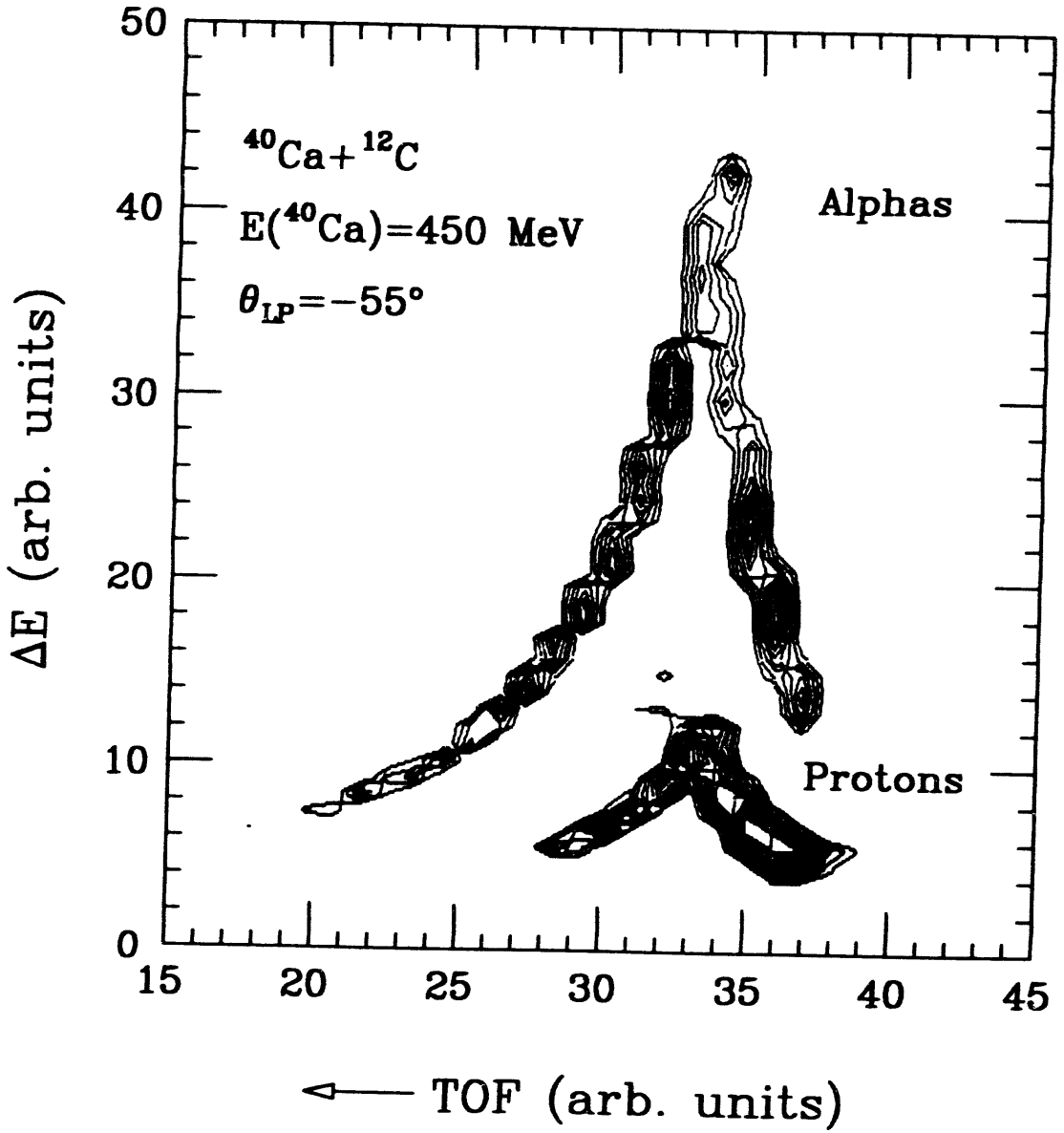
50
40
30
20
10
0
15
20
25
30
35
40
45
ΔE (arb. units)
← TOF (arb. units)
$^{40}Ca+^{12}C$
E(^{40}Ca)=450 MeV
θ_{LP}=−55°
Alphas
Protons

Fig 2

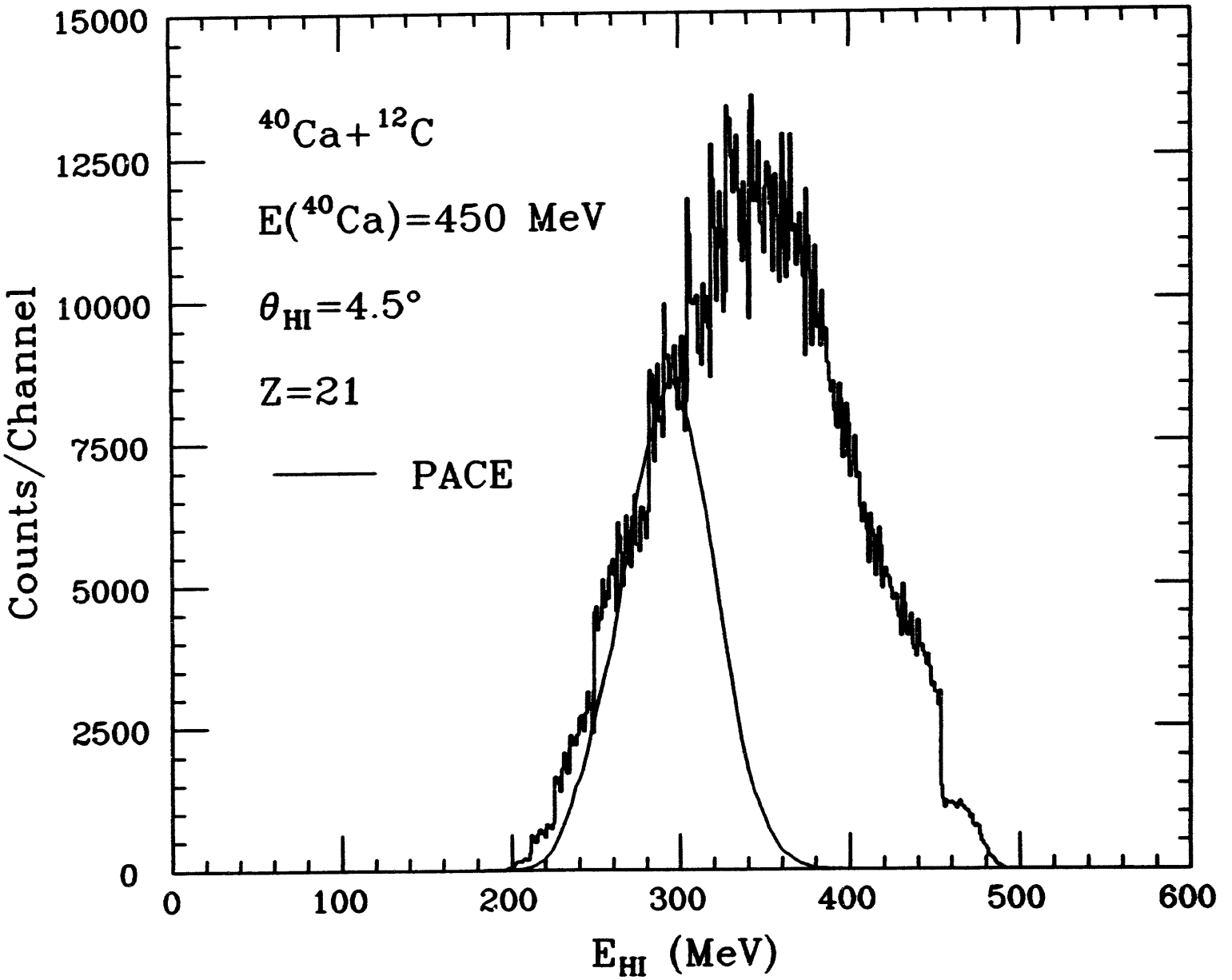
15000
12500
10000
7500
5000
2500
0
Counts/Channel
$^{40}Ca+^{12}C$
E(^{40}Ca)=450 MeV
θ_{HI}=4.5°
Z=21
PACE
0
100
200
300
400
500
600
E_{HI} (MeV)

Fig 3

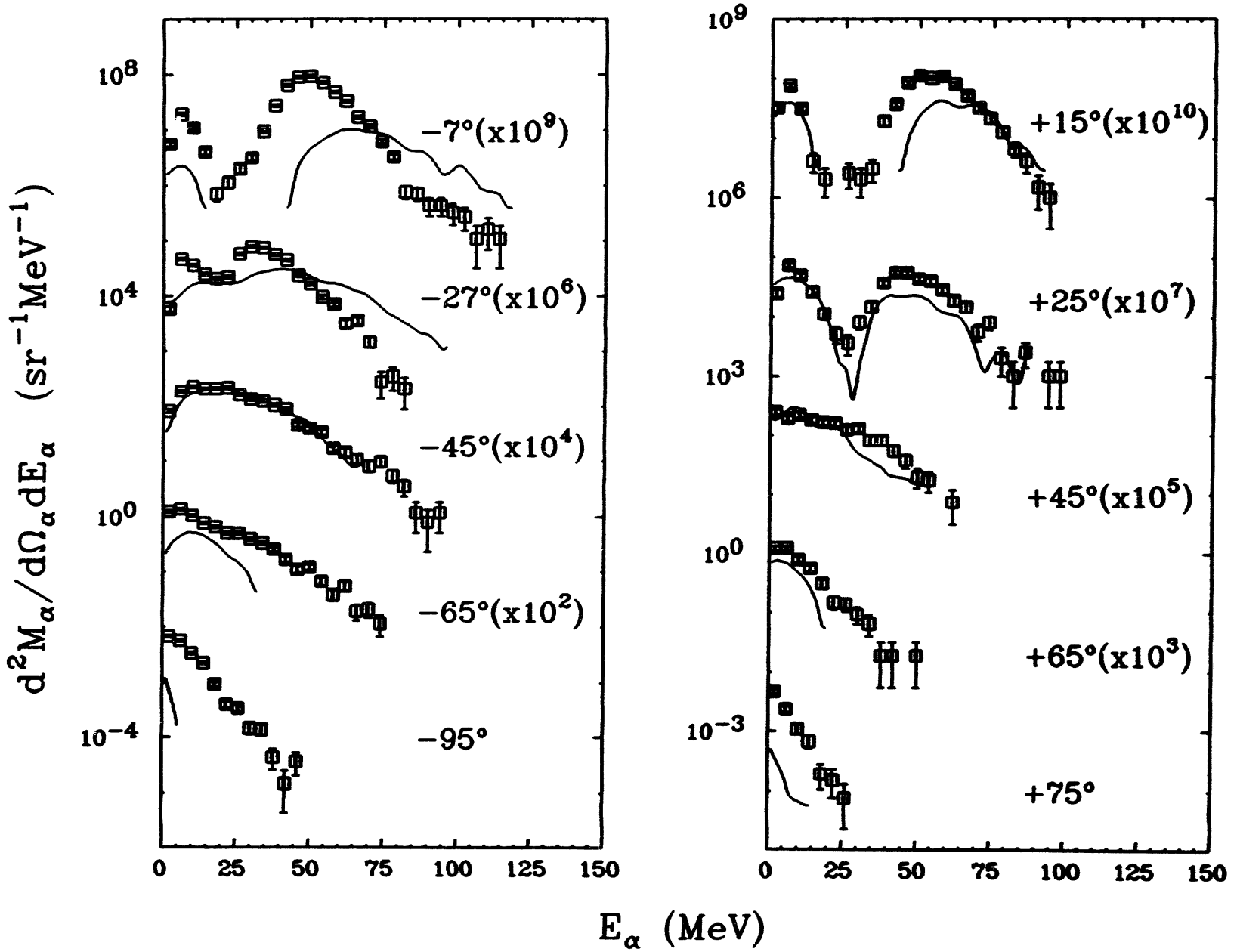
$d^2M_\alpha/d\Omega_\alpha dE_\alpha$ (sr^{-1}MeV^{-1})
E_α (MeV)
−7°(x10^9)
−27°(x10^6)
−45°(x10^4)
−65°(x10^2)
−95°
+15°(x10^{10})
+25°(x10^7)
+45°(x10^5)
+65°(x10^3)
+75°
10^8
10^4
10^0
10^{-4}
10^9
10^6
10^3
10^0
10^{-3}
0
25
50
75
100
125
150

Fig 4

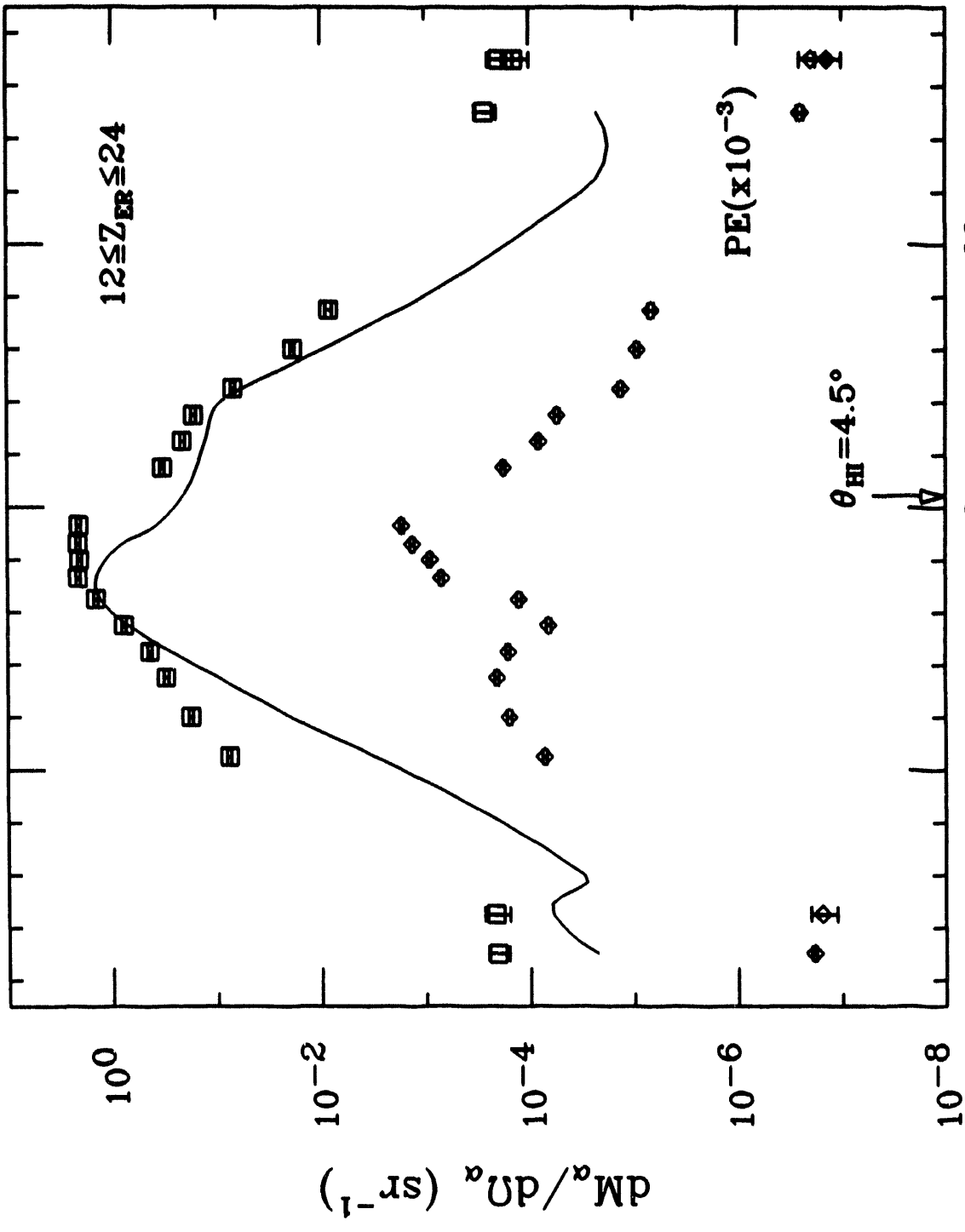
$dM_\alpha/d\Omega_\alpha$ (sr^{-1})
10^0
10^{-2}
10^{-4}
10^{-6}
10^{-8}
$12 \leq Z_{ER} \leq 24$
PE(x10^{-3})
θ_{HI}=4.5°
-100
0
100
θ_α (deg)

Fig 5

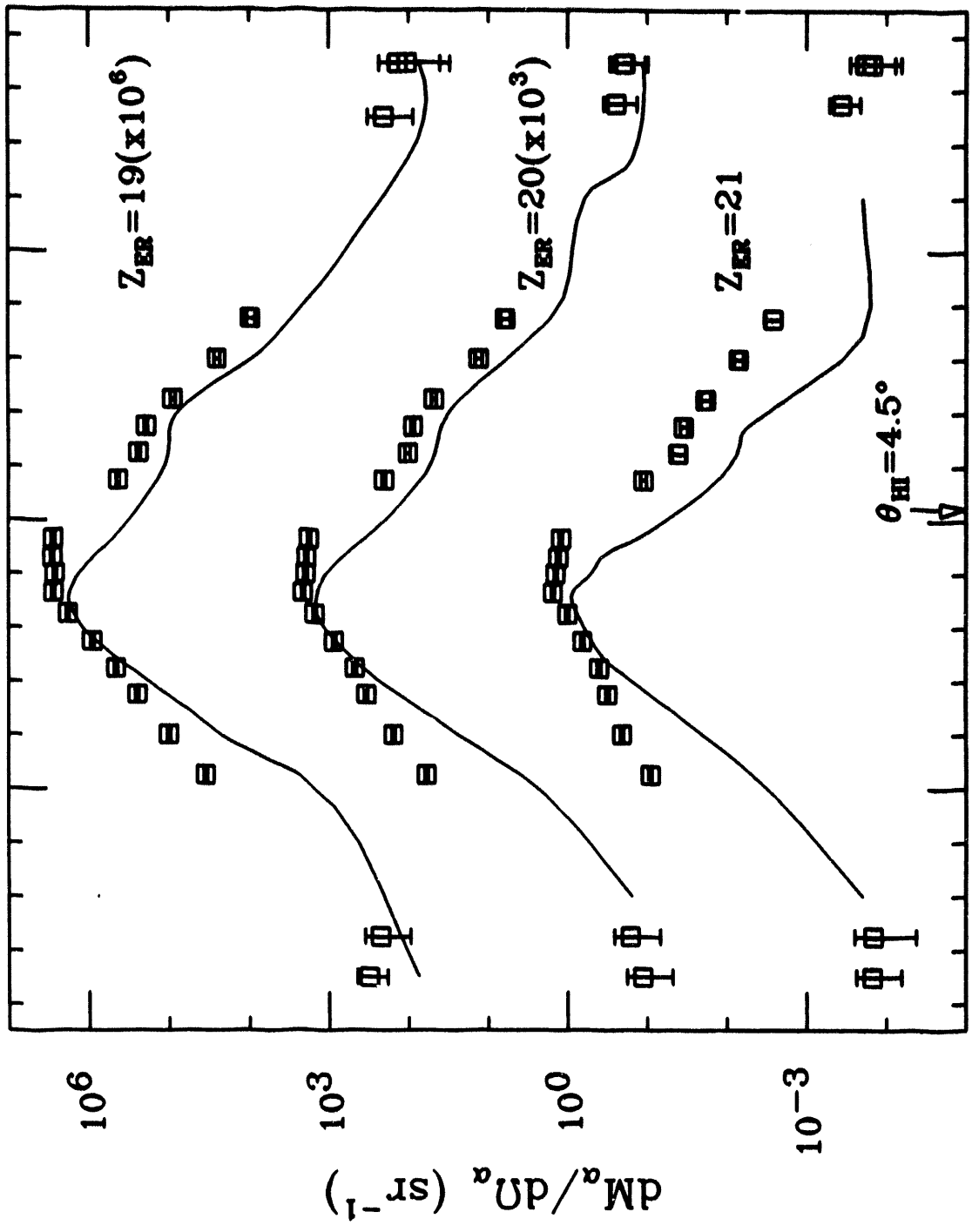
$dM_\alpha/d\Omega_\alpha$ (sr^{-1})
10^6
10^3
10^0
10^{-3}
Z_{ER}=19(x10^6)
Z_{ER}=20(x10^3)
Z_{ER}=21
θ_{HI}=4.5°
-100
0
100
θ_α (deg)

Fig 6

2 of 2

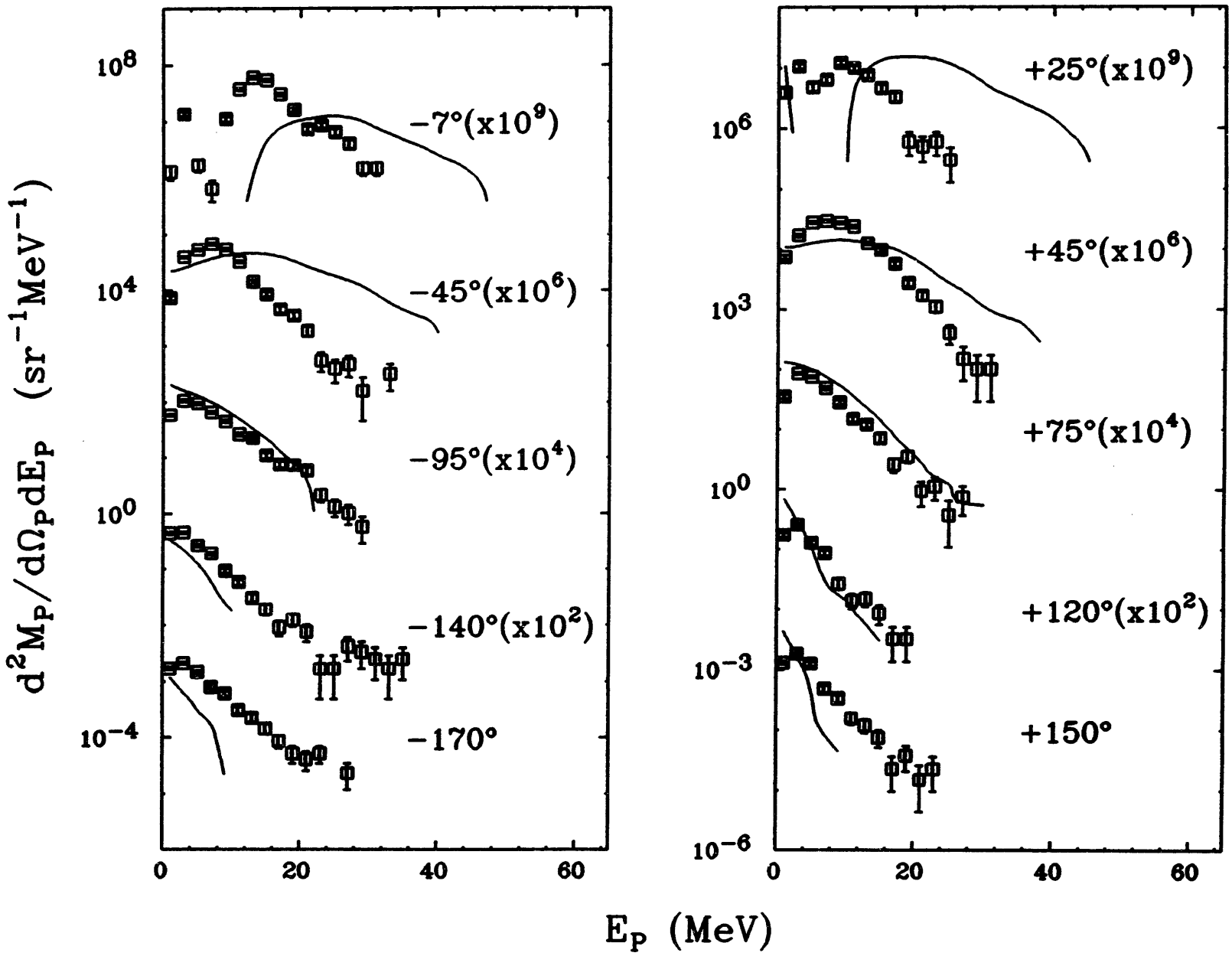
$d^2M_P/d\Omega_P dE_P$ (sr^{-1}MeV^{-1})
10^8
10^4
10^0
10^{-4}
10^6
10^3
10^0
10^{-3}
10^{-6}
−7°(x10^9)
−45°(x10^6)
−95°(x10^4)
−140°(x10^2)
−170°
+25°(x10^9)
+45°(x10^6)
+75°(x10^4)
+120°(x10^2)
+150°
0
20
40
60
E_P (MeV)

Fig 7

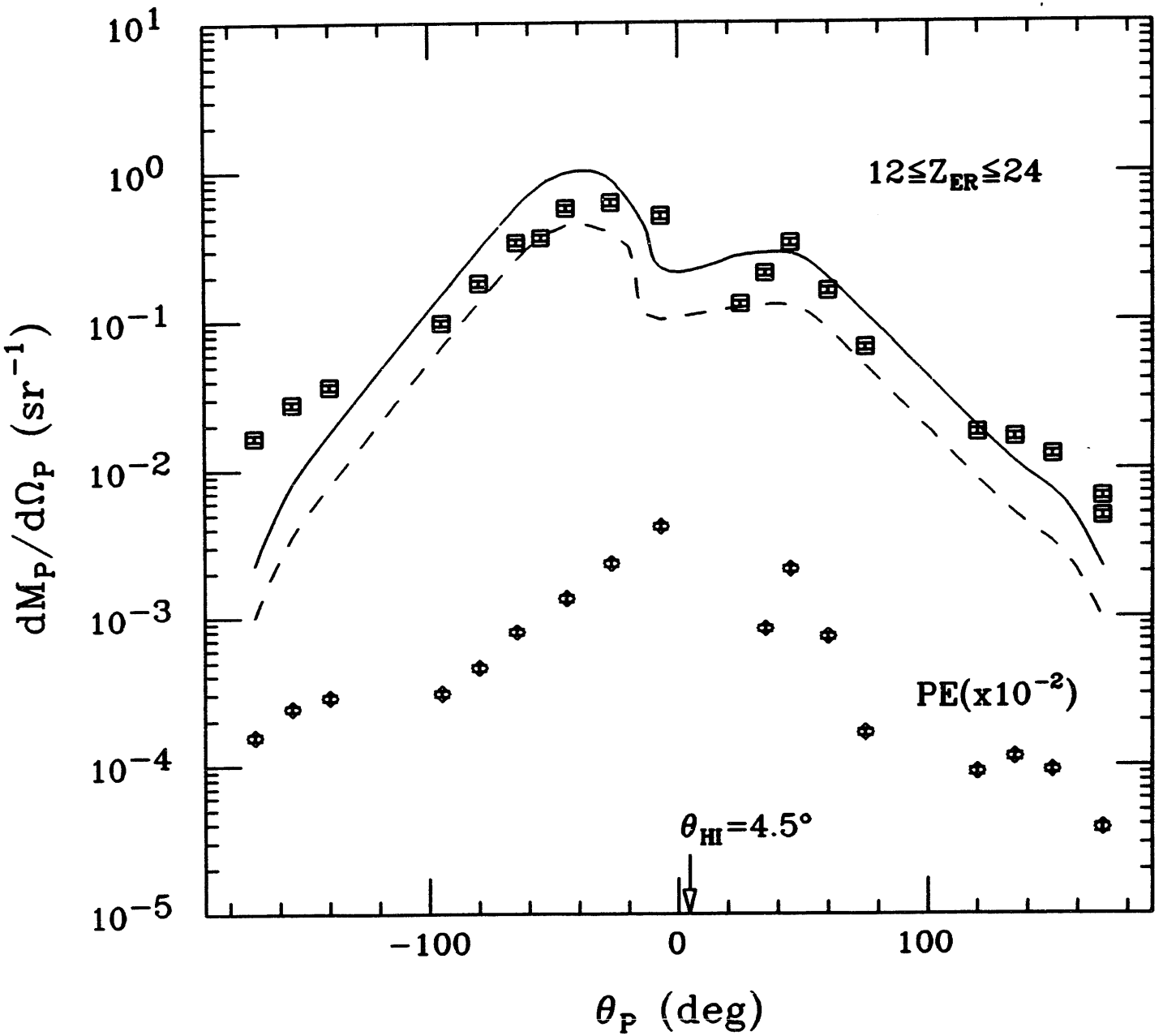
10^1
10^0
10^{-1}
10^{-2}
10^{-3}
10^{-4}
10^{-5}
$dM_P/d\Omega_P$ (sr^{-1})
$12 \leq Z_{ER} \leq 24$
PE(x10^{-2})
θ_{HI}=4.5°
-100
0
100
θ_P (deg)

Fig 8

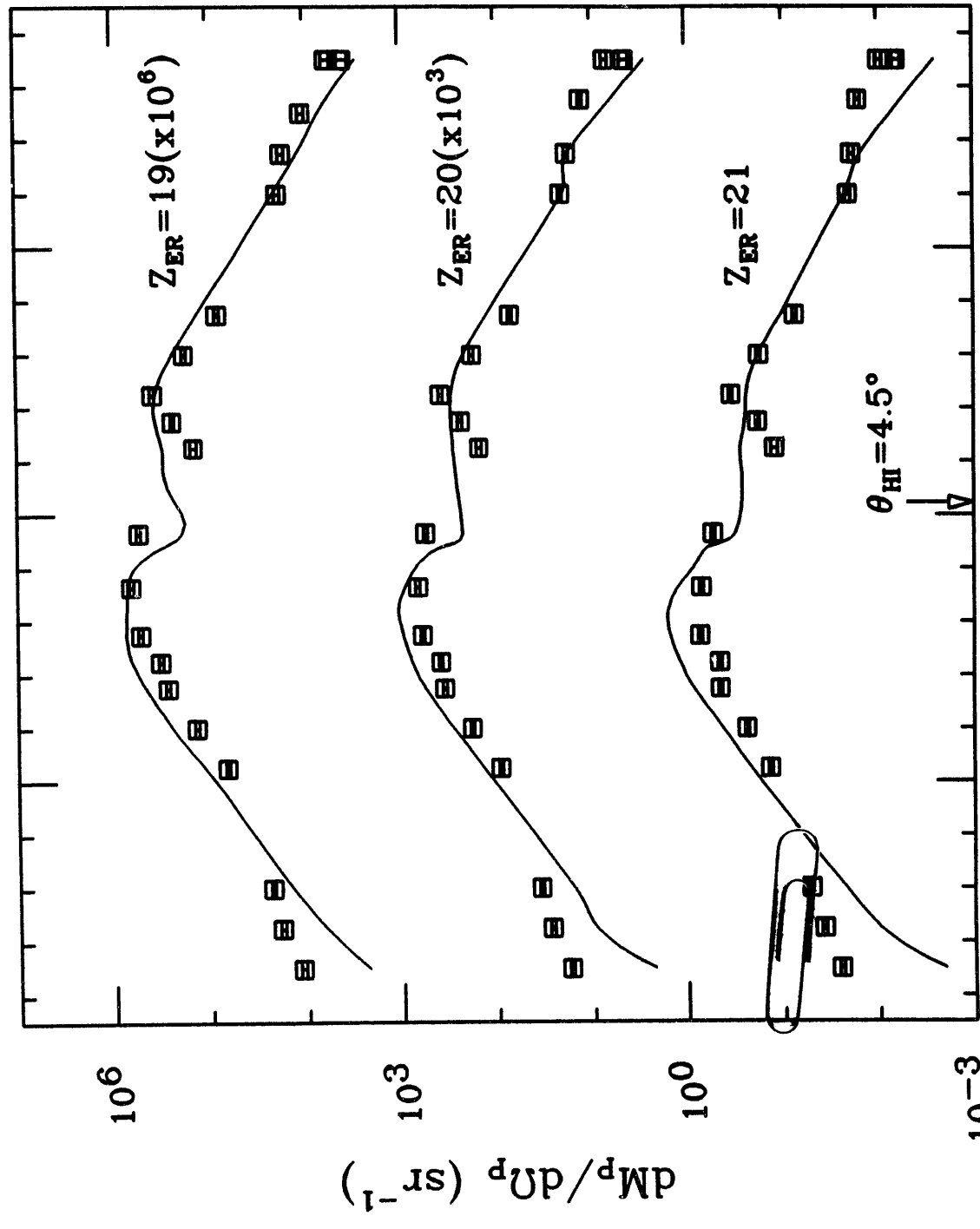
Z_{ER}=19(x10^6)
Z_{ER}=20(x10^3)
Z_{ER}=21
θ_{HI}=4.5°
10^6
10^3
10^0
10^{-3}
$dM_p/d\Omega_p$ (sr^{-1})
-100
0
100
θ_P (deg)

Fig 9

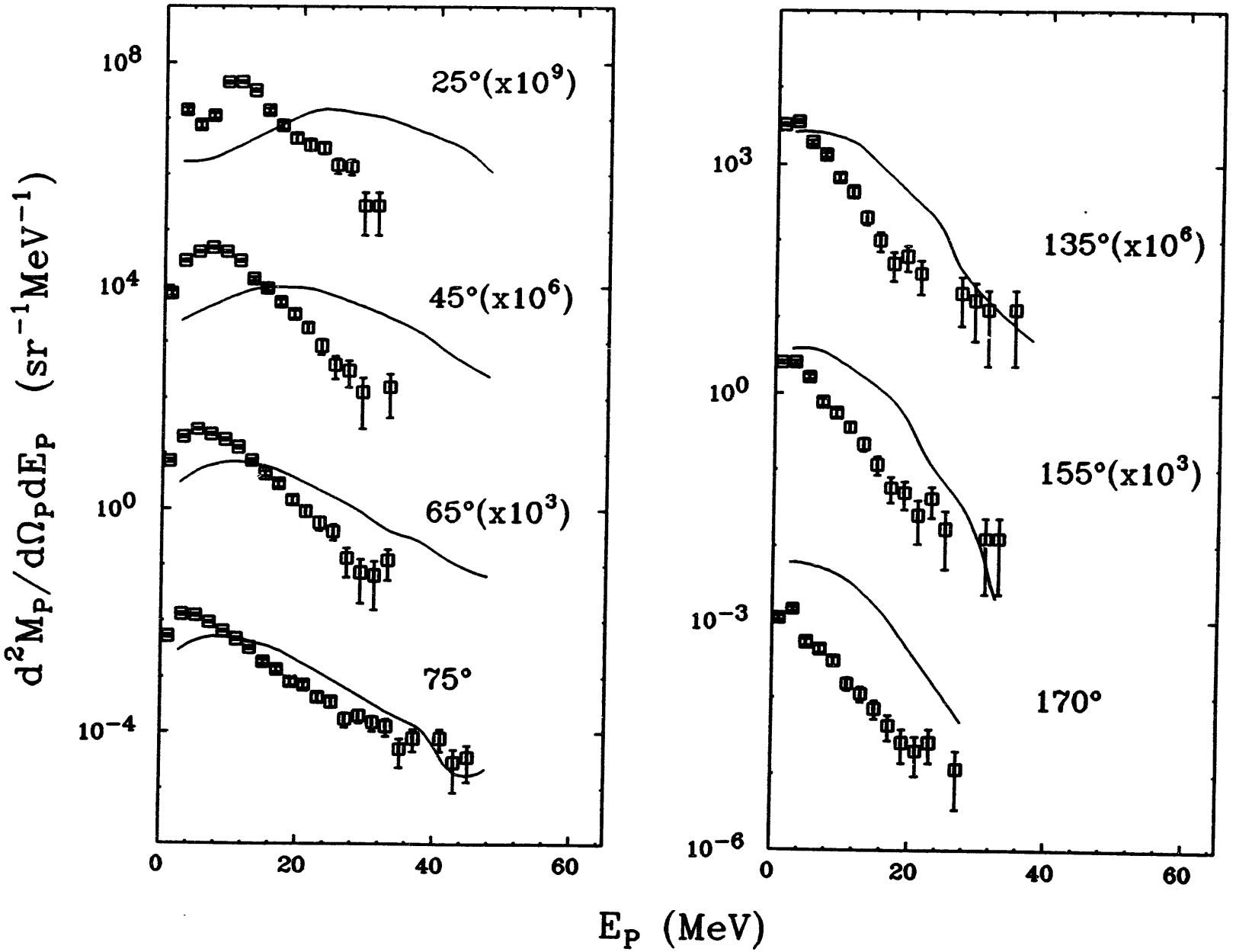
$d^2M_P/d\Omega_P dE_P$ (sr^{-1}MeV^{-1})
10^8
10^4
10^0
10^{-4}
25°(x10^9)
45°(x10^6)
65°(x10^3)
75°
10^3
10^0
10^{-3}
10^{-6}
135°(x10^6)
155°(x10^3)
170°
0
20
40
60
E_P (MeV)

Fig 10

Coincidence Measurements of Light Particles and Heavy Ions in the $^{28}Si + ^{24}Mg$ Reaction

Vineyard, Atencio, Cardounel, Gilfoyle, Glagola, Henderson, Mateja, Ohl, Prosser, Snyder, and Wuosma

We have measured the charged, light particles in coincidence with heavy ions produced in the $^{28}Si + ^{24}Mg$ reaction at E(^{28}Si) = 315 and 400 MeV. This system forms the same complete-fusion compound nucleus (^{52}Fe) as the $^{40}Ca + ^{12}C$ system studied in our earlier work [1]. The two sets of data will enable us to investigate the mass-asymmetry dependence of the incomplete-fusion process which has been suggested in previous studies of inclusive evaporation-residue velocity spectra [2-11]. The 315-MeV bombarding energy permits the study of this system at the same relative center-of-mass velocity at the Coulomb barrier as the $^{40}Ca + ^{12}C$ reaction at E(^{40}Ca) = 450 MeV. The measurements at 400 MeV were made to investigate the energy dependence of the pre-equilibrium emission process.

The experiment was performed with pulsed ^{28}Si beams obtained from the Argonne National Laboratory ATLAS facility. The time resolution of the beam pulses was approximately 300 ps (FWHM) with a period of 82.5 ns. The beams were incident on a 227 $\mu g/cm^2$ ^{24}Mg target mounted in the ATLAS 91-cm scattering chamber. The heavy ions were detected at 6° in a large solid-angle time-of-flight detector system [12]. This system consists of a parallel-plate avalanche counter for timing and position information and a Bragg-Curve Spectrometer [13] to obtain the energy and Z-identification of the heavy ions. The detector was mounted on the vacuum extension box of the scattering chamber at a distance of 1.00 m from the target and subtended a solid angle of 5.5 msr. The Z-resolution is illustrated in Fig. 1 where the Bragg peak is plotted as a function of the range of the heavy ions detected in the Bragg-Curve Spectrometer.

The light particles were measured at 20 in-plane angles and four out-of-plane angles with twelve telescopes consisting of surface barrier ΔE detectors and lithium-drifted silicon E detectors. The distance of these telescopes from the target ranged from 19.5 to 40.0 cm. Identification of the light particles was achieved using the rf beam timing of ATLAS.

The data are being analyzed by undergraduate students at the University of Richmond. The energy and time-of-flight calibrations have been determined and software gates have been

constructed to isolate each of the heavy-ion Z groups and light-particle species. The data tapes are being read to construct the energy and angular distributions of protons and α particles in coincidence with each of the heavy-ion Z groups. These distributions will be compared with the results of model calculations and the complimentary data for the $^{40}Ca + ^{12}C$ system in an attempt to gain some insight on the apparent mass-asymmetry dependence of incomplete fusion.

Shown in Fig. 2 is an energy spectrum of evaporation residues with Z = 18 produced at a bombarding energy of 315 MeV and detected at a laboratory angle of 6°. The solid line is the result of a PACE [14] calculation for complete fusion and equilibrium decay. The experimental energy distribution is shifted to higher energy than predicted by the PACE calculation indicating significant incomplete fusion due to pre-equilibrium emission from the ^{28}Si projectile.

References

[1] M. F. Vineyard, S. E. Atencio, J. F. Crum, G. P. Gilfoyle, B. G. Glagola, D. J. Henderson, D. G. Kovar, C. F. Maguire, J. F. Mateja, R. G. Ohl, F. W. Prosser, J. H. Rollinson, and R. S. Trotter, accepted for publication in Phys. Rev. C.

[2] H. Morgenstern, W. Bohne, K. Grabisch, D. G. Kovar, and H. Lehr, Phys. Lett. **113B**, 463 (1982); H. Morgenstern, W. Bohne, K. Grabisch, H. Lehr, and W. Stoffler, Z. Phys. **A313**, 39 (1983).

[3] Y. Chan, M. Murphy, R. G. Stokstad, I. Tserruya, S. Wald, and A. Budzanowski, Phys. Rev. **C27**, 447 (1983).

[4] H. Morgenstern, W. Bohne, W. Galster, K. Grabisch, and A. Kyanowski, Phys. Rev. Lett. **52**, 1104 (1984).

[5] G. Rosner, J. Pochodzalla, B. Heck, G. Hlawatsch, A. Miczaika, J. H. Rabe, R. Butsch, B. Kolb, and B. Sedelmeyer, Phys. Lett. **150B**, 87 (1985).

[6] G. S. F. Stephans, D. G. Kovar, R. V. F. Janssens, G. Rosner, H. Ikezoe, B. Wilkins, D. Henderson, K. T. Lesko, J. J. Kolata, C. K. Gelbke, B. V. Jacack, Z. M. Koenig, G. D. Westfall, A. Szanto De Toledo, E. M. Szanto, and P. L. Gonthier, Phys. Lett. **161B**, 60

(1985).

[7] C. Beck, D. G. Kovar, S. J. Sanders, B. D. Wilkins, D. J. Henderson, R. V. F. Janssens, W. C. Ma, M. F. Vineyard, T. F. Wang, C. F. Maguire, F. W. Prosser, and G. Rosner, Phys. Rev. **C39**, 2202 (1989).

[8] M. F. Vineyard, J. S. Bauer, C. H. Gosdin, R. S. Trotter, D. G. Kovar, C. Beck, D. J. Henderson, R. V. F. Janssens, B. D. Wilkins, G. Rosner, P. Chowdhury, H. Ikezoe, W. Kuhn, J. J. Kolata, J. D. Hinnefeld, C. F. Maguire, J. F. Mateja, F. W. Prosser, and G. S. F. Stephans, Phys. Rev. **C41**, 1005 (1990).

[9] M. F. Vineyard, J. S. Bauer, J. F. Crum, C. H. Gosdin, R. S. Trotter, D. G. Kovar, C. Beck, D. J. Henderson, R. V. F. Janssens, B. D. Wilkins, C. F. Maguire, J. F. Mateja, F. W. Prosser, and G. S. F. Stephans, Phys. Rev. **C45**, 1784 (1992).

[10] M. F. Vineyard, J. F. Mateja, C. Beck, S. E. Atencio, L. C. Dennis, A. D. Frawley, D. J. Henderson, R. V. F. Janssens, K. W. Kemper, D. G. Kovar, C. F. Maguire, S. J. Padalino, F. W. Prosser, G. S. F. Stephans, M. A. Tiede, B. D. Wilkins, and R. A. Zingarelli, Phys. Rev. **C47**, 2374 (1993).

[11] G. P. Gilfoyle, M. S. Gordon, R. L. McGrath, G. Auger, J. M. Alexander, D. G. Kovar, M. F. Vineyard, C. Beck, D. J. Henderson, P. A. DeYoung, and D. Kortering, Phys. Rev. **C46**, 265 (1992).

[12] B. Wilkins, D. Henderson, C. Beck, B. Glagola, D. G. Kovar, and T. Wang, Bull. Am. Phys. Soc. **32**, 1032 (1987).

[13] M. F. Vineyard, B. D. Wilkins, D. J. Henderson, D. G. Kovar, C. Beck, C. N. Davids, and J. J. Kolata, Nucl. Instr. and Meth. **A255**, 507 (1987).

[14] PACE is the modification of the code JULIAN described by A. Gavron, Phys. Rev. **C21**, 230 (1980).

Figure Caption

Fig. 1 Two-dimensional spectrum of Bragg peak versus range of heavy ions detected in the Bragg-Curve Spectrometer for $^{28}Si+^{24}Mg$ at $E(^{40}Ca)=400$ MeV and $\theta_{HI}=6^{o}$. A gate on the two-dimensional energy versus time-of-flight spectrum was used to exclude quasielastic events from this spectrum.

Fig. 2. Energy spectrum of Z=18 residues detected at 6° for $^{28}Si+^{24}Mg$ at $E(^{28}Si)=315$ MeV. The solid curve is the result of a PACE [14] calculation for the complete-fusion equilibrium-decay process.

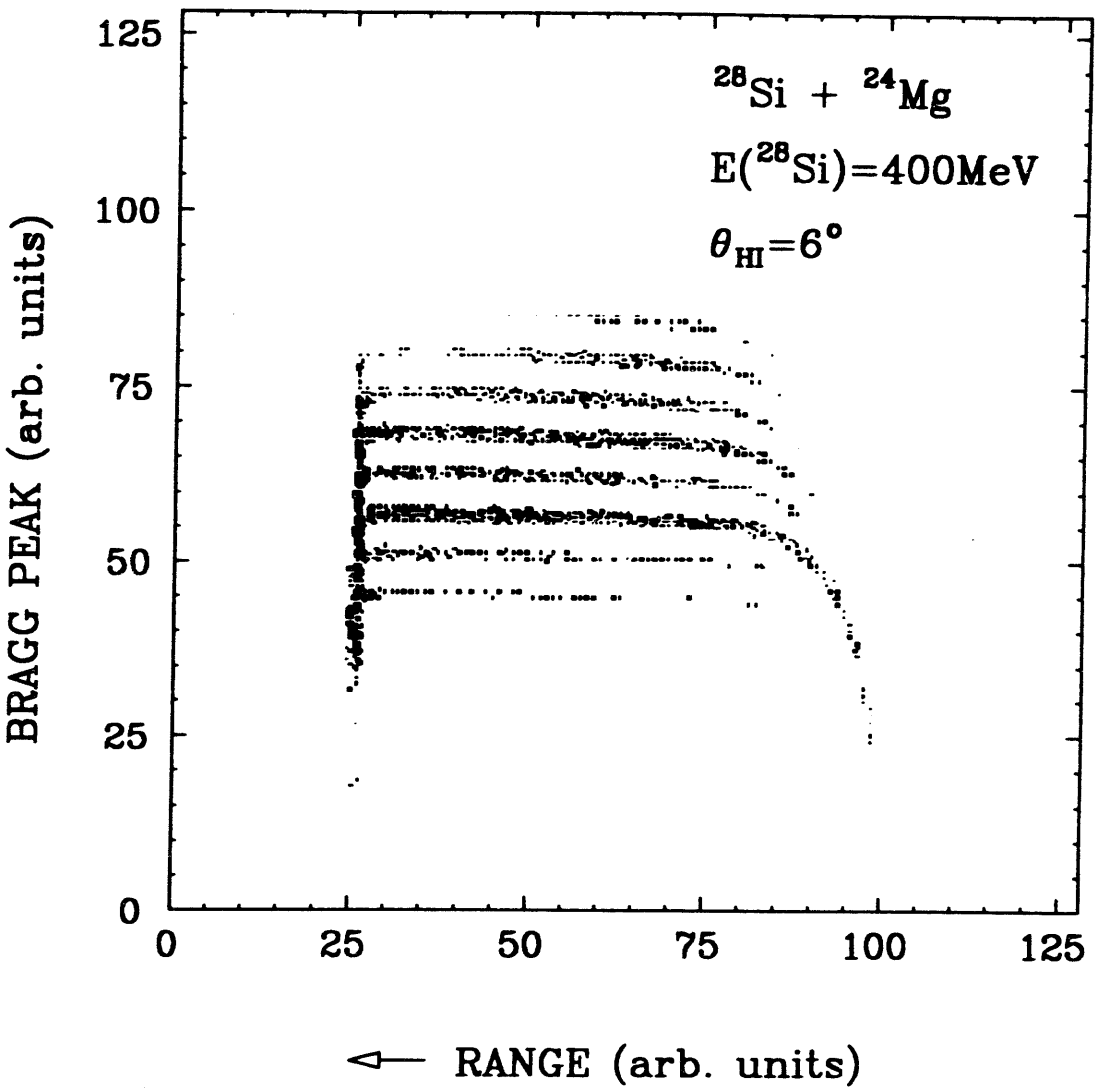
^{28}Si + ^{24}Mg
E(^{28}Si)=400MeV
θ_{HI}=6°
BRAGG PEAK (arb. units)
RANGE (arb. units)
0
25
50
75
100
125

Fig 1

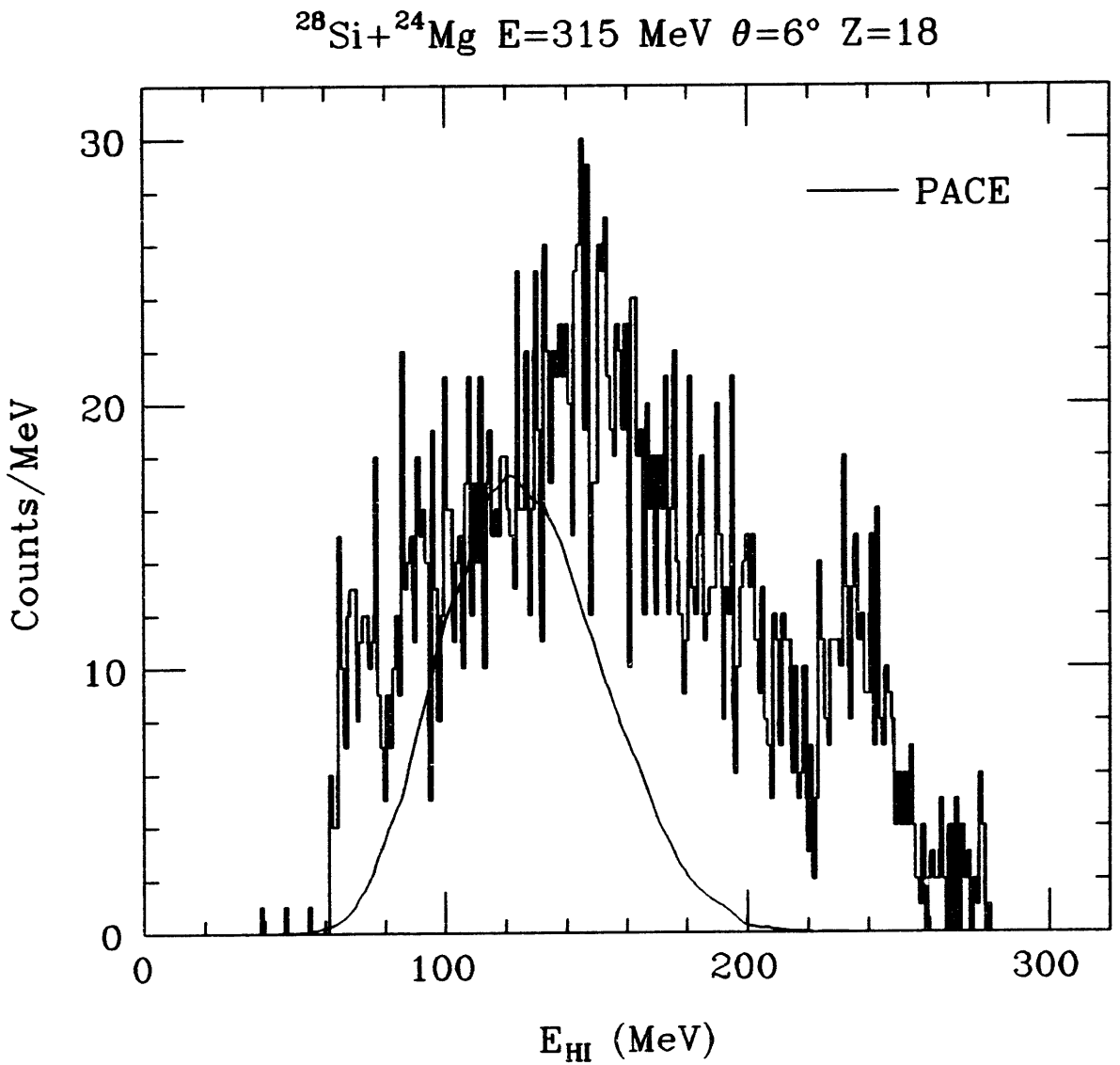
$^{28}Si+^{24}Mg$ E=315 MeV θ=6° Z=18
PACE
Counts/MeV
0
10
20
30
0
100
200
300
E_{HI} (MeV)

Fig.2

Resonances in the $^{12}C(^{13}C,\alpha)^{21}Ne$ Reaction

G.P.Gilfoyle, A.S.Snyder, C.A.Cardounel, C.Smith
J.Rollinson, M.McGhee, and S.Sigworth
Physics Department, University of Richmond, VA, 23173

H.T.Fortune, R.W.Zurmühle, M.McKenzie, J.Arrison, and M.Simpson
Physics Department, University of Pennsylvania, Philadelphia, PA, 19104

PACS 25.70Ef

I. Introduction

The last three decades have witnessed a broad effort to understand a unique state of matter, the nuclear 'molecule' or quasimolecular resonance [1-7] This state is formed when two heavy ions collide and form a rotating dinuclear complex analogous to the dumbbell molecule of atomic physics. Under the extreme conditions of temperature and density that nuclei are subjected to in heavy-ion (HI) collisions one expects the many-body features of the nucleus to come to the fore and produce relatively unstructured spectra. Even in the most celebrated case, that of $^{12}C + ^{12}C$, the density of states near the Coulomb barrier is of the order of 10-100 levels per MeV - any interesting features should dissolve in a sea of compound nucleus states. This is not what is seen. Instead, a rich array of structure has been found in the excitation functions of a number of reactions whose understanding is far from complete. Typically, these structures are of two kinds: broad, gross structure peaks with widths in the several MeV range and intermediate structures with widths of the order of hundreds of keV. A classic example of this phenomenon is the $^{12}C + ^{12}C$ system which exhibits a number of resonances that have been identified as quasimolecular states in ^{24}Mg (the compound nucleus formed in the entrance channel).[1]

The gross structure associated with light heavy-ion systems can be related to the nature of the optical-model potentials that are used to fit the elastic scattering. For most light, HI systems, the potentials are surface transparent. The deep interior of the nucleus is black and any particle penetrating to this region forms a thermally equilibrated compound nucleus. Near the periphery of each fragment, though, the ions can interact without fusing (the density of high spin states that couple to the incoming channel at these excitations energies is low). This surface transparency is responsible for the presence of an l window, a region of low absorption lying between the yrast line and an area of strong absorption at higher excitation energy in the compound nucleus. Most of the resonances experimenters

have found lie in this l window.

The narrow intermediate width structures are not so amenable to our understanding. A variety of schemes have been proposed by theorists to explain various sets of data, but no single prescription has been successful in describing a significant fraction of the data. The common starting point for most of these theories is the doorway state mechanism [8]. A simple eigenstate of some angular momentum, J, is fragmented by a weak residual interaction that spreads the incoming flux over a set of more complex states. The choice of these more complex configurations that couple to the doorway state is a critical component of such theories. Some of the most spectacular resonances exist in systems in which the ions consist of an integral number of α particles. Michaud and Vogt attributed the intermediate structure in the $^{12}C + ^{12}C$ system to special configurations of ^{24}Mg consisting of a ^{12}C core and three α particles [9]. Others have classified systems of α nuclei from $^{12}C + ^{12}C$ to $^{16}O + ^{28}Si$ in an attempt to explain the features of heavy-ion reactions in these systems as excitations of α particles [10].

If the residual interaction does couple the incoming channel to α-particle excitations of the ions then one expects the addition of valence nucleons would disrupt this pattern as the α-particle substructure disappears. However, a rich spectrum of resonance phenomena has been observed in C+C systems which have one or more valence neutrons added to the $^{12}C + ^{12}C$ system. A fusion study by Frawley, *et al* [11], of the $^{12}C + ^{13}C$ system (the one valence neutron case) found it to be similar to the $^{12}C + ^{12}C$ system while other studies of light-charged particle production from reactions that pass through the same intermediate nucleus (^{25}Mg) produced ambiguous results [12-17]. Further evidence from the $^{12}C(^{13}C,\alpha)^{21}Ne$ reaction will be presented below which will resolve this ambiguity.

Investigations of the $^{12}C + ^{14}C$ system (a two valence neutron case) have produced contradictory results [18-20], but a study by Konnerth, *et al* [21] found strong evidence of intermediate structure. The gross structure of the elastic and inelastic scattering of the $^{13}C+^{13}C$ system (a two valence nucleon system with no α nuclei) is consistent with the two carbon nuclei orbiting around one another [22] and a global study of the $^{12}C(^{13}C,\alpha)^{21}Ne$ reaction by us uncovered extensive intermediate structure [23-26]. Fusion studies did not

reveal resonant structure, but nevertheless the data were fitted with a surface transparent optical potential similar to that of other resonant systems [27]. The $^{14}C + ^{14}C$ elastic, inelastic, and transfer channels were also measured by Konnerth, *et al* who observed gross structure similar to that in $^{16}O + ^{16}O$ (a resonating system) in the 90° elastic scattering excitation function [21]. The weight of evidence is tilting against the α-particle degrees of freedom as the dominant source of intermediate structure.

In this paper we will present data for the $^{12}C(^{13}C,\alpha)^{21}Ne$ reaction. The angle-integrated cross sections over a broad energy range for the ground state, the first two excited states, and three multiplets will be exhibited along with a variety of tests and comparisons which establish the non-statistical nature of most of the cross section. We have used autocorrelation analysis, searched for exit channel correlations, and made comparisons with the predictions of the statistical model. The outcome of each method applied is characteristic of a large, non-statistical component. We also compare the angular distributions at correlated peaks in the excitation function to draw conclusions about the angular momentum of the interaction. We find the spin of the intermediate nuclear molecule is consistent with the values observed in other carbon-carbon interactions in the same energy range.

II. Experimental Details

The data were collected at the University of Pennsylvania Tandem Accelerator Laboratory with targets of self-supporting, isotopically-enriched ^{12}C foils of areal density 20 $\mu g/cm^2$. The beam lost about 100 keV (in the center-of-mass system) in the target. The α particles were measured with two large-solid-angle, position-sensitive, slice detectors designed and built by Zurmühle and Csihas [28]. The forward-angle detector had a nickel foil placed in front of it to prevent ions heavier than the α's from reaching the detector, thus reducing radiation damage to the device and reducing the rate of pileup events. At back angles the presence of proton 'contamination' in the α spectra was eliminated by placing a ΔE gas counter in front of a second slice detector [28]. A position spectrum from the back-angle slice detector is shown in Figure 1a. The peaks correspond to the different

slices across the face of the detector. Angular distributions were measured over the range $\theta_{cm} = 10° - 160°$ and contain data at about 160-180 points depending on the configuration for that particular run. The ground and first excited states overlap one another so their yields were extracted by fitting each spectrum with two Gaussian distributions. The second excited state was resolved as were three multiplets, at $E_x(^{21}Ne) = 2.786 - 2.866$ MeV (three states), $E_x(^{21}Ne) = 3.662 - 3.883$ MeV (three states), and $E_x(^{21}Ne) = 4.432 - 4.726$ MeV (four states). The final states in ^{21}Ne above 5 MeV were not resolvable because of the large number of broad, overlapping peaks. A typical energy spectrum for a single slice is shown in Figure 1b.

III. Results and Analysis

The excitation functions for the angle-integrated cross sections for the transitions mentioned above are shown in Figure 2. The data reveal a pronounced peak in each of the excitation functions centered around 8.1 MeV and having a width of about 100-200 keV depending on the exit channel. In this section we will subject the data to a series of tests to establish the non-statistical, correlated nature of the reaction mechanism.

One test for the existence of resonances is to compare the data with the predictions of the statistical model. If the average, angle-integrated cross section exceeds the model prediction by a wide margin, then one must account for this extra yield with some other explanation. Energy-averaged total cross sections were calculated with the computer code STATIS [29]. The exit channels included in the calculation were: $^{12}C + ^{13}C$, $p + ^{24}Na$, $n + ^{24}Mg$, $\alpha + ^{21}Ne$, $2p + ^{23}Ne$, and $2n + ^{23}Mg$. Transmission coefficients derived from the optical model were used for the $^{12}C + ^{13}C$ and the $\alpha + ^{21}Ne$ channels and the code's internal parameterization was used for the remaining channels that make up a small portion of the total fusion cross section. The input parameters for STATIS and the optical model parameters used to calculate the transmission coefficients are displayed in Table I. We found three sets of optical model parameters for the entrance channel. The results of the calculations using the sets from the work of Hallock, *et al* [30], and Delic, *et al* [31] are shown in Figure 1 as the solid curve and dashed figure, respectively. The parameters from

the work of Westfall, *et al* produced a curve close to zero and we have not included it in the figure [32]. The data exceed the statistical model prediction at all energies and the average, angle-integrated cross section is typically a factor of 2-3 greater than the statistical model prediction. A large portion of the cross section is produced by a mechanism other than the formation of a thermally-equilibrated, compound nucleus.

The excitation functions exhibit gross structures of width which are fragmented into narrower structures of width $\Gamma_{cm} \approx 1.0 - 2.0$ MeV which are fragmented into narrower structures of width $\Gamma_{cm} \approx 200 - 400$ keV. The magnitude of the fluctuations is considerably more pronounced than what would be expected by the statistical model. This observation will be put on a more quantitative basis below. The problem of separating the resonant structure from the noise of statistical fluctuations is critical as described above. We calculate the auto-correlation function defined by the relation

$$R(\Gamma,\epsilon) = \frac{<\sigma(E)\sigma(E+\epsilon)>}{<\sigma(E)><\sigma(E+\epsilon)>} - 1$$

where $\sigma(E)$ is the angle-integrated cross section at energy E, ϵ is the energy interval, and Γ is the average width or coherence width of levels in the compound nucleus. The autocorrelation function can also be described by a Lorentzian shape so that

$$R(\Gamma,\epsilon) = \frac{\Gamma^2}{\Gamma^2+\epsilon^2}\frac{1-Y_{D_k}^2}{N_k}$$

where N_k is the effective number of channels contributing to a particular exit channel k, and Y_{D_k} is the ratio of the average direct cross section to the average total cross section. The mean square deviation, $R(\Gamma,0)$ for each state can be used to put limits on Y_{D_k} and N_k. At 0° , N_k is one and it rises to a maximum at 90° of $N_k = g/2$ (g even) or $(g+1)/2$(g odd)-with

$$g = (2i+1)(2I+1)(2i'+1)(2I'+1)$$

where i and I are the spins of the target and projectile and i' and I' are the spins of the final fragments. The allowed ranges of Y_{D_k} and N_k obtained in the present work are shown in Table II. The results clearly show that the majority of the cross section is due to non-statistical processes.

The existence of correlations between different channels is usually a distinctive feature that separates resonances from a fluctuating background[3]. Consider the deviation function

$$D(E) = \frac{1}{N}\sum_{k=1}^{N}\left[\frac{\sigma_k(E)}{<\sigma_k(E)>} - 1\right]$$
$$= \frac{1}{N}\sum_{k=1}^{N}[Y_k - 1]$$

where N is the number of excitation functions and $<\sigma_k(E)>$ is a running average of the angle integrated cross section with an averaging interval of $\Delta E_{cm} = 1.50$ MeV. The size of the interval is determined by the behavior of $D(E)$ as the interval is increased. When it becomes sufficiently greater than the coherence width of levels in the compound nucleus the shape of $D(E)$ will remain essentially constant. The averaging interval we obtained in this manner is consistent with the coherence width of 125 keV that we measured with the autocorrelation function. We use the running average in order to eliminate any kinematic effects on the average cross section, such as the presence of the Coulomb barrier at $E_{cm} \approx 6.5$ MeV. The probability density $p(Y_k)$ for a given channel, Y_k, is given by

$$p(Y_{D_k}) = \frac{N_k}{Y_{D_k}}\left[\frac{Y_k}{Y_{D_k}}\right]^{N_k-1}\exp\left[-N_k\left[\frac{Y_k + Y_{D_k}}{1 - Y_{D_k}}\right]\right] \times I_{N_k-1}\left[\frac{2N_k(Y_k Y_{D_k})^{1/2}}{1 - Y_{D_k}}\right]$$

where I_N is a modified Bessel function of order N. The probability distribution for the deviation function, $p(D)$, is given for statistically independent Y_k by the Fourier transform of the product of the characteristic functions, $\Phi_k(t)$, of the original probability densities for the different states, $p(Y_k)$. The characteristic unction for each channel is

$$\Phi_k(t) = \int_0^\infty p_k(Y_k)e^{itY_k}dY_k \quad .$$

The characteristic function of D (E) is then

$$\Phi_D(t) = \prod_{k=1}^{N} e^{-it/N_k}\Phi_k\left[\frac{t}{N_k}\right] \quad .$$

The probability density of $D(E)$ is given by the Fourier transform of Φ_D,

$$p(D) = \frac{1}{2\pi}\int_{-\infty}^{\infty}\Phi_D(t)e^{-iDt}dt \quad .$$

We can now calculate the probability or confidence level for $D(E)$ using the parameters from the autocorrelation analysis. The percentage of data points with a deviation greater than x_T or less than x_B is defined by

$$Q(x_T) = \int_{x_T}^{\infty} p(D)dD \quad ,$$

$$Q(x_B) = \int_{-\infty}^{x_B} p(D)dD \quad .$$

In Fig. 3 we have plotted $D(E)$ for the first three states and the next three multiplets in ^{21}Ne along with the lines representing the 3Because we are using a running average the points that are closer to the end of the data set than one-half the averaging interval cannot be treated properly. Those points have not been included. Outside the 3containing three data points out of a total of sixteen. Whereas statistical considerations would lead us to expect at most a few events (maybe one), we find three. Thus, we observe evidence for correlated structure in ^{13}C(^{13}C,α)^{22}Ne.

One expects that the ground state transition at these correlated maxima should have angular distributions dominated by a few l values. The angular distributions for transition to the ^{21}Ne ground state are shown in Figure 4. They display the typical oscillatory behavior one expects in resonant reactions, but there are two points to note. The background varies considerably with energy. The two minima on either side of the peak at 8.1 MeV are at 7.92 MeV and 8.28 MeV and each has a considerably different angular distribution. This rapidly changing background is similar to what is seen in other C+C reactions [23-26]. The second point is the angular distributions do not exhibit the deep minima and large peak-to-valley ratios of reactions with zero-spin nuclei in the exit channel (in this case, the ^{21}Ne has $J^{\pi} = \frac{3}{2}^{+}$). The contribution of different magnetic substates to the final angular distribution tends to 'wash out' the structure. Nevertheless, one can still extract some information about the angular momentum of the intermediate nucleus by examining the angular distribution at the maximum in the angle-integrated cross section.

If the transition to the ^{21}Ne ground state were due to a single angular momentum

quantum number the differential cross section could be expressed as

$$\begin{aligned}\frac{d\sigma}{d\Omega} &= |c^2_{l-1}Y^2_{l-1}(\theta,\phi) + c^2_{l+1}Y^2_{l+1}(\theta,\phi)|^2 \\ &= |c^1_{l-1}Y^1_{l-1}(\theta,\phi) + c^1_{l+1}Y^1_{l+1}(\theta,\phi)|^2 \\ &= |c^0_{l-1}Y^0_{l-1}(\theta,\phi) + c^0_{l+1}Y^0_{l+1}(\theta,\phi)|^2\end{aligned}$$

where the c^m_l's are are proportional to the scattering matrix. The angular distribution at the 8.1-MeV peak in the excitation function is shown in Figure 5 with the curve one expects for a transition arising from a pure $|Y^1_5(\theta,\phi)|^2$. The similarity between the curves implies this spherical harmonic is dominating the cross section and the angular momentum of the intermediate nucleus is from either $l = 4$ or $l = 6$. The differential cross section, alone, is not sufficient to resolve this ambiguity between the different possible l values.

It is worthwhile at this point to compare the evidence for resonances in this energy range in the ^{12}C +^{13} C system with the evidence in other C+C systems in which the phenomenon has been observed. In the ^{12}C+^{12}C system a prominent 4^+ state is observed at a bombarding energy of E_{cm} = 7.7 MeV that is correlated in several final states. The spin assignment is based on the resemblance of the angular distribution at 7.7 MeV to a pure $|P_4(cos\theta)|^2$ [33]. A correlated 4^+ state has also been observed in the ^{13}C+^{13}C system [25]. Both resonances have similar widths and exceed the statistical model prediction of the cross section by similar amounts [25]. Hence, $l = 4$ resonances exist at or near this center-of-mass energy in the C+C systems for the zero- and two-valence-nucleon cases and o'' lata here are consistent with the same assignment in the one-valence-nucleon case. We favor the assignment of an $l = 4$ to the resonance observed here.

IV. Conclusions

We have measured full angular distributions for the ^{12}C(^{12}C,α)^{20}Ne reaction for the transitions to the $\neq$ ground state, first and second excited states, and three multiplets at $E_x(^{21}Ne) = 2.786-2.866$ MeV (three states), $E_x(^{21}Ne) = 3.662-3.883$ MeV (three states), and $E_x(^{21}Ne) = 4.432 - 4.726$ MeV (four states). We have observed a correlated peaks in the angle-integrated cross section including one at 8.1 MeV whose measured cross section exceeds a statistical model prediction. The differential cross section at the correlated peak

is consistent with the formation of an $l = 4$ resonance in the intermediate ^{25}Mg nucleus. The resonance is similar in character to ones observed in the $^{13}C + ^{13}C$ and $^{12}C + ^{12}C$ systems and hints at the possibility of a common mechanism among all three. If a common mechanism did exist to explain the presence of the resonance is the three systems it would call into question the explanation of the $^{12}C + ^{12}C$ nuclear molecular states in terms of α particle degrees of freedom.

Acknowledgements

We acknowledge financial support from the National Science Foundation, the United States Department of Energy, and the Research Corporation.

REFERENCES

[1] T.M.Cormier, Ann. Rev. Nucl. Part. Sci. **32**, 271(1982).

[2] N.Cindro, Rivista del Nuovo Cimento **4** , No. 6 (1981) and references therein.

[3] R.M.Freeman, in **Proceedings of the International Conference on the Resonant Behavior of Heavy-Ion Systems, Aegean Sea-1980**, edited by G.Vourvopoulos(Greek Atomic Energy Commission), Athens, (1981), p.41.

[4] R.Koennecke, W.Greiner, J.Y.Park, and W.Scheid, see Ref. 2, p.163.

[5] W.Greiner , see Ref. 2, p.391.

[6] R.L.Phillips, K.A.Erb, D.A.Bromley, J.Weneset, Phys. Rev. Lett. **42**, 566(1979).

[7] S.Ohkubo and D.M.Brink, Phys. Rev. **C36**, 1375(1987).

[8] H.Feshbach, A.K.Kerman, and R.H.Lemmer, Annals of Phys. **41**, 230(1967).

[9] G.J.Michaud and E.W.Vogt, Phys. Rev. **C5**, 350(1970).

[10] M.Gai, see Ref. 2, p.495.

[11] A.D.Frawley, N.R.Fletcher, L.C.Dennis, and K.M.Abdo, Nucl. Phys., **A394**, 292(1983).

[12] D.J.Crozier and J.C.Legg, Phys. Rev. Lett., **33**, 782(1974).

[13] W.von Oertzen, B.Imanishi, H.G.Bohlen, W.Treu, and H.Volt, Phys. Lett. **B93**, 21(1980).

[14] K.R.Cordell, L.C.Dennis, T.C.Schweizer, S.T.Thornton, P.G.Lookado, J.L.C.Ford, J.Gomez del Campo, and D.Shapira, Nucl. Phys. **A323**, 146(1979).

[15] H.Voit, G.Ischenko, F.Siller, and H.D.Helb, Nucl. Phys. **A179**, 23(1972).

[16] R.A.Dayras, R.G.Stokstad, Z.E.Switkowski, and R.M.Wieland, Nucl. Phys. **A265**, 153(1976).

[17] E.Haindl, W.Galster, P.Duck, W.Treu, F.Siller, and H.Voit, Phys. Rev. Lett. **35**, 1478(1975).

[18] W.Galster, P.Dück, H.Fröhlich, W.Treu, and H.Voit, Nucl. Phys., **A277**, 16(1977).

[19] M.Feil, W.von Oertzen, H.G.Bohlen, A.Gamp, and R.L.Walter, Z.Phys. **260**, 271(1973).

[20] R.M.Freeman, F.Haas, and G.Korschinek, Phys. Lett. **90B**, 229(1980).

[21] D.Konnerth, W.Trombik, K.G.Bernhardt, K.A.Eberhard, R.Singh, A.Strzalkowski, and W.Trautmann, Nucl. Phys. **A436**, 538(1985).

[22] S.K.Korotky, K.A.Erb, R.L.Phillips, S.J.Willet, and D.A.Bromley, Phys. Rev. **C28**, 1(1983).

[23] G.P.Gilfoyle and H.T.Fortune, Phys. Rev. **C32**, 865(1985).

[24] G.P.Gilfoyle, L.C.Bland, R.Gilman, M.Carchidi, K.S.Dhuga, J.W.Sweet, A.H.Wuosmaa, G.S.F.Stephans, R.W.Zurmühle, and H.T.Fortune, Phys. Rev. **C32**, 861(1985).

[25] G.P.Gilfoyle, J.Richards, and H.T.Fortune, Phys. Rev. **C34**, 152(1986).

[26] G.P.Gilfoyle and H.T.Fortune, Phys. Rev. **C40**, 762(1989).

[27] J.L.Charvet, R.Dagras, J.M.Fieni, S.Joly, J.L.Uzureau, Nucl. Phys. **A376**, 292(1982).

[28] R.W.Zurmühle and L.Csihas, Nucl. Instr. and Meth. **203**, 261(1982).

[29] R.G.Stokstad, private communication.

[30] J.N.Hallock, H.A.Enge, J.D.Garrett, R.Middleton, and H.T.Fortune, Nucl. Phys. **A252**, 141(1975).

[31] G.Delic, Phys. Rev. Lett., **34**, 1468(1975).

[32] G.P.Westfall and S.A.A.Zaidi, Phys. Rev., **C14**, 610(1976).

[33] K.A.Erb, R.R.Betts, D.L.Hanson, M.W.Sachs, R.L.White, P.P.Tung, and D.A.Bromley, Phys. Rev. Lett., **37**, 670(1976).

Table I. Optical-model parameters for statistical model calculations.

Channel	Ref.	V_R (MeV)	R_R (fm)	a_R (fm)	V_I (MeV)	R_I (fm)	a_I (fm)	V_{so}
$^{12}C+^{13}C$	30	14.0	1.35	0.35	A^a	1.40	0.35	
$\alpha+^{21}Ne$	30	180.0	1.42	0.56	16.5	1.42	0.56	
$p+^{24}Na$	30	B^b	1.25	0.65	C^c	1.25	0.47	D^d
$n+^{24}Mg$	30	F^e	1.306	0.66	G^f	1.189	0.48	
$^{12}C+^{13}C$	31	67.79	1.019	0.701	50.82	1.077	0.1002	
$^{12}C+^{13}C$	32	86.6	1.08	0.59	9.56	1.27	0.33	

[a] $A = 0.4 + 0.1E_{cm}$
[b] $B = 53.3 - 0.55E_{cm} + 27(N-Z)/A + 0.4Z/A^{1/3}$
[c] $C = 3A^{1/3}$
[d] $D = 8.5$ for $E \geq 17$, 7.5 for $E < 17$
[e] $F = 47.01 - 0.267E_{cm} - 0.00118E_{cm}^2$
[f] $G = 9.52 - 0.053E_{cm}$

Table II. Autocorrelation Analysis Results.

	N_k		Y_{D_k}		
Channel	Min	Max	Min	Mean	Max
0.0	1	4	0.90	0.94	0.98
0.351	1	6	0.89	0.94	0.98
1.4556	1	8	0.73	0.86	0.97
2.7885-2.8656	1	4.7	0.95	0.97	0.99
3.6621-3.8829	1	5.3	0.92	0.95	0.99
4.432-4.726	1	6.5	0.89	0.94	0.98

FIGURE CAPTIONS

Fig. 1 Typical position and energy spectra for the $^{12}C(^{13}C,\alpha)^{21}Ne$ reaction. The position spectrum from the back-angle, position-sensitive, solid-state, surface-barrier detector is shown in the upper panel. Each peak represents another slice or scattering angle. The lower panel is a typical energy spectrum and shows the overlapping ground and first excited states, the resolved second excited state, and the three multiplets at higher excitation energy in ^{22}Ne. Each peak is labelled with the energy or energies of the states composing it.

Fig. 2 The excitation functions of the angle-integrated cross sections for the $^{12}C(^{13}C,\alpha)^{21}Ne$ reaction leading to the ground state, first two excited states, and the three multiplets discussed in the text. The dashed curves are Hauser-Feshbach calculations for each transition.

Fig. 3 Deviation function for the first three isolated states and the first three multiplets in ^{21}Ne. The solid lines represent the 3% confidence levels described in the text.

Fig. 4 Angular distributions for $^{12}C(^{13}C,\alpha)^{21}Ne(0.0)$ reaction in the range $E_{c.m.}$ = 7-9 MeV.

Fig. 5 The angular distribution for the transition to the ^{22}Ne ground state at E_{cm} = 8.10 MeV. The solid curve is from a pure $|Y_5^1(\theta,\phi)|^2$ corresponding to an $l = 4$ or $l = 6$ in the intermediate ^{25}Mg nucleus.

[20] D.L.Gay, L.C.Dennis, and N.R.Fletcher, Phys. Rev. **C34**, 2144(1986).

[21] P.Braun-Munzinger and J.Barrette, Nucl. Phys., **32**, 353(1982).

[23] B.H.Wildenthal, private communication.

[24] P.D.Kunz, private communication.

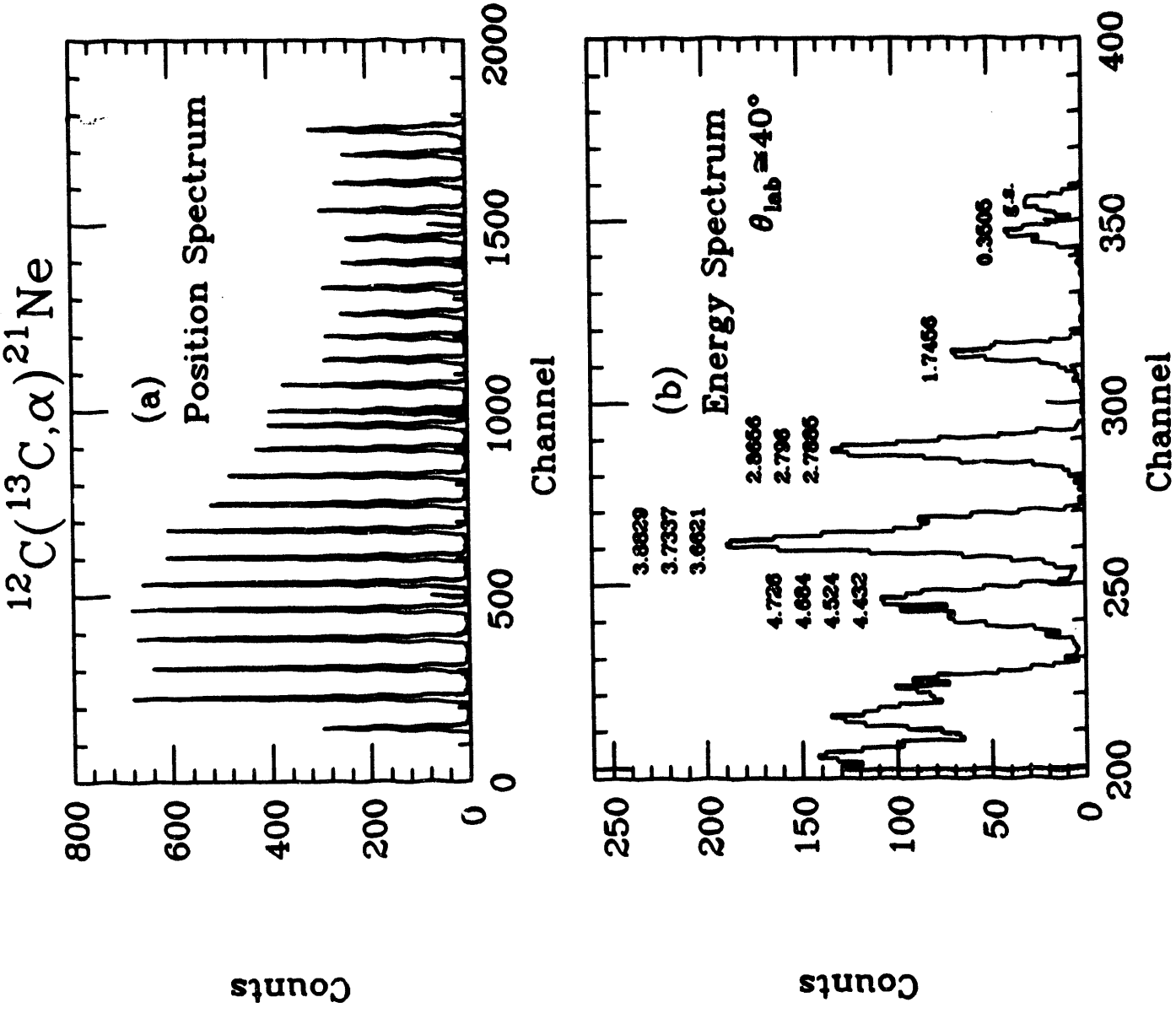
$^{12}C(^{13}C,\alpha)^{21}Ne$
(a)
Position Spectrum
Counts
Channel
(b)
Energy Spectrum
$\theta_{lab} \cong 40°$
3.8829
3.7337
3.6621
2.8656
2.795
2.7665
4.726
4.684
4.524
4.432
1.7456
0.3505
Counts
Channel

Figure 1

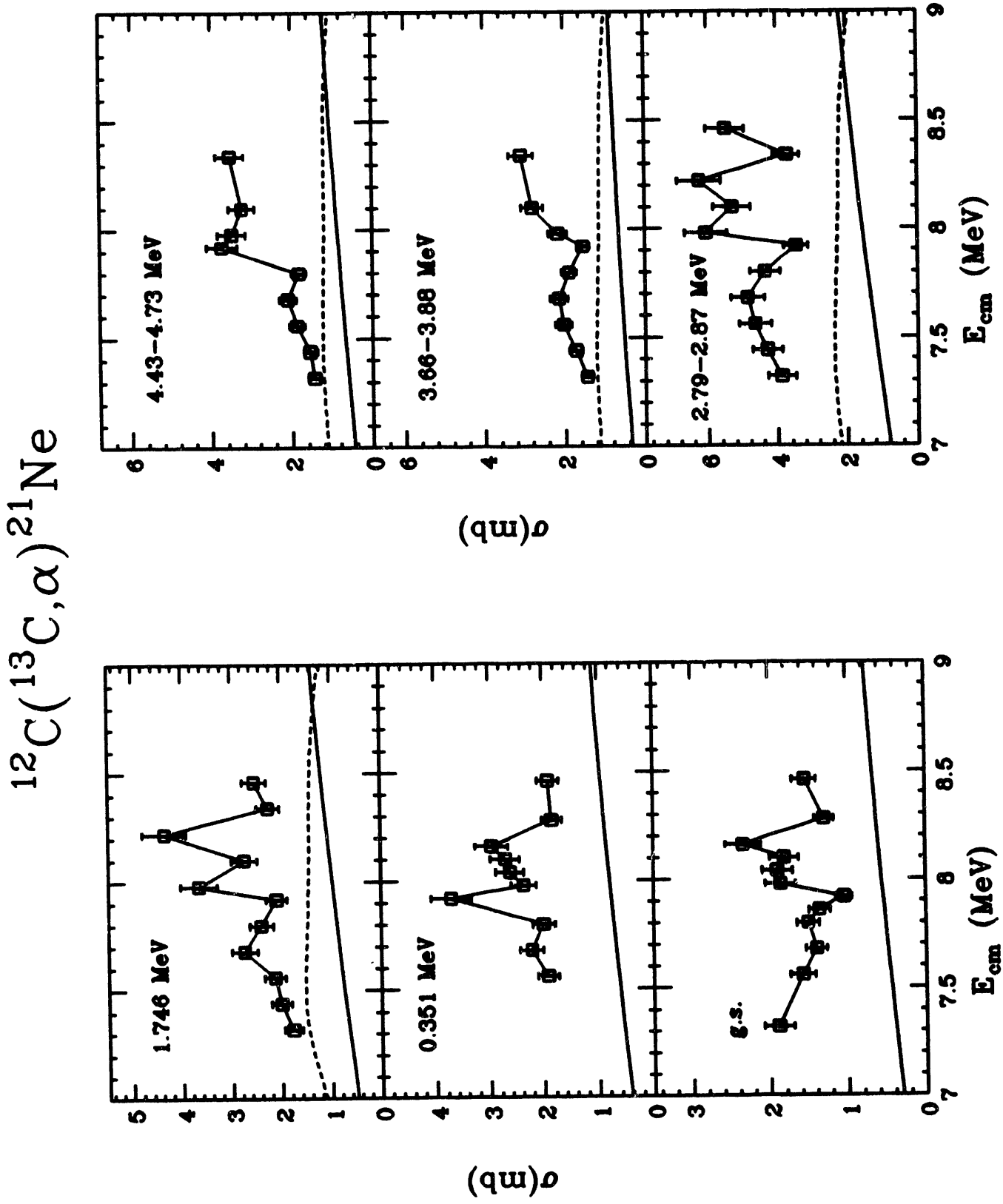
$^{12}C(^{13}C,\alpha)^{21}Ne$
4.43–4.73 MeV
3.66–3.88 MeV
2.79–2.87 MeV
1.746 MeV
0.351 MeV
g.s.
σ(mb)
E_{cm} (MeV)

Figure 2

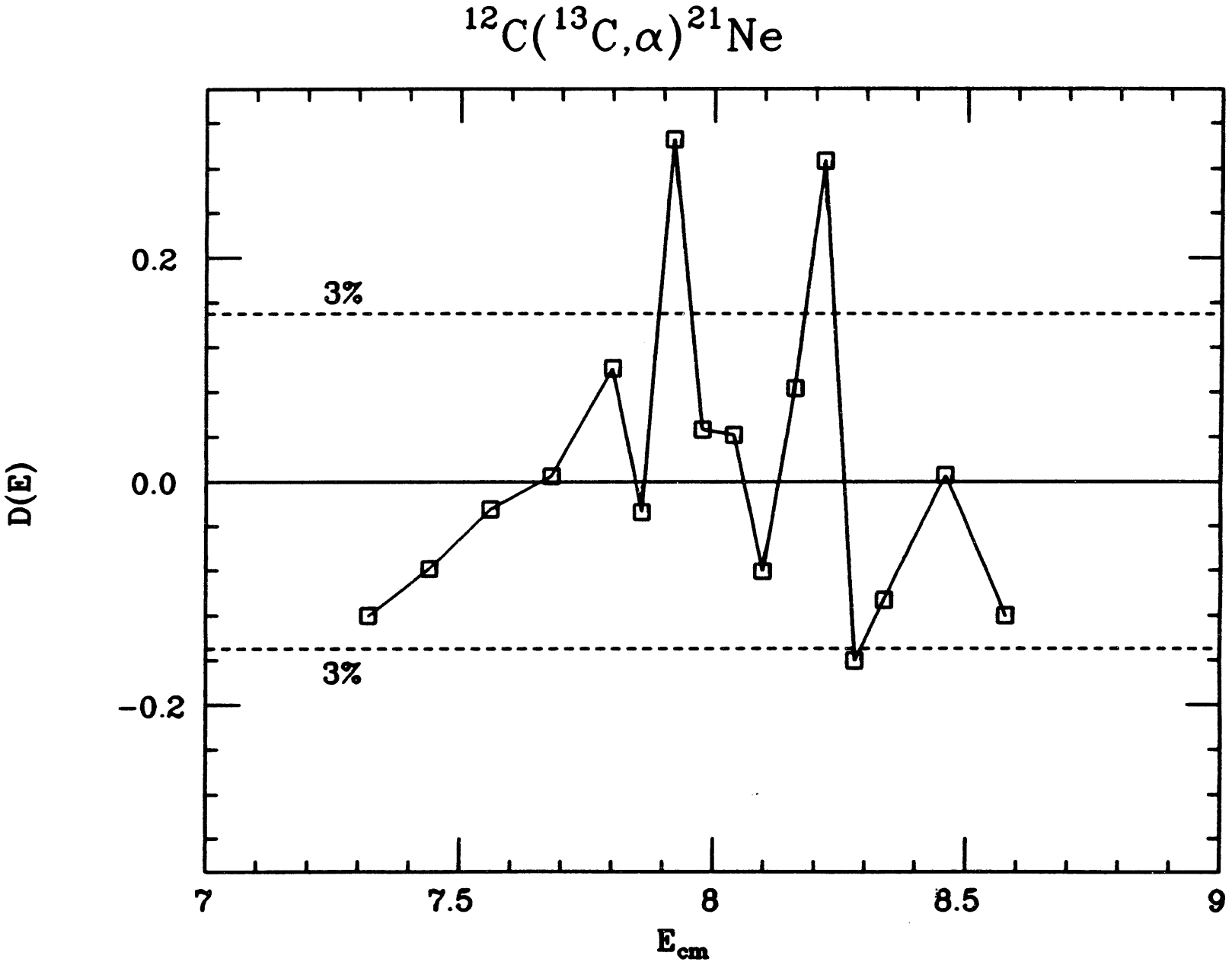

Figure 3

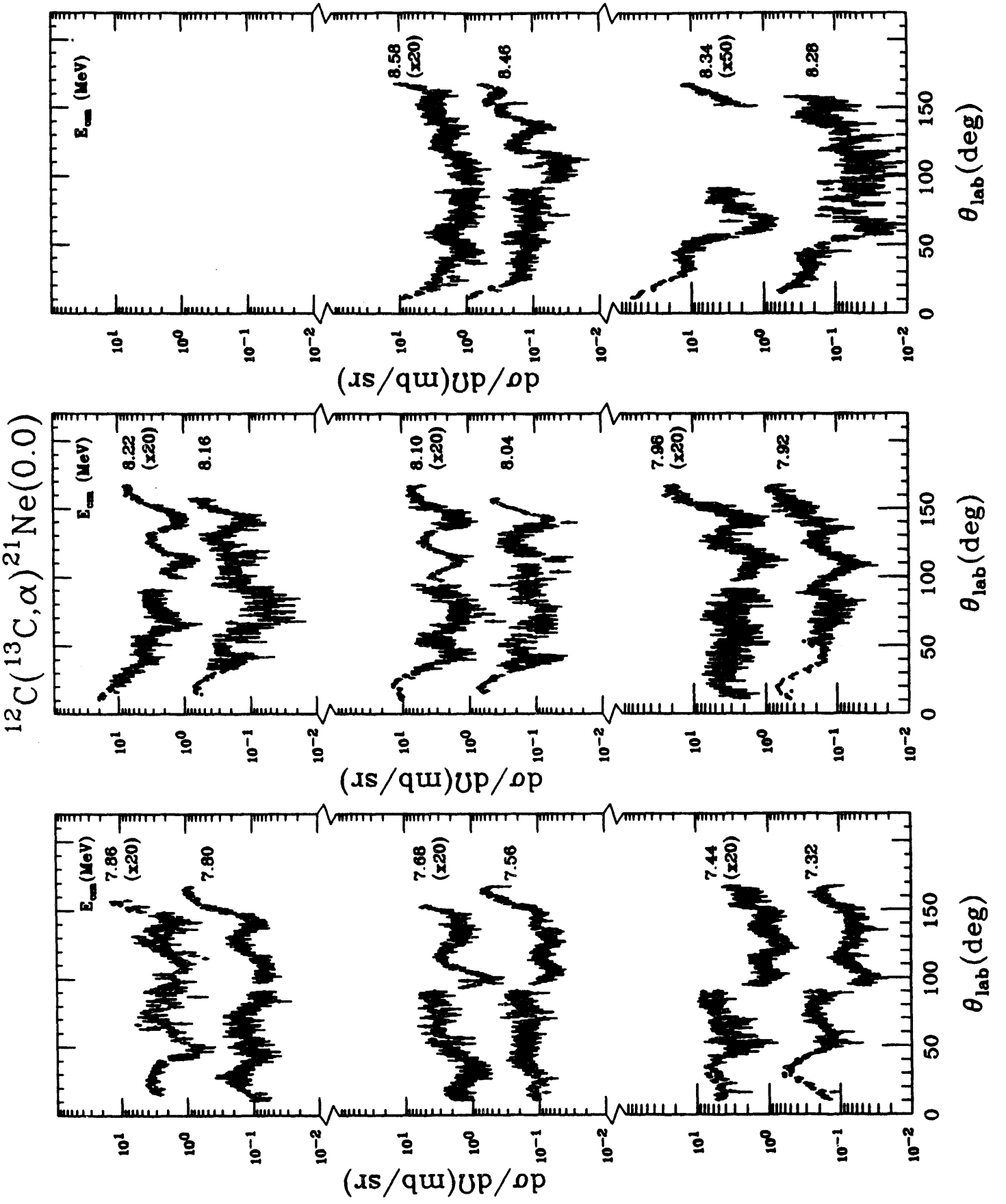
$^{12}C(^{13}C,\alpha)^{21}Ne(0.0)$
E_{cm} (MeV)
8.58 (x20)
8.46
8.34 (x50)
8.28
8.22 (x20)
8.16
8.10 (x20)
8.04
7.98 (x20)
7.92
7.86 (x20)
7.80
7.68 (x20)
7.56
7.44 (x20)
7.32
$d\sigma/d\Omega$(mb/sr)
θ_{lab}(deg)

Figure 4

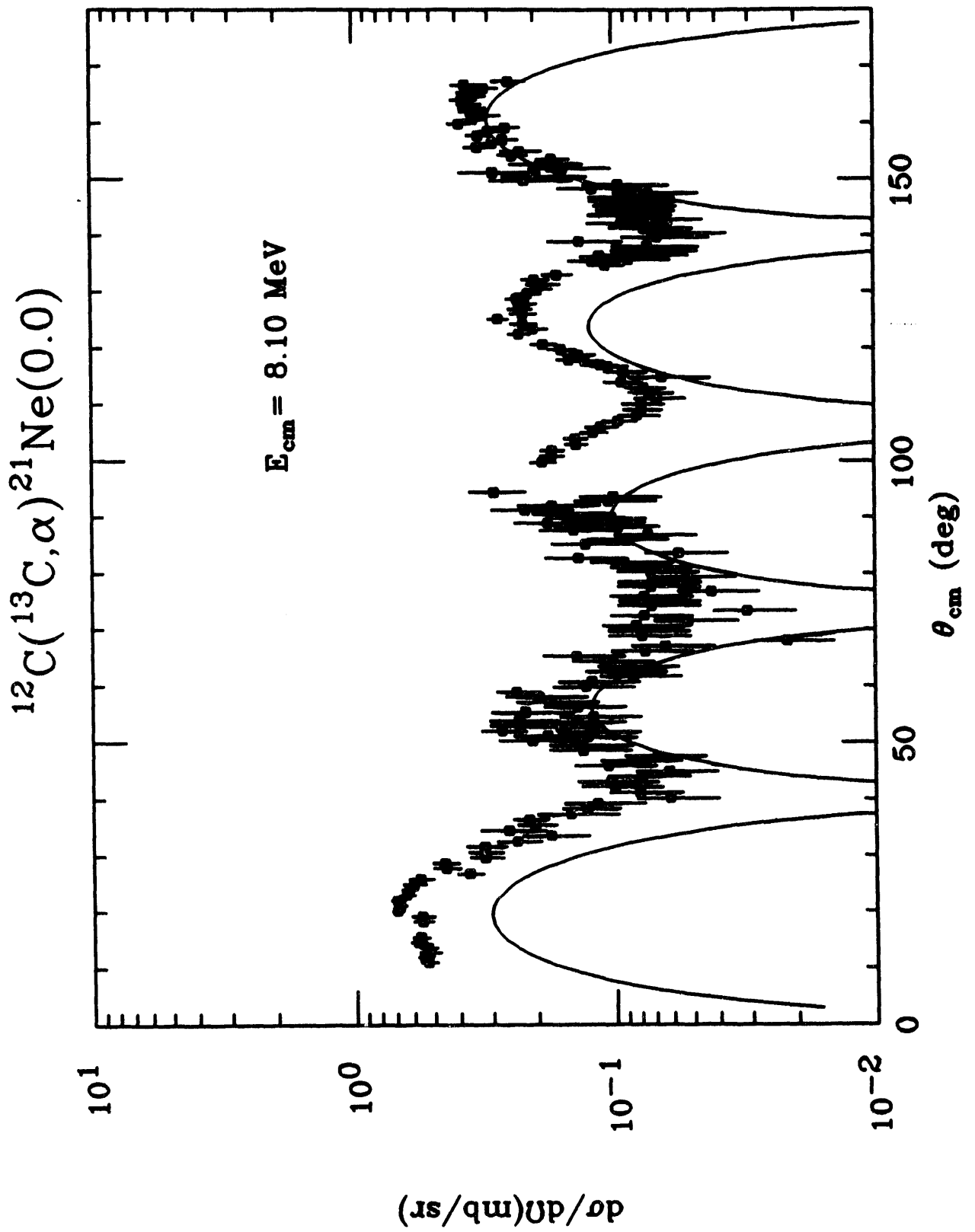
$^{12}C(^{13}C,\alpha)^{21}Ne(0.0)$
E_{cm} = 8.10 MeV
θ_{cm} (deg)
$d\sigma/d\Omega$(mb/sr)
10^1
10^0
10^{-1}
10^{-2}
0
50
100
150

Figure 5

Neutron-neutron and neutron-deuteron correlations

Gilfoyle, Snyder, Nimchek, DeYoung, Peterson, Shaw,

Hinnefeld, Kolata, Glagola, and Kryger

Physics Justification: The goal of the experiment is to make accurate measurements of the n-n and n-d correlation functions for a well-characterized system. Such measurements can provide extremely valuable information for assessing the role of the Pauli Exclusion Principle in two-particle correlations. The proton-proton (p-p) correlation function in nuclear collisions has been extensively studied over a wide range of energies, since it is sensitive to the space- time characteristics of the emitting source (see, e.g., Ref. 1). The most striking feature of this correlation function is the strong anti-correlation at low relative momentum that results primarily from Coulomb repulsion but may have some contribution from Pauli effects. In principle, the Pauli component might be evaluated by investigating n-n correlations however, systematic studies of n-n correlations simply do not exist. In fact, only three experiments have been done to date. The first, a study[2] of the proton + Pb reaction at 7.5 GeV/c, reported no Pauli anticorrelation and concluded that the correlation is dominated by the attractive n-n singlet-state final state interaction (FSI). The second group[3], which investigated the $^{18}O + ^{26}Mg$ system at incident energies of 64 and 88 MeV, did identify Pauli repulsion in their data. They attributed their success to the fact that the average neutron emission time from the ^{44}Ca compound nucleus resulted in a mean distance between successively emitted neutrons that was large compared with the 16 fm n-n singlet-state scattering length. Finally, the most recent study[4], an investigation of $^{20}Ne+^{12}C$ and $^{20}N + ^{59}Co$ at 600 MeV, again reported domination by attractive FSI effects. Only in the latter work was a comparison made with p-p correlation data from the same system.

We have measured n-n correlations resulting from the $^{16}O + ^{27}Al$ reaction at 216 MeV. This is a very well-studied system for which many two-particle correlations have been measured

[5,6,7], including the first and to date the only measurement of neutron-charged particle correlations (Ref. 7). From these data, it has been determined[8] that the effective source size for neutron-proton correlations is 50 fm, thus perhaps satisfying the emission-time requirement given in Ref. 3. In addition, n-n coincidences were observed in this experiment, although insufficient statistics coupled with problems due to scattering of neutrons from one detector to another (this experiment was optimized for neutron-charged particle coincidence detection) prevented us from constructing a believable correlation function. We therefore believe that this reaction provides an ideal testing ground for the possible effects of Pauli repulsion on the n-n correlation.

A further goal of the experiment is to extract a higher-statistics n-d correlation function. In Ref. 7, we noted an intriguing anticorrelation at low relative momentum in this two- particle correlation function (Fig. 1), which may result from the strongly repulsive nature of the J=3/2 s-wave interaction. Interestingly enough, this repulsion appears to be due to Pauli effects between the two neutrons[9]. If this is in fact the case, and if the n-n correlation proves to be nearly always dominated by FSI effects, then the n-d correlation may well be the cleanest way to investigate Pauli repulsion in two-particle correlations. Unfortunately, our data (Fig. 1), though strongly suggestive of an effect, is of limited statistical significance. Thus, a second goal of the proposed work will be to obtain a higher statistics n-d correlation function that can be analyzed with some confidence. At the same time, we also be recorded other neutron-charged particle and charged particle-charged particle correlations at higher statistics. All this information will be factored into the analysis of the new experimental data. The result will be an exceptionally complete body of information that will be very important for the study of Pauli repulsion and other effects in two-particle correlations.

Experimental Configuration: The neutron charged-particle experiment[7] in 1989 was primarily focused on n-p coincidences but did have provisions in the electronic set up to measure both n-d and n-n coincidences. As detailed above an interesting result was found for the n-d but the n-n

results were not reliable. However, this measurement did give us some very solid rate information and pointed out what changes need be made before attempting to measure either of these channels. The improvements which were made fall in several broad areas. For both the n-n and n-d correlations the statistics were improved, the lower limit in q (relative momentum) was too high for n-d, and the background (primarily neutrons scattering from one detector to another or "in-out scattering") was unacceptably large for n-n. The statistics problem was addressed by having more detector pairs. Two parameters affect the lower limit for q; the opening angle and the statistics. The proposed configuration will have roughly the same opening angles as the 1989 work and will yield an absolute lower limit of 2 MeV/c for n-d and 2.2 MeV/c for n-n. These are significantly lower than the limit seen in figure 1 because of low statistics in that case. At any finite opening angle the available phase space in the pn-pd space becomes ever smaller as q is lowered requiring infinite statistics to realize the limit set by the opening angle. Of course a smaller opening angle acts to increase the available phase space but simulations of the previous and proposed geometries show that the biggest gains are made by increasing the statistics rather than decreasing opening angles (with associated smaller solid angles). The problem of in- out scattering required a radical change in detector placement. The placement is driven by several competing effects. The simplest way to reduce in-out scattering is to move the detectors farther apart thereby reducing the solid angle for detecting the scattered neutron. Since we needed to preserve small opening angle this means that the detectors were placed at different distances from the target to achieve the solid angle reduction. Unfortunately, this gain is partially offset by the increase in in-out scattering due to the forward peaked laboratory angular distribution of the scattered neutron. A second order effect is the fact that neutrons scattered at small angle usually produce little light (little energy lost) in the first detector and so are not registered there. Certainly, aside from considerations of the size of the reduction of the in-out scattering achieved with a staggered array, one can absolutely reject in-out scatters with restrictions on the time of flight. By requiring that the forward n detector (closest to the target) fire at a later time than the time at which the back neutron would have passed the

forward detector, based on the energy measured by time of flight in the back detector, in-out scattering is absolutely rejected. Unfortunately, this also eliminates half the statistics (which was accounted for in the rate estimates below). This procedure has been checked with simulations and it was found that essentially all spurious events would be rejected for the geometry described below.

We used two separate arrays (one on each side of the beam at 45°): one for n-n coincidence measurements and the smallest angle n-d coincidences, and one primarily for n-d measurements (higher solid angles but somewhat bigger opening angle). This array (figure 2a) will be composed of 16 neutron detectors (five inch diameter) where detectors with short flight paths (2 meter flight path) alternate with those having larger distances (2.9 meter flight). The distances were chosen as a compromise between maximizing the in-out scatter and preserving solid angle. The center-to-center distance (5.5 inches when projected onto a plane at 2 m) gives a 4° opening angle. Simulations of the geometry indicate that with 50000 coincidences the minimum q (based on acceptable error bars) will be on the order of 3 MeV/c; more than adequate based on either quantum models or measurements.[4] In the center of the squares formed by the neutron detectors we placed 9 CsI detectors (1.5 cm in diameter) at a distance of 90 cm from the target inside the vacuum chamber (see figure 2a). These gave an opening angle of 2.8° for the n-d coincidences. The second array (figure 2b) was composed of 8 neutron detectors and 6 CsI detectors alternating at the vertices of a square lattice. In this array the neutron detectors were placed 2 meters from the target (no staggering) and so were not useful for n-n coincidences because of the high in-out scattering anticipated for closely spaced detectors. The CsI detectors were located at a distance of 55 cm. This configuration had a minimum opening angle of 3.3° which is larger than the first array but this arrangement gave a large number of small angle pairs with relatively high solid angle. Having two arrays allowed good measurements of the wide angle correlations.

In-out scattering is an insidious contaminant process as it registers as a n-n small-angle coincidence. Even though it is relatively rare, it is still a small fraction of the huge singles rate in comparison to the much lower coincidence rate. Initially, our hope was that shadow bar

measurements would allow all n-n detector pairs to be used. To this end simulations of in-out scattering were performed for the first array described above. After including geometrical solid angle effects, angular distributions, kinematics, and neutron efficiencies the in-out probability was found to be .06%. Unfortunately, the n-n coincidence to n singles ratio was 10^{-4} giving about 5 rescattered events to every 1 real coincidence. This requires an unacceptably high correction factor. (In the 1989 work with adjacent detectors the ratio was 20 scattered events for every real coincidence.)

In addition to the changes in detector configuration, we also increased the target thickness to 1.6 mg/cm^2 both to increase statistics and increase the real/background ratio (a concern with the beam dump in the target room). We required a 250 ns beam pulse spacing (as in 1989) to accommodate the long neutron flight paths.

The data were collected in the summer of 1993 in five days of running at ATLAS. The data are currently being analyzed by our collaborators at Hope College and at Michigan State University.

References

1. D.H. Boal, C.K. Gelbke, and B.K. Jennings, Rev. Mod. Phys. 62,553 (1990).
2. Y.D.Bayukov, et. al., Phys.Lett B189,291 (1987).
3. W. Dunnweber, et. al., Phys. Rev. Lett. 65, 297 (1990).
4. B. Jakobsson, et. al., Phys. Rev. C44, R1238 (1991).
5. P.A. DeYoung, et. al., Phys. Rev. C39, 128 (1989).
6. P.A. DeYoung, et. al., Phys. Rev. C41, R1885 (1990).
7. R.A. Kryger, et. al., Phys. Rev. Lett. 65, 2118 (1990).
8. R.A. Kryger, private communication.
9. H.W. Bartz, et.al., Phys. Rev. C37, 2910 (1988).

Figure Captions

Figure 1: The correlation functions from O+Al at 215 MeV involving neutrons. (Results from the 1989 experiment.)

Figure 2: Schematic representations of the detector geometry. The circles show the effective size of the various detectors as projected onto a plane 2 meters from the target. The solid circles are the CsI, the open circles are neutron detectors 2 m from the target and the cross hatched circles are the offset neutron detectors at a distance 2.9 m.

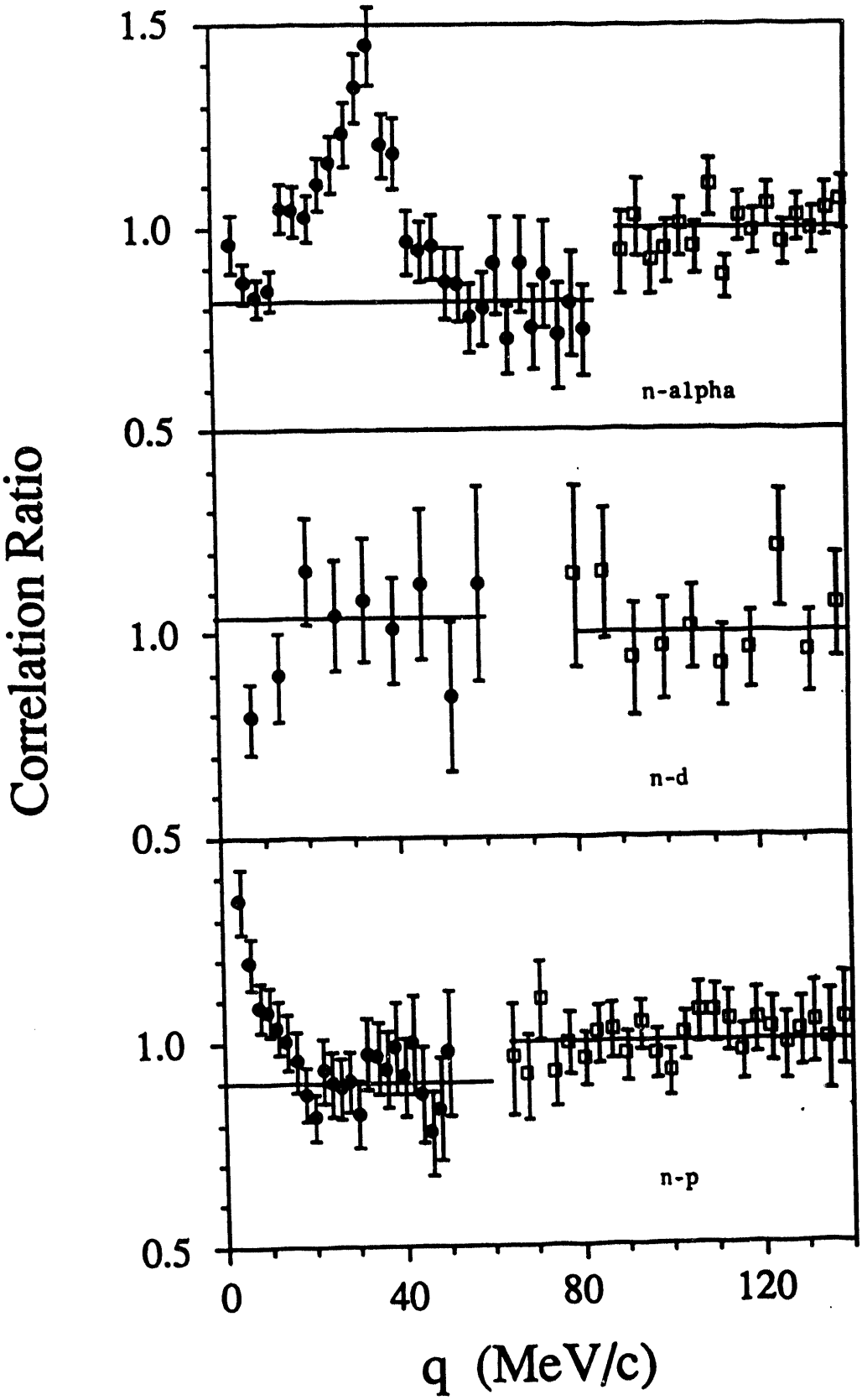
Correlation Ratio
1.5
1.0
0.5
n-alpha
1.0
0.5
n-d
1.0
0.5
n-p
0
40
80
120
q (MeV/c)

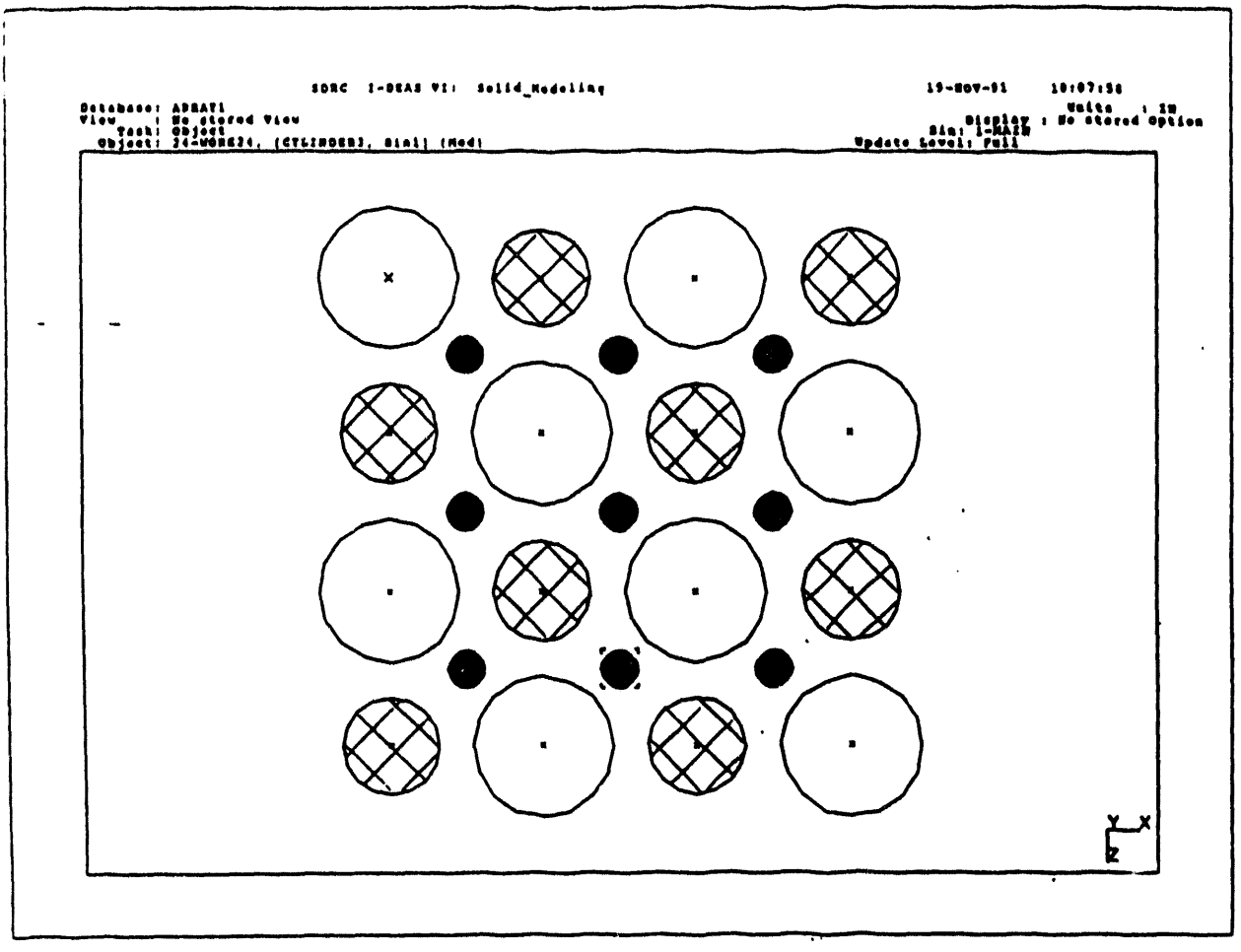
SDRC I-DEAS V1: Solid_Modeling
19-NOV-91 10:07:56
Database: ARRAY1
View : No stored View
Task: Object
Object: 24-WORK24, (CYLINDER3, Bin1) (Mod)
Units : IN
Display : No stored option
Bin: 1-MAIN
Update Level: Full
Y
X
Z

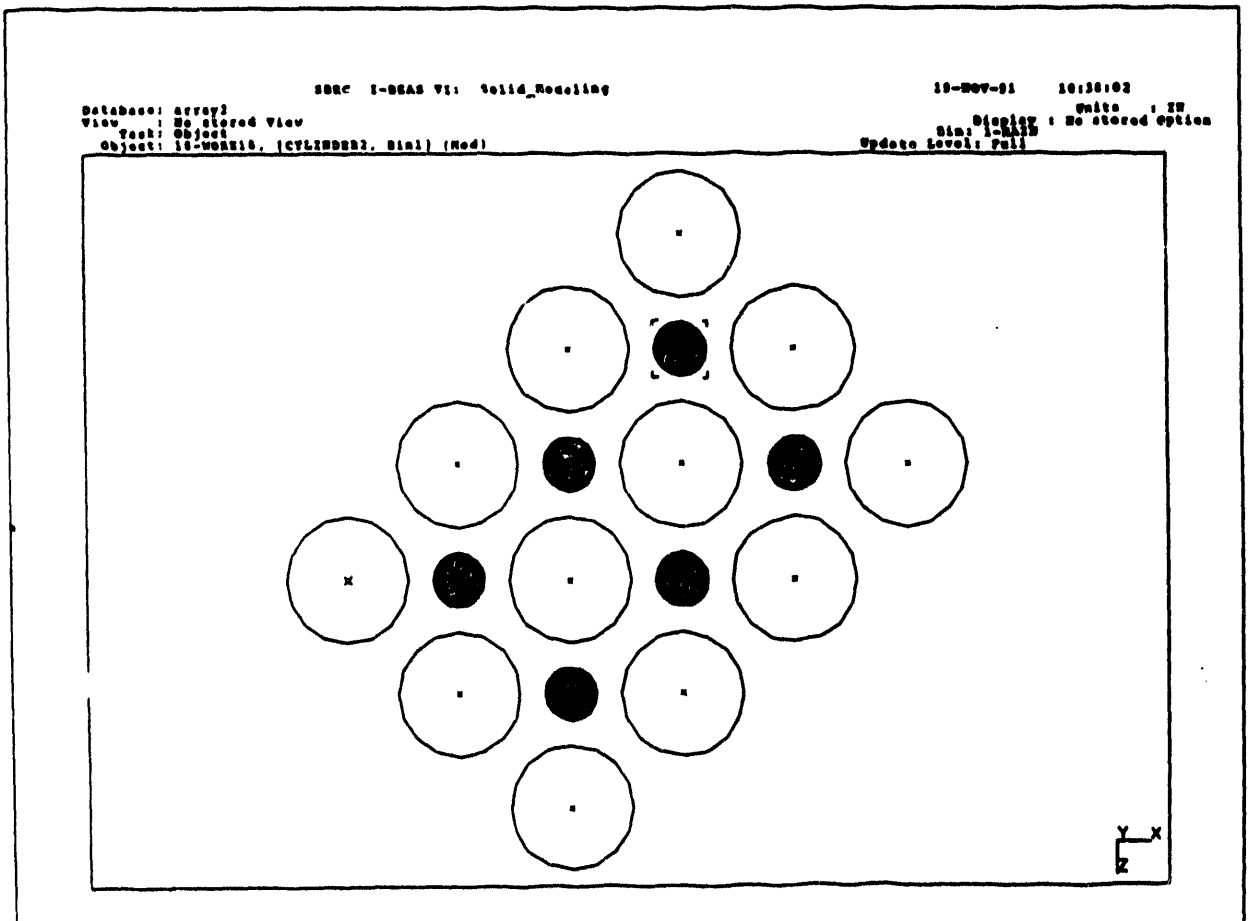
SDRC I-DEAS V1: Solid_Modeling
19-NOV-91 10:38:02
Database: array2
View : No stored View
Task: Object
Object: 19-WORK19, (CYLINDER2, Bin1) (Mod)
Units : IN
Display : No stored option
Bin: 1-MAIN
Update Level: Full
Y
X
Z

Abstract Presented
to the National Conference on Undergraduate Research
University of Utah, Salt Lake City Utah
March 25-28, 1993

THE SEARCH FOR NUCLEAR MOLECULES IN THE $^{12}C+^{13}C$ SYSTEM. A.Snyder, C.A. Cardounel, S.Sigworth, C. Smith, (G.P. Gilfoyle), University of Richmond, R. Zurmuhle,H.T. Fortune, J. Arrison, M. McKenzie, M. Simpson, University of Pennsylvania. When two nuclei collide they can form a dumbbell-like complex called a nuclear molecule, analogous to molecules formed by atoms. We have studied the $^{12}C + ^{13}C$ system for evidence of these di-nuclear complexes. The ground state and first excited state peaks in the energy spectrum of this reaction are often not well seperated. A FORTRAN code was written which fits these two peaks with a double gaussian. The best fit is determined by minimizing the χ^2. This code allowed us to satisfactorily seperate the ground and first excited states, and thus calculate the angular distributions for this reaction. This work was supported by the Research Corporation and DOE.

Computing Facilities

Gilfoyle, Rubin, and Vineyard

The University of Richmond Physics Department has a computer system dedicated to the research needs of its faculty and students. The system is built around two Digital Equipment Corporation (DEC) computers, a VAXstation 3100 and a VAXstation 3200. These machines form a cluster communicating via an Ethernet connection with the VAXstation 3100 acting as the boot node (see Figure 1). The system is supported by 1.0 Gbyte of disk storage, a 9-track, 1/2-inch tape drive, and a smaller TK-50 tape drive. A terminal server provides connections to all faculty offices (five), to student terminals (four), and an LN03+ laser printer. We have been using a DECstation 3100 for development of the computer interface to control the parameters of the gas system of the CLAS (see section on slow controls for the CLAS drift chamber gas system). That machine will be replaced with a new device in the fall of 1993 (see below). The Vaxes and some of the other resources in the Department are part of a campus-wide ethernet network that also provides access to Internet. The entire system is in an air-conditioned room in the Department for easy student and faculty access. The system is managed by one faculty member (G.P.Gilfoyle) and has been up and running nearly continuously for three and a half years with few interruptions of service.

As part of its teaching facilities the Department has an array of Macintosh computers with software packages for mathematical analysis and data acquisition plus two PostScript laser printers. Two of these computers are located in faculty offices and are part of the ethernet network. Another five are located in a teaching laboratory and have also been connected to the ethernet network. Although primarily for teaching use these machines are a resource for faculty and student research. We have already begun using some of the software like *Mathematica* for the analysis of the projects described in this report.

We have already ordered a new addition to our computing resources, a Hewlett-Packard

(HP) 715/75 Unix-based machine with 1 Gbyte of disk space, 64 Mbytes of RAM, and an 86 MIP processor. It will used to write code and will be part of a prototype data acquisition system that we intend to build as part of the software development projects we are involved in at CEBAF. This new machine will also make our facilities compatible with those of our collaborators at CEBAF. To take full advantage of the new resource we will also equip a number of the Department's Macintosh computers with software that will enable them to act as X-terminals for faculty and student use.

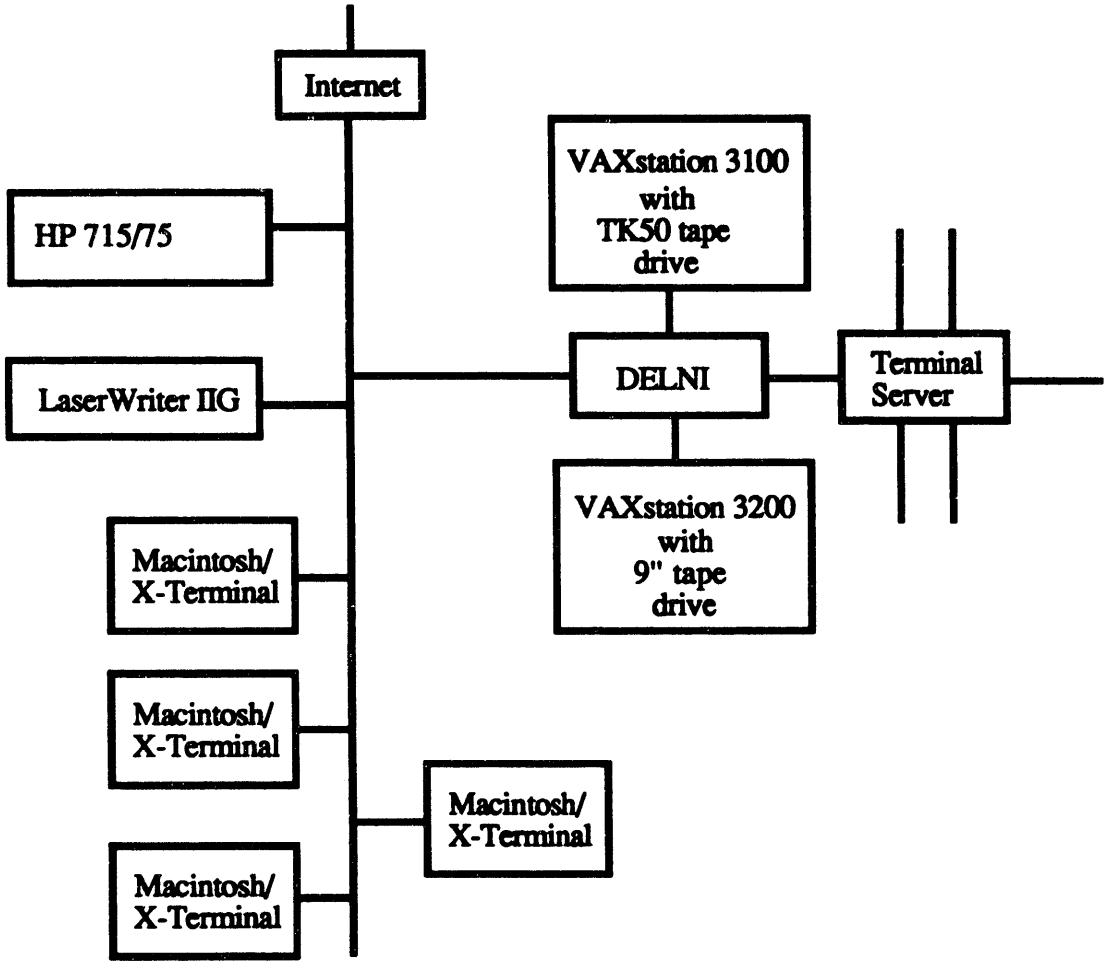

Fig. 1 A schematic view of the University of Richmond Physics Department computer system is shown. The system is solely for the Department and to satisfy its research needs.

Contract Related Activities

Publications and Submissions

M. F. Vineyard, J. F. Mateja, C. Beck, S. E. Atencio,* L. C. Dennis, A. D. Frawley, D. J. Henderson, R. V. F. Janssens, K. W. Kemper, D. G. Kovar, C. F. Maguire, S. J. Padalino, F. W. Prosser, G. S. F. Stephans, M. A. Tiede, B. D. Wilkins, and R. A. Zingarelli, "Energy dependence of fusion evaporation-residue cross sections in the $^{28}Si+^{12}C$ reaction", Phys. Rev. **C47**, 2374 (1993).

M. F. Vineyard, S. E. Atencio,* J. F. Crum,* G. P. Gilfoyle, B. G. Glagola, D. J. Henderson, D. G. Kovar, C. F. Maguire, J. F. Mateja, R. G. Ohl,* F. W. Prosser, J. H. Rollinson,* and R. S. Trotter,* "Light-particle correlations with evaporation residues in the $^{40}Ca+^{12}C$ reaction at $E(^{40}Ca)$=450 MeV", accepted for publication in Phys. Rev. C.

Abstracts

A. Snyder,* C. A. Cardounel,* S. Sigworth,* C. Smith,* G. P. Gilfoyle, R. Zurmuhle, H. T. Fortune, J. Arrison, M. McKenzie, and M. Simpson, "The Search for Nuclear Molecules in the $^{12}C+^{13}C$ System", abstract presented to the National Conference on Undergraduate Research, University of Utah, Salt Lake City, Utah, March 25-28, 1993.

* Undergraduate Student Author

Collaborators

Name	Institution	Name	Institution
S. Ahmad	Rice	J.Arrison	Pennsylvania
P. Bonneau	CEBAF	B. E. Bonner	Rice
S. Christo	CEBAF	P. A. DeYoung	Hope College
S. A. Dytman	Pittsburgh	H. T. Fortune	Pennsylvania
H. Funsten	William & Mary	B. G. Glagola	ANL
D. J. Henderson	ANL	J. Hinnefeld	IU South Bend
C. E. Hyde-Wright	Old Dominion	J.J.Kolata	Notre Dame
D. G. Kovar	ANL/DOE	R.A.Kryger	Michigan State
B. J. Lieb	George Mason	C. F. Maguire	Vanderbilt
J. F. Mateja	ANL	M. McKenzie	Pennsylvania
B.A.Mecking	CEBAF	M. D. Mestayer	CEBAF
R. A. Miskimen	Massachusetts	G. S. Mutchler	Rice
F. W. Prosser	Kansas	B. G. Ritchie	Arizona State
P. D. Rubin	Richmond	J. B. Seaborn	Richmond
M. Simpson	Pennsylvania	H. Stroeher	Giessen
A. Wuosmaa	ANL	A. Yegneswaran	CEBAF
R. Zurmuhle	Pennsylvania		

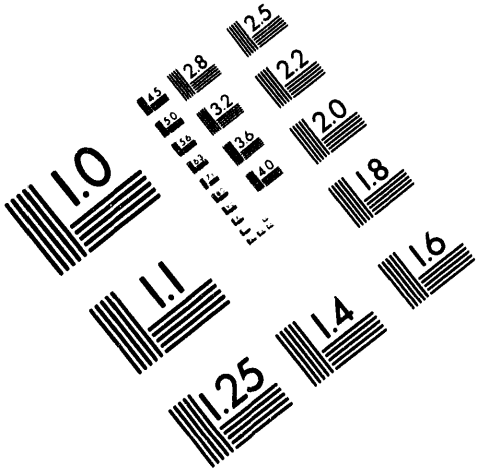

Association for Information and Image Management

1100 Wayne Avenue, Suite 1100
Silver Spring, Maryland 20910

301/587-8202

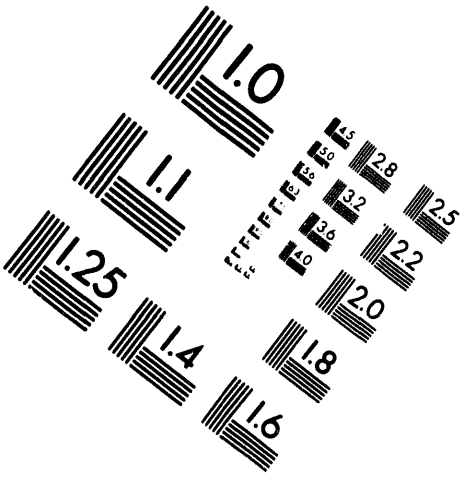

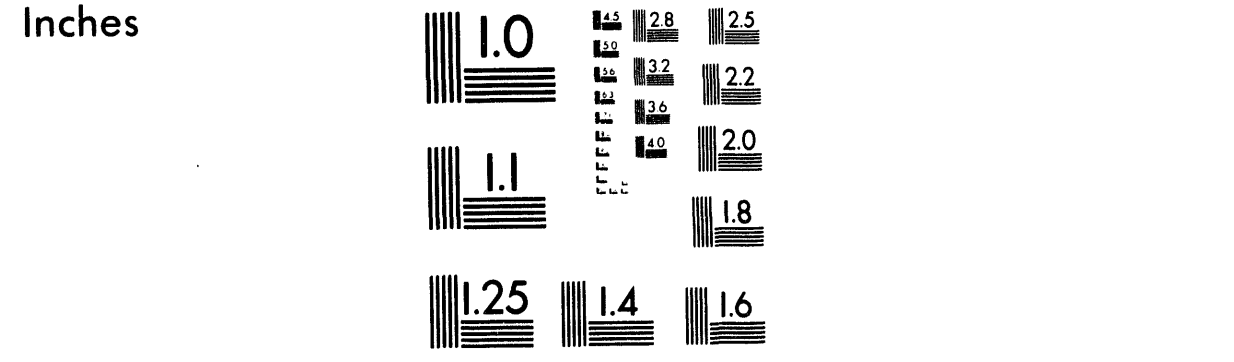

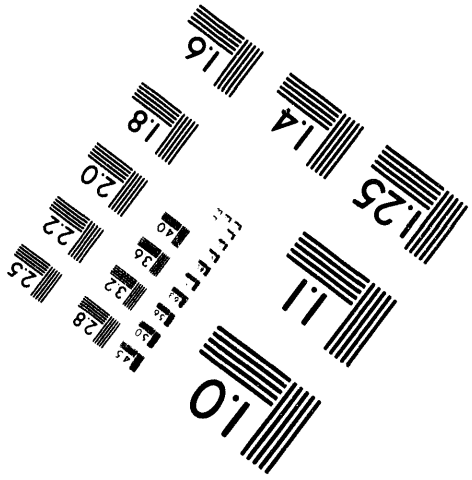

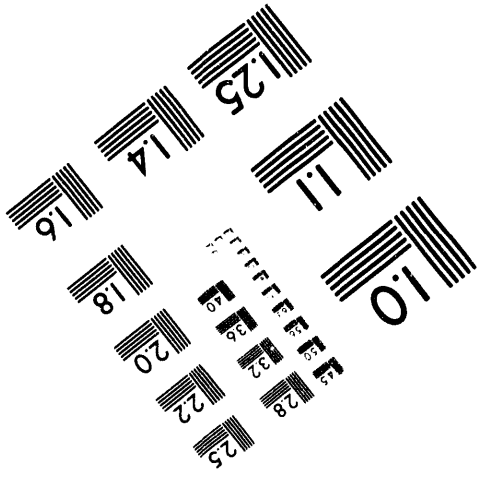

MANUFACTURED TO AIIM STANDARDS
BY APPLIED IMAGE, INC.

DATE
FILMED
12/14/94

END